ADVANCING CYANOBACTERIAL PRODUCTION OF SUSTAINABLE CHEMICAL FEEDSTOCKS

by

Darrian M. Newman

A thesis submitted to the Faculty and the Board of Trustees of the Colorado School of Mines in partial fulfillment of the requirements for the degree of Master of Science (Chemical Engineering).

Golden, Colorado

Date _____

Signed: _____

Darrian M. Newman

Signed: _____

Dr. Nanette R. Boyle
Thesis Advisor

Golden, Colorado

Date _____

Signed: _____

Dr. Anuj Chauhan
Department Head and Professor
Department of Chemical and Biological Engineering

ABSTRACT

The temperature on earth is rising. Studies show that the average surface temperature is already 1°C higher than in pre-industrial times. This rise in temperature is directly linked to anthropogenic carbon emissions and will only continue to rise if immediate action is not taken. Work to improve sustainability in our society has already begun, with vast improvements in solar, wind, geothermal, and other forms of sustainable energy production being made every day. Fossil fuel dependency is pumping carbon dioxide into our atmosphere at unsustainable rates, and cyanobacteria present a feasible means to combat emissions and close the carbon loop for a more sustainable future. Cyanobacteria are prokaryotic, photosynthetic microorganisms with the capability to produce a wide range of chemicals, from biofuels to plastics to sugar to rubber, all while utilizing minimal resources. Only sunlight, trace minerals, unarable land, and sub-optimal water such as ocean water are needed for growth and production of valuable specialty and commodity chemicals. With a higher photosynthetic efficiency and genetic tractability than plants and no competition for arable land or fresh water, cyanobacteria have the potential to be pivotal in the fight against climate change. In this thesis, I characterize the central metabolism of a biofuel producing strain of cyanobacteria to gain a better understanding of how to manipulate cyanobacterial metabolism for increased production of not only biofuels but a range of valuable products. I probe pathways of primary and secondary metabolism using metabolic engineering techniques in an effort to glean useful information and help demystify the complex metabolic network of these complex organisms. Additionally I improve and validate existing tools needed to accelerate the design-build-test-learn cycle and establish cyanobacteria as a commercially viable sustainable producer of valuable products.

TABLE OF CONTENTS

ABSTRACT iii

LIST OF FIGURES viii

LIST OF TABLES xi

LIST OF SYMBOLS xii

LIST OF ABBREVIATIONS xiii

ACKNOWLEDGMENTS xvi

CHAPTER 1 INTRODUCTION 1

CHAPTER 2 THE 2-C-METHYL-D-ERYTHRITOL-4-PHOSPHATE (MEP) PATHWAY 6

2.1 Terpenoid Production in Cyanobacteria 6

2.2 Fosmidomycin: The MEP Pathway Inhibitor 10

CHAPTER 3 METHOD DEVELOPMENT 16

3.1 Arresting Metabolism in *Synechococcus* 7002 Using Partially Frozen Saline Solution 16

3.1.1 Partially Frozen Saline Versus Methanol Quenching Solutions 17

3.1.2 Mathematical Predictions 18

3.1.3 Experimental Verification of Temperature Changes 19

3.2 Metabolic Engineering in Cyanobacteria 21

3.2.1 Synthetic Biology Toolkit in Cyanobacteria 21

3.2.2 Vector Construction and Transformations in *E. coli* 25

3.2.3 Cyanobacterial Transformations 27

3.3 Promoter Characterization 28

3.4 CRISPRi Repression of *dxr* 32

3.5 Overexpression of Native Genes 35

3.5.0.1 *dxr* Overexpression and Knockout 35

3.5.0.2 Overexpression of bifunctional fructose-1,6-biphosphatase/Sedoheptulose-1,7-Bisphosphatase enzyme (SBPase) in *Synechococcus* 7002 37

CHAPTER 4 QUANTIFICATION OF THE CENTRAL METABOLISM OF A LIMONENE PRODUCING *SYNECHOCOCCUS* SP. PCC 7002 42

4.1 Background 42

4.1.1 Isotopically Non-stationary ^{13}C Metabolic Flux Analysis (INST-^{13}CMFA) 42

4.2 Isotopically Non-stationary ^{13}C Metabolic Flux Analysis (INST-^{13}CMFA) on Limonene Producing *Synechococcus* sp. PCC 7002 48

4.2.1 Abstract 48

4.2.2 Introduction 49

4.2.3 Methods 51

4.2.3.1 Strains and Cultivation Conditions 51

4.2.3.2 Dynamic Labeling and Quenching Experiment 51

4.2.3.3 Metabolite Extraction 52

4.2.3.4 LC/MS-MS Quantitation of Metabolites 52

4.2.3.5 Isotopically Non-stationary 13C Metabolic Flux Analysis . . . 53

4.2.4 Results and Discussion 53

4.2.5 Conclusions 59

CHAPTER 5 THE EFFECT OF CHANGING BIOMASS COMPOSITION ON THE OUTCOME OF CONSTRAINT BASED METABOLIC MODELS 60

5.1 Abstract 60

5.2 Introduction 61

5.3 Materials and Methods 63

5.3.1 Metabolic Model 63

5.3.2 Biomass Formation Equations 63

5.3.3 Biomass Yield on Light Calculations 64

5.3.4 Sensitivity Analysis 64

5.4 Results 64

5.5 Discussion 66

5.6 Conclusions 69

5.7 Conflicts of Interest 70

CHAPTER 6 CONCLUSION 71

6.1 Future Works 72

REFERENCES 74

APPENDIX A EXPERIMENTAL PROCEDURES 90

A.1 Growth Conditions 90

A.1.1 *E. coli* 90

A.1.2 *Synechococcus* 7002 90

A.1.3 *Synechocystis* 6803 90

A.2 Plasmid Construction and Screening 91

A.3 Cyanobacterial Transformation 93

APPENDIX B PLASMIDS, PRIMERS, AND DNA SEQUENCES 97

APPENDIX C COPYRIGHT PERMISSIONS 120

C.1 Copyright Permission for NOAA Data 120

C.2 Copyright Permission for ^{13}C Workflow from Sake et al. 121

C.3 Copyright Permission for CRISPRi Description Figure from Hogan et al. . . 122

APPENDIX D SUPPLEMENTARY INFORMATION FOR CHAPTER 4 123

APPENDIX E SUPPLEMENTARY INFORMATION FOR CHAPTER 5 131

LIST OF FIGURES

Figure 1.1 Levels of atmospheric CO_2 since 1958. 2

Figure 1.2 Levels of atmospheric CO_2 over the last 800,000 years. 3

Figure 2.1 The 2-C-methyl-D-erythritol-4-phosphate (MEP) pathway in cyanobacteria. 8

Figure 2.2 Chemical structure of limonene. 9

Figure 2.3 Fosmidomycin inhibits growth in *E. coli* 12

Figure 2.4 Change in growth rate of *E. coli* DH5α in response to changing concentrations of fosmidomycin in the extracellular growth medium. . . . 13

Figure 2.5 *Synechococcus* 7002 growth in high fosmidomycin concentration. 14

Figure 3.1 Action of restriction endonucleases 23

Figure 3.2 Function of the CRISPRi system in vivo. 24

Figure 3.3 Restriction-Ligation reaction unidirectionally ligating two parts. 26

Figure 3.4 Growth of *Synechocystis* 6803 in BG-11 media altered to contain either only NH_4 or only NO_3, as well as an equally split molar ratio of both nitrogen sources. 29

Figure 3.5 Self-replicating plasmid expressing the eYFP gene promoted by either the inducible NirA promoter, or the synthetic J23119 promoter outfitted with the same RBS sequence as nirA. 30

Figure 3.6 Growth of *Synechocystis* 6803 mutant strains expressing the eYFP protein behind either the NirA or J23119 promoter. 31

Figure 3.7 Promoter characterization of the inducible NirA and J23119 synthetic promoter in *Synechocystis* 6803. 32

Figure 3.8 Self-replicating plasmid expressing the dCas9 protein and sgRNA sequence specific to *dxr* for transcript repression. 33

Figure 3.9 Growth of *Synechocystis* 6803 Cr178 strain in different nitrogen conditions, compared to growth of the WT strain. 34

Figure 3.10 Two vector system for the inducible expression of an extra copy of the *dxr* on a self-replicating plasmid, followed by a knockout of the genomic copy. 35

Figure 3.11 Growth of *Synechocystis* 6803 DXR overexpressing strain in different nitrogen conditions, compared to growth of the WT strain. 37

Figure 3.12 Overexpression of *fbp1* amplified from 7002 genomic DNA. 39

Figure 3.13 Phenotypic differences between the three *fbp1* overexpressing strains. . . . 40

Figure 3.14 Growth of the *Synechococcus* 7002 SBPJ23119, *Synechococcus* 7002 SBPJ23109 and *Synechococcus* 7002 SBPJ23108 strains compared to the WT strain. 41

Figure 4.1 Complete workflow for INST-^{13}CMFA in cyanobacteria. 43

Figure 4.2 Example of metabolite pool labeling of a three carbon intracellular metabolite when fed a cocktail of unlabeled, uniformly labeled, and a 1-^{13}C labeled six carbon substrate. 44

Figure 4.3 Example of transient metabolite pool labeling of a three carbon intracellular metabolite when fed a single carbon ^{13}C labeled substrate. . 45

Figure 4.4 MIDs for the intracellular metabolites 3PG and FUM describing the change in labeling over time as cells incorporated more isotopically labeled ^{13}C into metabolite pools. 46

Figure 4.5 Example flux map of the CBB cycle depicting carbon flow through reactions from metabolite to metabolite. 47

Figure 4.6 *Synechococcus* 7002 WT and LS solved flux maps. 55

Figure 4.7 Transient labeling patterns for PEP. 56

Figure 4.8 Associated energy and reducing power transfer reactions accompanying the two reaction pathways cyanobacteria use to synthesize PYR from PEP. 58

Figure 5.1 Comparison of published, experimentally determined biomass composition for a variety of algae and cyanobacteria species. 62

Figure 5.2 Comparison of growth rate and yield predictions for the Imam et al. *Chlamydomonas reinhardtii* genome scale model using several different biomass formation equations. 66

Figure 5.3 Flux sensitivity analysis for changing biomass compositions. 67

Figure A.1 Protocol for restriction/ligation reactions to assemble modular level 0 parts into level 1 constructs for transformation into *E. coli* and blue/white screening. 91

Figure A.2 Protocol for LB plates with the appropriate concentrations of various antibiotics and other necessary ingredients for compatibility with *E. coli* blue-white screening procedures as described in Gale et al.. 92

Figure A.3 protocol for colony PCR in cyanobacteria to test for segregation of genes in a single colony of transformants. 93

Figure A.4 Natural transformation of *Synechococcus* 7002 94

Figure A.5 Electroporation of *Synechocystis* 6803. 95

Figure A.6 Conjugation in *Synechocystis* 6803. 96

Figure C.1 Copyright Permission for NOAA Data 120

Figure C.2 Copyright Permission for ^{13}C Workflow Figure 121

Figure C.3 Copyright Permission for CRISPRi Description Figure 122

Figure D.1 Labeling dynamics of measured metabolites: GAP, DHAP, FUM, PEP, AKG 125

Figure D.2 Labeling dynamics of measured metabolites: FBP, 3PG, RU5P, G1P, FBP, G6P 126

Figure D.3 Growth curve of *Synechococcus* 7002 WT strain and LS strain. 130

LIST OF TABLES

Table 2.1 Previous attempts to engineer cyanobacteria for high titers of terpenoid products through the MEP pathway. 10

Table 3.1 Predicted instantaneous temperatures of quenching 19

Table 3.2 Measured instantaneous temperatures of quenching. 20

Table B.1 List of Final Level T Plasmids 98

Table B.2 List of Plasmids 100

Table B.3 List of Primers 105

Table B.4 List of Custom Sequences 113

Table D.1 Metabolic network and Associated Atom Transitions. 123

Table D.2 Simulated Flux Values and Bounds. 127

Table E.1 Exchange Reaction Fluxes for Simulations Run to Predict Growth Rate and Biomass Yield. 132

Table E.2 Exchange Reaction Fluxes for Simulations Run to Predict Growth Rate and Biomass Yield. 134

Table E.3 Reactants and products consumed and formed in the biomass formation equation and their coefficients for each of the equations constructed for this study. 136

LIST OF SYMBOLS

Inhibited percent growth in Hill equation . . . . . E/E_{max}

Inhibitor concentration in Hill equation . . . . . [A]

half maximal effective concentration . . . . . EC_{50}

heat of melting for water . . . . . ΔH_{fus}

mass of ice . . . . . m_{ice}

methanol-water heat of mixing . . . . . ΔH_m

mixture mass . . . . . m_{mix}

mixture specific heat . . . . . $C_{p,mix}$

mixture temperature . . . . . T_f

quenching solution temperature . . . . . T_q

sample mass . . . . . m_s

sample specific heat . . . . . $C_{p,s}$

sample temperature . . . . . T_s

LIST OF ABBREVIATIONS

α-ketoglutarate	AKG
1-deoxy-D-xylulose5-phosphate	DXP
1-hydroxy-2-methyl-2-(E)-butenyl 4-diphosphate	HMBPP
2-C-Methyl-D-erythritol 4-phosphate	MEP
2-C-methyl-d-erythritol-2,4-cyclodiphosphate	ME-cDP
2-phosphoglycolate	2PG
3-phosphoglycerate	3PG
4-(cytidine 5'-diphospho)-2-C-methyl-D-erythritol	CDP-ME
5-Bromo-4-Chloro-3-Indolyl -D-Galactopyranoside	X-gal
CDP-ME kinase	ispE
CDP-ME synthase	ispD
CRISPR associated protein 9 dead	dCas9
Calvin-Benson-Bassham cycle	CBB cycle
Colorado School of Mines	CSM
DXP reductase	DXR
DXP synthase	DXS
Deoxyribonucleic acid	DNA
Escherichia coli	*E. coli*
HMBPP reductase	ispH
HMBPP synthase	ispG

IPP isomerase . . . . . IDI

ME-cDP synthase . . . . . ispF

National Oceanic and Atmospheric Administration . . . . . NOAA

carbon dioxide . . . . . CO_2

clustered regularly interspaced short palindromic repeats interference . . . . . CRISPRi

cytidine triphosphate . . . . . CTP

dihydroxyacetone phosphate . . . . . DHAP

dimethylallyl diphosphate . . . . . DMAPP

dxr . . . . . DXP reductase gene

erythrose 4-phosphate E4P

fructose 1,6-bisphosphate . . . . . FBP

fructose 6-phosphate F6P

fructose-1,6-bisphosphatase/sedoheptulose- 1,7-bisphosphatase . . . . . SBPase

fumarate . . . . . FUM

geranyl pyrophosphate . . . . . GPP

glucose 6-phosphate G6P

glyceraldehyde 3-phosphate . . . . . GAP

isopentenyl diphosphate . . . . . IPP

limonene synthase . . . . . LS

malate . . . . . MAL

mass isotopomer distribution . . . . . MID

mevalonate . . . . . MVA

micromolar . . . . . μM

millimolar . . . . . mM

nanometers . . . . . nm

open reading frame . . . . . ORF

oxygen . . . . . O_2

parts per million . . . . . ppm

pentose phosphate pathway . . . . . PPP

phosphoenolpyruvate . . . . . PEP

pyruvate . . . . . PYR

reverse transcription quantitative polymerase chain reaction . . . . . RT-qPCR

ribose 5-phosphate R5P

ribosome binding site . . . . . RBS

ribulose 1,5-bisphosphate . . . . . RUBP

ribulose 5-phosphate RU5P

ribulose-1,5-bisphosphate carboxylase-oxygenase . . . . . RuBisCO

sedoheptulose 7-phosphate S7P

small guiding ribonucleic acid . . . . . sgRNA

small regulatory ribonucleic acid . . . . . sRNA

succinate . . . . . SUC

wild type . . . . . WT

xylulose 5-phosphate X5P

yellow fluorescent protein . . . . . eYFP

ACKNOWLEDGMENTS

Firstly, thank you Nanette. Thank you for taking me on as an undergrad, and seeing my potential for graduate school. Thank you for giving me the freedom in research and in life to become who I am today, and for the guidance that I simply could not have succeeded without. I am forever grateful of the chance you gave me to pursue the research I have come to love, and have fun doing it too. From you I have learned the right way to do science, and how to not take no for an answer, two skills among many that I will never forget. I'm honored to have been a part of the amazing team you have built, and would like to thank Cara, Alex, and Michelle for the endless support, ideas, and damage control throughout this wild ride. I can't wait to see all of the amazing things each of you accomplish. Thanks to my undergraduate prodigy, Evan. Thanks as well to my committee, Dr. Josh Ramey and Dr. Melissa Krebs for your support through my time here.

I would also like to thank my parents. Mom, thank you for listening, thank you for picking me up when I was down, and thank you for helping me to think outside the box when I was stuck. I've grown up to be a scientist, just like you. Dad, thank you for pushing me, not just in school but in life. I'm so grateful for both of you, even though sometimes I didn't want to do multiplication in the car. You both taught me how to think and how to learn, and more credit goes to you than I am even willing to admit.

CHAPTER 1

INTRODUCTION

The earth has experienced an average surface temperature rise of 1°C since pre-industrial times, and is projected to reach an absolute rise of 1.5°C compared to pre-industrial times by the year 2040[1]. The evidence is clear and abundant: emissions from human activity is adding nearly 100 megatons of CO_2 into the atmosphere every day [2] and is directly linked to the rising temperatures we experience on earth [3]. We burn petroleum to drive our cars and planes, coal and natural gas to supply electricity and heat to our houses, all the while pumping carbon dioxide (CO_2), the main product of the combustion reaction, into our atmosphere. Non-renewable fossil fuels are the main source of energy and materials for modern society.

CO_2 levels in the atmosphere are measured in parts per million (ppm). Our atmosphere contained on average 412.5 ppm CO_2 in the year 2020, a full 43.5 ppm increase since the year 2000 according to the National Oceanic and Atmospheric Administration (NOAA) [4]. Since 1958 the average concentration has risen from 316 ppm to 417 ppm in October of 2021 at the Mauna Loa Observatory in Hawaii (Figure 1.1, where CO_2 levels are being continuously tracked. Rising and falling levels of atmospheric CO_2 are not uncommon in earth's history; the problem lies in the *RATE* of CO_2 increase, which is exceptionally high over a very short (relative) span of time. Over the last 800,000 years CO_2 concentrations have remained stable, oscillating between 175 and 300 ppm through glacial and interglacial periods (Figure 1.2). Industrialization by humankind has changed these oscillatory patterns, and the NOAA clearly demonstrates the unprecedented rise in atmospheric CO_2 levels compared to earth's past.

Since the conception of life on earth, nature has depended on the stability our environment provides to grow and thrive. Life on earth is incapable of adapting quickly

enough to these immense changes, and as a result we already see coral bleaching in our oceans and rises in endangered species[5]. The consequences of anthropogenic emissions are beginning to take effect, not only for wildlife but for the humans as well. Future generations will battle rising sea levels, mass extinctions, severe droughts, wildfires, temperature extremes, and other erratic weather patterns.

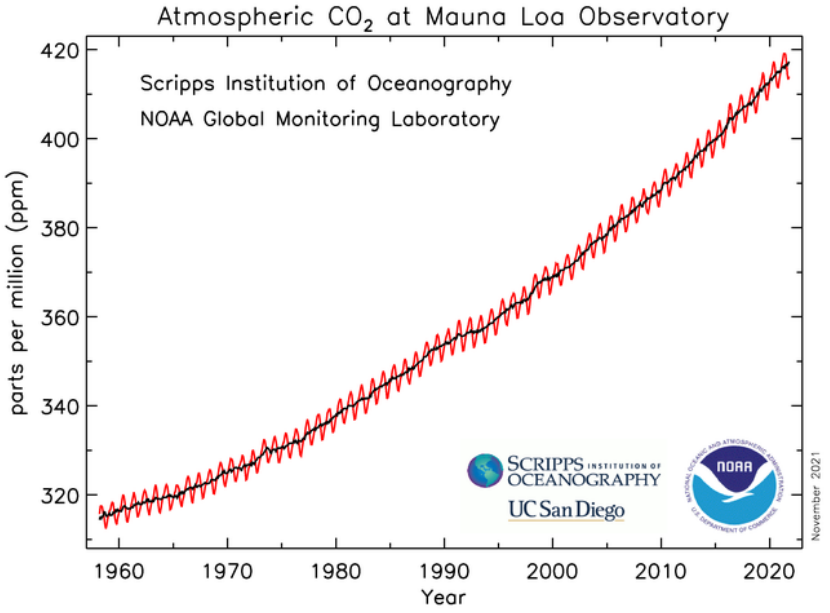

Figure 1.1 Levels of atmospheric CO_2 since 1958.The red line represents monthly mean CO_2 concentrations at the Mauna Loa Observatory, with black representing the same measurement, corrected for average seasonal cycles. Data compiled by the NOAA, recorded at the Mauna Loa Observatory(https://gml.noaa.gov/ccgg/trends/). Permission statement in Figure C.1.

Research into sustainable energy generation, like wind and solar, have dramatically increased in recent years in response to increasing evidence of the negative impact CO_2 have on our environment. Solar, wind, hydro-thermal, and similar electricity producing sustainable options have provided us with promising avenues toward a more sustainable future. However, the energy density of batteries cannot match that of liquid fuel, such as gasoline or diesel. In order to build upon our existing, petroleum based infrastructure, sustainable methods of producing large amounts of biofuel must be developed.

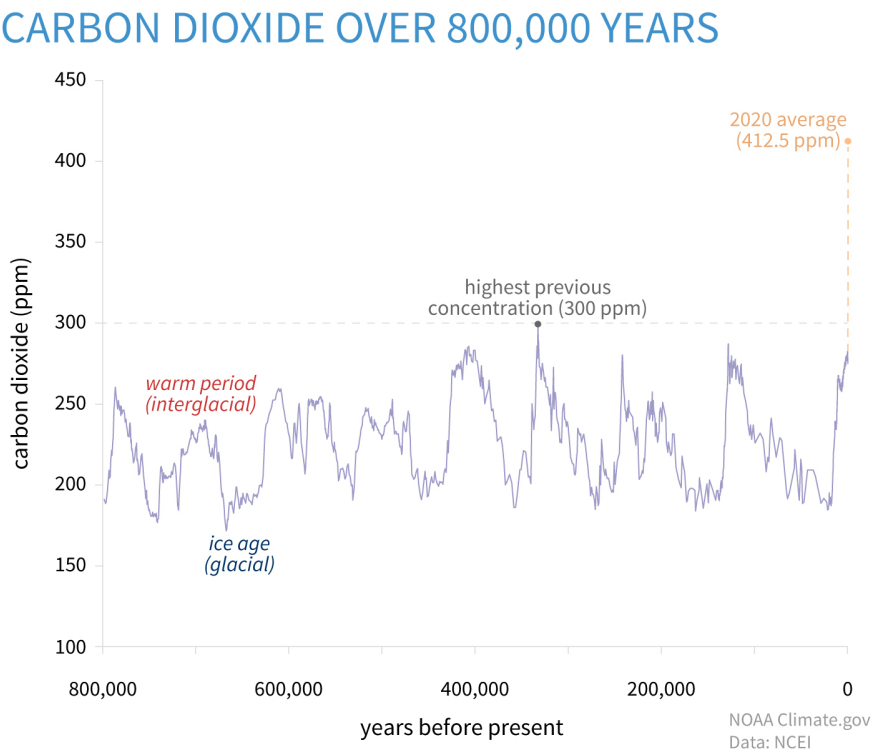

Figure 1.2 Levels of atmospheric CO_2 over the last 800,000 years. Data obtained from https://www.climate.gov/media/13611 [4]. Permission statement in Figure C.1.

Research into sustainable bioproducts has seen a similar boom, with the production of sustainable chemicals by *E. coli* and yeast. Now the field looks to harness the power of photosynthesis to produce carbon negative chemicals and carbon neutral fuels directly from the atmospheric CO_2 in an effort to reduce CO_2 concentrations and alleviate our societies' dependency on fossil fuels. Here, cyanobacteria have an important role to play. These microorganisms have been identified as promising and effective tools for biofuel and biochemical production [6][7], with many important advances already made toward improving cyanobacteria for industrial purposes [8].

Cyanobacteria are a particularly intriguing candidate for sustainable chemical and fuel production. Sometimes called blue-green algae, these prokaryotic microorganisms are more efficient at light harvesting and produce biomass at higher rates than plants [9][10]. This gives these simple organisms an advantage over existing methods of biofuel production,

such as the fermentation of corn by yeast. Additionally, cyanobacteria do not compete with food/feed products, and instead can be engineered to grow and synthesize valuable products on non-arable land and with sub-optimal water supply, such as brackish water or waste water. Some species, such as *Synechococcus* sp PCC 7002 (herafter *Synechococcus* 7002) are able to tolerate high salinity and light intensity, broadening their range of potential applications [11][12]. Cyanobacteria have the potential to close the carbon loop, enabling our societies to reuse carbon from our atmosphere for the production of fuels and materials, rather than relying on unsustainable fossil fuel feed stocks. In a sustainable future, essential carbon-containing goods like plastics, rubbers, and commodity chemicals will not come from untapped oil reserves, they will be recycled again and again from existing feedstocks. Cyanobacteria provide the unique opportunity to weave sustainability into the current oil-based economy, providing our planes and transportation with carbon-neutral sources of energy dense liquid fuel.

Cyanobacteria are vital organisms in nature already. These creatures fix CO_2 and produce O_2 in all of the worlds oceans, and fresh water as well. Some species are capable of fixing atmospheric nitrogen into reduced forms [13], providing a valuable source of biologically active nitrogen to the environment around them. In order to use these microorganisms for our purposes, we must rewire metabolism and direct carbon to the products in which we are interested. The relative simplicity of cyanobacteria compared to their eukaryotic counterparts and their genetic tractability make this goal more attainable [12].

One major roadblock in the use of cyanobacteria is an underdeveloped synthetic biology toolbox for the manipulation of phenotypes. In recent years, the toolbox has been drastically improved, but more work is needed in order to develop the same tools for cyanobacteria that have been developed and effectively used for modification of model organisms such as *E. coli* and yeast. The faster we are able to efficiently engineer strains and learn from the resulting phenotypes, the faster we can accelerate these organisms to

industrially relevant producers of fuels and materials. The faster we are able to produce industrially relevant strains, the more valuable cyanobacteria will be in the fight to reduce the effects of anthropogenic climate change caused by carbon emissions. In this thesis I use synthetic biology, analytical chemistry, and computational biology together to develop and validate experimental techniques for metabolic engineering of cyanobacteria, and deepen our understanding of cyanobacterial metabolism through experimental and computational research.

CHAPTER 2

THE 2-C-METHYL-D-ERYTHRITOL-4-PHOSPHATE (MEP) PATHWAY

The MEP pathway is an integral part of secondary metabolism, and is utilized by prokaryotes and eukaryotes. This linear, seven step pathway connects central metabolism to a class of molecules called terpenoids, essential building blocks of life, and an extremely diverse group of secondary metabolites. The MEP pathway has been the subject of a lot of research due to the array of valuable chemicals that can be synthesized using this pathway. In this chapter, I describe the MEP pathway, describe my efforts to engineer the MEP pathway in cyanobacteria, and delve into conflicting evidence in the literature describing the function and architecture of this pathway.

2.1 Terpenoid Production in Cyanobacteria

Terpenoids are the largest class of secondary molecules, encompassing over 55,000 known chemicals, with many more likely to be discovered [14]. The class terpenoid includes many complex molecules used for a wide variety of functions throughout animals, plants and bacteria. Photosynthetic molecules like chlorophyll, carotenoids, plastoquinone all fall within this category [15]. Likewise, terpenoids represent a diverse suite of currently utilized and potential industrial compounds including flavors, fragrances, chemical solvents, rubbers and biofuel precursors [16], all with the potential for sustainable production, as cyanobacteria naturally produce the precursors to all terpenoids.

In the scientific literature, the term terpenoid is often used interchangeably with isoprenoid and terpene. Isoprenoid and terpene are synonyms that refer to molecules that are directly formed by the condensation of sequential isoprene units, the five carbon building blocks of all isoprenoids, terpenes and terpenoids alike. Terpenoid is simply a more general term that also encompasses molecules with added functional groups beyond

five carbon isoprene units[15]. I will continue to use the more general term, terpenoid, throughout the rest of this thesis.

Terpenoids are known to be produced through two separate pathways, the mevalonate (MVA) pathway, and the MEP pathway, also referred to as the mon-mevalonate pathway. Cyanobacteria, and all other prokaryotic organisms only possess the MEP pathway, while eukaryotic organisms are equipped with both, usually with the MEP pathway at work in either the chloroplast and mitochondria, and the MVA pathway in a different compartment. Both pathways provide cells with the same five carbon isoprene units isopentenyl diphosphate (IPP) and dimethylallyl diphosphate (DMAPP) from which all terpenoids are produced [17][18][19].

Prokaryotes draw upon glyceraldehyde 3-phosphate (GAP) and pyruvate (PYR) pools to initiate the first step to the MEP pathway in the formation of 1-deoxy-D-xylulose 5-phosphate (DXP)(Figure 2.1). This step is catalyzed by DXP synthase (DXS). DXP is converted to MEP in a second step by DXP reductase (DXR), which is the first committed step to the linear pathway. All MEP is converted to IPP and DMAPP, the universal terpenoid precursors, by the HMBPP reductase (ispH) enzyme HMBPP reductase produces both IPP and DMAPP, with the ratio heavily dependent on the strain [20]. IPP and DMAPP can be inter-converted with the isopentenyl diphosphate isomerase (IDI) enzyme. The IDI enzyme is not essential in cyanobacteria, as ispH produces both IPP and DMAPP[15], but has been studied as a tool for optimization of IPP/DMAPP ratios in cyanobacteria[21]. For a more in-depth review of the MEP pathway, consult Zhao et al.[22]. All steps from the central metabolism of cyanobacteria to the universal terpenoid preucursors of IPP and DMAPP are shown in Figure 2.1.

Terpenoids can be used as sustainable fule sources and limonene is one such terpenoid receiving attention from the metabolic engineering field as a candidate for use as a sustainable drop-in bio-diesel jet fuel additive. Limonene ($C_{10}H_{16}$) is an energy-dense 10 carbon cyclic hydrocarbon molecule with properties similar to cold-weather performance

diesel jet fuel. Limonene is currently extracted from the peels of citrus fruit as a byproduct of juice processing, a production method that is energy-intensive and subject to volatile pricing fluctuations from seasonal farming yields [23]. The global market for limonene as of 2018 was $160 million, with an average market price of $7/kg [24]. Multiple techno-economic analyses of limonene production using microbial technologies report that vast improvements are needed for the molecule to become economically relevant as a bio-fuel precursor [24][25].

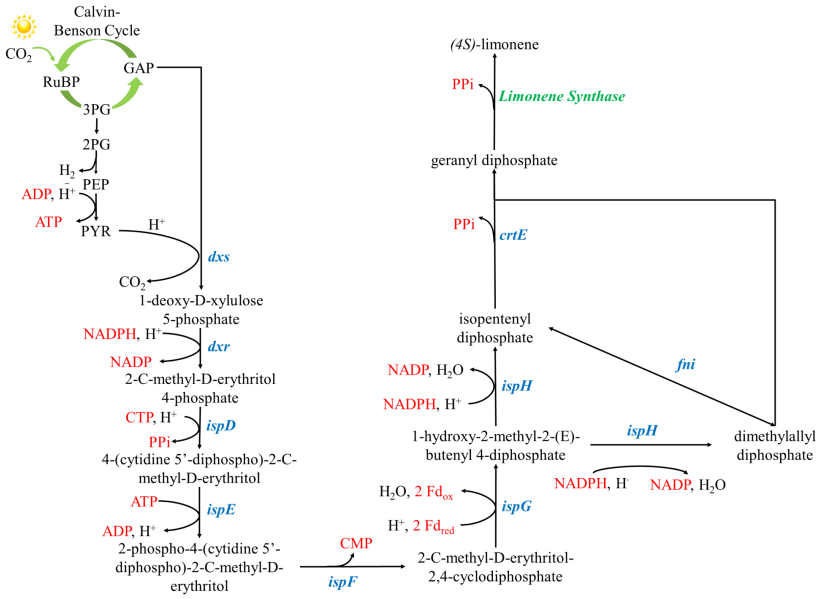

Figure 2.1 The 2-C-methyl-D-erythritol-4-phosphate (MEP) pathway in cyanobacteria. Pathway describes each reaction (black arrows) from the CBB cycle to geranyl diphosphate, along with enzymes mediating each reaction (blue), and cofactors (red) produced and consumed. The green limonene synthase describes the heterologous insertion of the enzyme for endowing organisms with the ability to produce limonene.

Limonene is classified as a cyclic monoterpene (Figure 2.2), synthesized from geranyl pyrophosphate (GPP) in a single step of the limonene synthase (LS) enzyme. GPP is produced by the condensation of IPP and DMAPP [26] and is considered one of the simplest terpenoid structures, hence limonene's classification as a monoterpenoid(ten carbon) as opposed to the more complex classes of structure such as sesquiterpenoid(C15),

diterpenoid(C20), triterpenoid(C30), or tetraterpenoid(C40) [15]. Due to ease of integrating a single gene for the production of limonene and the potential market for this molecule, it has already been expressed in many organisms, like heterotrophic *E. coli* [27] and yeast [28], as well as autotrophic cyanobacteria. The ability to produce other terpenoid molecules besides limonene have also been conferred to cyanobacteria (see Table 2.1). In *Synechococcus elongatus* 7942 for example, attempts have been made to overexpress upstream MEP pathway bottlenecks, but with limited success. Consistently, attempts to alleviate bottlenecks in the MEP pathway and increase the pool sizes of terpenoid precursors, IPP and DMAPP, are met with limited or no success.

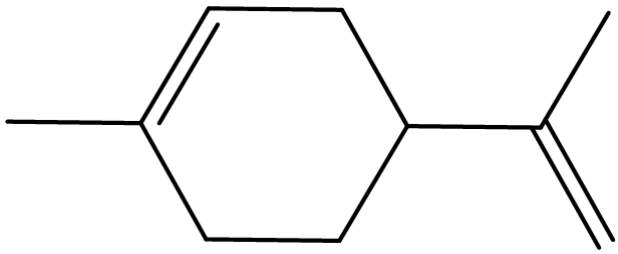

Figure 2.2 Chemical structure of limonene.

Regulatory elements likely play a role in these low partition rates toward the MEP pathway, and the limited success of metabolic engineering attempts to increase flux toward the production of terpenoid products. Unfortunately, much is still known about the specific mechanisms involved in such regulation[29]. Given this information, attempts have even been made to bypass host regulation altogether by inserting the entire MVA pathway from eukaryotic organisms into *Synechocystis* 6803 [30]. Even this strategy was met with the same limited success. Whether the availability of precursor molecules or regulation of the pathways are responsible for low terpenoid titers among cyanobacterial producers, a new strategy is needed to produce industrially relevant cyanobacterial strains capable of economically feasible production of terpenoid products.

Table 2.1 Previous attempts to engineer cyanobacteria for high titers of terpenoid products through the MEP pathway.

Strain	Target Molecule	Expression Targets	Titer	Days	References
Synechococcus 7002	Limonene	LS[1]	4 mg/L	4	[31]
Synechcoccus elongatus 7942	Limonene	LS	2.5 mg/L	4	[32]
Synechcoccus elongatus 7942	Isoprene	IDI, ispS[2], DXS, ispG	1.26 g/L	21	[33]
Synechcoccus elongatus 7942	Amorphadiene	dxs, idi, ispA[3], ads[4]	19.8 mg/L	10	[34]
Synechocystis 6803	Phellandrene	MVA pathway	10 mg/gDCW	2	[30]

Given the lack of tools necessary to elucidate the mechanisms of low terpenoid titers, I propose zooming out of the MEP pathway, and characterizing cyanobacterial metabolism from a whole-cell perspective. A more global approach to carbon partitioning and regulatory control may be needed to better understand cyanobacterial metabolism and design strategies for increased production.

2.2 Fosmidomycin: The MEP Pathway Inhibitor

Fosmidomycin is an antibiotic that targets the active site of *dxr* in many microorganisms, shown to inhibit growth and terpenoid production in plants like *Populus nigra* and *Chelidonium majus*[35], and microorganisms like *Mycobacterium tuberculosis* and *Plasmodium falciparum*[36]. Interestingly, fosmidomycin is ineffective in most species of cyanobacteria, which calls into question the role of DXR in cyanobacterial metabolism.

[1]limonene synthase
[2]isoprene synthase
[3]farnesyl diphosphate synthase
[4]amorpha-4,11-diene synthase

The *dxr* has been studied previously as a potential bottleneck to the MEP pathway [34][37]. Alleviation of this bottleneck however, as well as attempts to alleviate many other bottlenecks in the MEP pathway (Table 2.1) have proven unsuccessful at substantially increasing carbon flux through the MEP pathway toward valuable products. These results indicate the presence of intense regulation restricting carbon flux through the MEP pathway, but little is known about the mechanisms of such regulation [19][38][39].

Another intriguing explanation for the lack of success in overexpressing MEP pathway enzymes is that perhaps the MEP pathway isn't the main source of terpenoid production in cyanobacteria. Conflicting evidence exists in the literature as to the essentially of the DXR enzyme in cyanbacteria, and more broadly the assumption of the MEP pathway as the sole metabolic route in cyanobacteria for terpenoid production. The MEP pathway as described in cyanobacteria has been inferred from the MEP pathway in *E. coli*. The MEP pathway is undoubtedly a universally conserved pathway, and orthologous proteins to those in each step of the MEP pathway have been identified in cyanobacteria such as the model organism *Synechocystis* 6803 [40]. Figure 2.3 provides evidence of *E. coli* growth inhibition in the presence of varying concentrations of fosmidomycin.

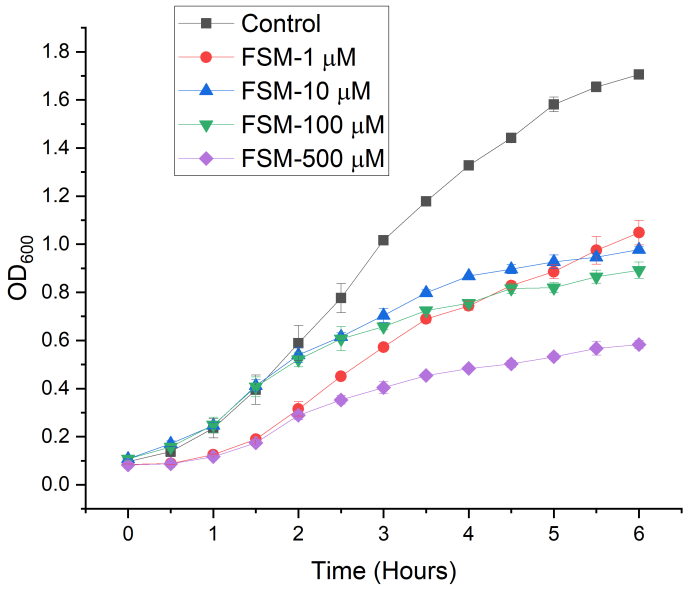

Figure 2.3 Fosmidomycin inhibits growth in *E. coli*. We grew E. coli in various concentrations of fosmidomycin, a known inhibitor of *dxr*. Increasing concentrations of fosmidomycin results in a larger detrimental impact on growth. Error bars represent standard deviation of biological replicates(n=3).

Furthermore, *E. coli* show a characteristic response to increasing dosage of the antibiotic(Figure 2.4), which can be fit to the hill equation [41] (Equation 2.1):

$$\frac{E}{E_{max}} = \frac{1}{1 + (\frac{EC_{50}}{[A]})^n} \tag{2.1}$$

where E/E_{max} represents the percent growth compared to uninhibited growth, and [A] represents the concentration of fosmidomycin in the extracellular medium in μM. The inhibiting effect of fosmidomycin on the *E. coli* DH5α strain was confirmed in our lab by estimating a half maximal effective concentration (EC_{50}) of 0.9 μM.

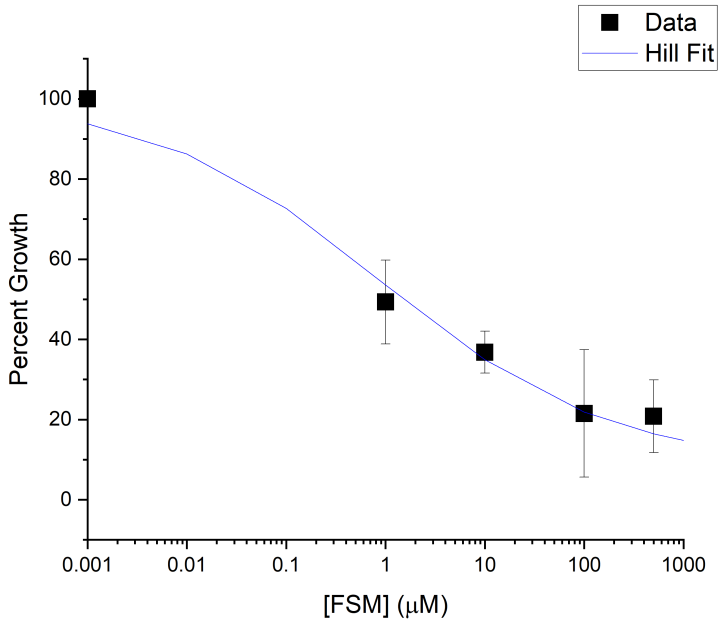

Figure 2.4 Change in growth rate of *E. coli* DH5α in response to changing concentrations of fosmidomycin in the extracellular growth medium. The hill equation (2.1) was used to estimate an EC_{50} value for the effect of fosmidomycin on *E. coli* growth. Error bars represent standard deviation of biological replicates(n=3).

In contrast, we see no significant difference in growth when *Synechococcus* 7002 is grown in the presence of fosmidomycin, even at concentrations over 1000x the EC_{50} for *E. coli*. This apparent tolerance is not due to inactivation of the antibiotic, because we grew *E. coli* in the spent medium from cyanobacterial cultures and saw the same growth defect as shown in Figure 2.3. This could be due to mechanisms present in cyanbacteria that rapidly expel the antibiotic, block it's entry into the cell altogether, or simply have a *dxr* that is not susceptible to fosmidomycin. The other, more intriguing possibility is that the DXR enzyme IS susceptible to fosmidomycin inhibition, but not essential for the production of terpenoid products in cyanobacteria. Evidence from Ershov et al. [42] corroborates this theory. Using cell-free extracts, Ershov et al. demonstrated a higher incorporation of ^{14}C radio-labeled carbon into downstream terpenoid products when labeled pentose phosphate pathway intermediates like E4P, G6P, F6P, and GAP were

added to the system, rather than when labeled PYR or DXP. This study found significant incorporation of labeled MEP as well, indicating that the first two steps of the MEP pathway in cyanobacteria may not operate as described by *E. coli*. It was concluded that X5P was the most likely candidate for the connection between the pentose phosphate pathway and terpenoid production in cyanobacteria.

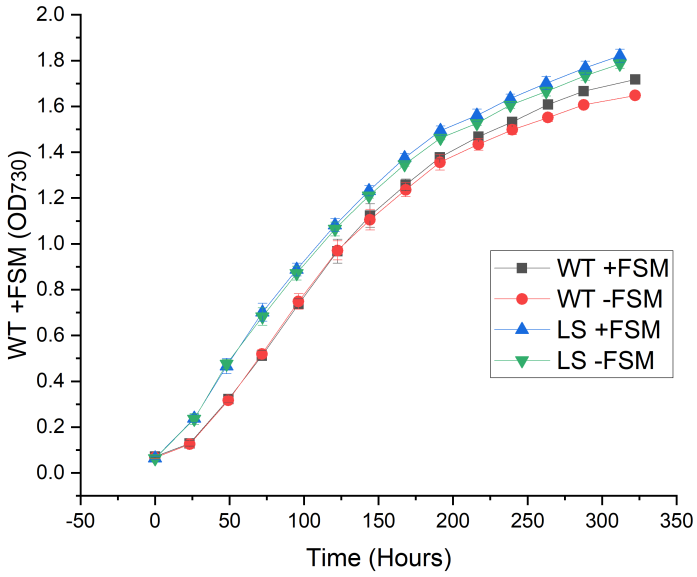

Figure 2.5 *Synechococcus* 7002 growth in high fosmidomycin concentration. Cultures were grown at atmospheric CO_2 levels and a light intensity of 80μmol $m^{-2}s^{-1}$, in a fosmidomycin concentration of 10 mM, 20x higher than the highest concentration used in *E. coli*. Error bars represent standard deviation of biological replicates(n=3).

A subsequent study by the same group was published later, identifying the sll1556 gene in *Synechocystis* 6803, an apparent ortholog to the IDI enzyme in *E. coli* as a key player in pentose phosphate incorporation into MEP products[43]. Inactivation of this gene impaired the ability of *Syenchocystis* 6803 to incorporate pentose phosphate intermediates into downstream terpenoid products, indicating that versions of the IDI enzyme in cyanbacteria may have been re-purposed for drawing carbon from the pentose phosphate pathway into terpenoid biosynthesis. This evidence is contrasted by studies engineering IDI enzymes for

optimized IPP/DMAPP ratios in cyanbacteria, showing that IDI maintains it's function as an isomerase between IPP and DMAPP[44][21]. One study on limonene production in *Synechocystis* 6803 showed improved titers upon engineering the pentose phosphate pathway[45], but at a final titer of only 6.7 mg/L, much investigation into this potential alternative entry point into terpenoid biosynthesis is needed.

In the following chapter, I describe synthetic biology tools and metabolic engineering efforts focused on testing the essentiality of *dxr*. If the DXR enzyme is indeed nonessential in cyanobacteria, uncovering the actual architecture of terpenoid production would provide new avenues for pathway engineering and further accelerate the engineering of industrially relevant cyanobacterial strains.

CHAPTER 3

METHOD DEVELOPMENT

Model organisms such as *E. coli* and yeast have very well developed synthetic biology toolboxes, but often the same tools that are effectively wielded in these model organisms are not effective in cyanobacteria [46]. In order to engineer these organisms to convert CO_2 directly to sustainable fuels and feedstocks, more effort must be devoted to developing the tools used to probe cyanobacteria. In this section, I highlight work that functions to increase our understanding of cyanobacterial metabolism while improving and validating the tools designed to manipulate and characterize these photosynthetic microorganisms.

3.1 Arresting Metabolism in *Synechococcus* 7002 Using Partially Frozen Saline Solution

Quenching is a vital step in metabolomics studies, including INST-^{13}C-MFA. In order to study intracellular metabolite pools the metabolism of the organism must be completely halted as quickly as possible to preserve the information in the system at the time of sampling. Rapidly lowering the temperature of a sample of microbial culture is an effective way to accomplish this halt in metabolism, commonly accomplished using cold methanol quenching solution in *E. coli*[47] and yeast[48][49]. While these methods are effective in these model organisms, they are reported to induce extreme metabolite leakage and hinder the overall effectiveness of the quenching procedure in non-model organisms such as *Penicillium chrysogenum*[50]. Cold-shock is another phenomena encountered by microorganisms when subject to extreme temperature changes that also contributed to metabolite leakage and lowered efficiency in the quenching process[51]. Alternative methods of quenching have been explored in both model and non-model organisms.

Alternative quenching solutions have been employed, such as glyerol-saline [52], dry ice-ethanol[53], and many other variations of ethanol solutions. Additionally, fast-filtration

has been employed as a replacement to the centrifugation steps following quenching[54]. These alternative methods all fail to significantly reduce metabolite leakage[55]. Saline quenching solutions provide a much less harsh alternative, but at the cost of a significantly higher freezing point. The following data was collected and published in a paper by Sake et al. to compare the quenching efficiency of saline quenching solution, both unfrozen and partially frozen, to other common quenching solutions for arresting cellular metabolism in *Synechococcus* 7002[56].

3.1.1 Partially Frozen Saline Versus Methanol Quenching Solutions

Primarily, methanol has been used as a common quenching solution because of its capacity to remain liquid at very cold temperatures, down to -143.7°C at atmospheric pressure. This is favorable, as it allows quenching to occur at very low temperatures while facilitating the use of small working volumes. However, methanol is both less dense and has a lower heat capacity compared to water, thus making it a less effective heat sink. Therefore when used as a quenching solution, the temperature of the methanol will rise >2x as fast as water when cooling the same volume of cell culture [56]. Furthermore, there is a heat of mixing associated with the additionf of methanol and water, meaning heat is generated when aqueous cell culture solutions are quenched in methanol, further raising the temperature of the mixture. It has been previously shown that higher temperature quenching solutions (such as the combination of 20% methanol with 0.9% normal saline at -4°C) provide similar levels of metabolic inactivation of Lactobacillus plantarum as lower temperature methanol quenching solutions[57]. Along with metabolic inactivation, the higher temperature saline solution limited cell envelope damage in L. plantarum compared to solutions with higher concentrations of methanol. [56]

.

3.1.2 Mathematical Predictions

By accounting for energy transferred due to the heat of mixing generated in a methanol-aqueous mixture and the heat absorbed by ice in partially frozen saline quenching solutions, we estimated the instantaneous temperature of quenching for methanol and saline methods. Values were selected to mirror our experimental conditions. We assume no heat transfer with the surrounding environment over the short time of mixing and use the temperature of the quenching solution as the reference temperature. The heat stored in the 21 mL quenching solution and 14 mL sample to be quenched, along with the change of heat supplied by the heat of mixing in methanol, or consumed in the melting of ice in saline, must equal the heat stored by the final mixture. For methanol as the quenching solution, the energy of the final mixture must be equal to the energy stored in the 21 mL quench solution and 14 mL culture sample, plus the additional heat of mixing for a methanol/water mixture. For chilled saline, the heat of mixing is replaced with the heat absorbed when the frozen portion of the saline quench solution melts. The following equations describe the energy balance for the quenching approaches:

$$m_s C_{p,s} (T_s - T_q) + \Delta H_m = m_{mix} C_{p,mix} (T_f - T_q) \tag{3.1}$$

$$m_s C_{p,s} (T_s - T_q) - \Delta H_{fus} m_{ice} = m_{mix} C_{p,mix} (T_f - T_q) \tag{3.2}$$

Where m_s, $C_{p,s}$, and T_s represent the mass, specific heat, and temperature of the 14 mL cell culture sample, respectively. These same values for the final 35 mL mixture are m_{mix}, $C_{p,mix}$, and T_f. ΔH_m is the heat of mixing of methanol and water, T_q is the quenching solution temperature, ΔH_{fus} is the heat of melting of ice, and m_{ice} is the estimated mass of the saline solution that is frozen prior to quenching.

3.2 includes the heat of mixing (ΔH_m) generated through the addition of 14 mL of water to 21 mL of methanol. Likewise 3.1 includes the heat of melting (ΔH_{fus}) of water

and the heat consumed through the melting of ice as the sample is added to the partially frozen quenching solution. We estimated the instantaneous temperature of mixing (T_f) under various conditions and presented the results in Table 3.1.

Table 3.1 Predicted instantaneous temperatures of quenching

Quenching solution	Quenching solution temperature (°C)	Instantaneous temperature of mixing (°C)
100% Methanol	-70	-10.6
100% Methanol	-40	1.5
100% Methanol	-20	9.6
0% Frozen Normal Saline (9 g/L)	-3	6.9
15% Frozen Normal Saline (9g/L)	-3	0
20% Frozen Normal Saline (9 g/L)	-3	-2.7
50% Frozen Normal Saline (9 g/L)	-3	-17.1

While the energy balances provide reasonable estimations of the instantaneous temperature of mixing, many approximations were made: heat capacity of the cell sample, heat capacity of the final mixture, negligible heat transfer from surroundings, and instantaneous mixing. Factors such as the heat of metabolism and other interactions with the cells were also neglected.

3.1.3 Experimental Verification of Temperature Changes

To verify our mathematical approximations, the instantaneous temperature of mixing was experimentally determined for each case approximated in Table 2. The instantaneous temperature was recorded. In the event that the temperature was initially above 0°C, the time taken for the solution to reach 0°C while immersed in the bath was recorded. A partially frozen quenching solution of normal saline was prepared by pre-chilling in a -20°C freezer and periodically vortexing to produce a slightly frozen, visibly slushy mixture.

Table 3.2 Measured instantaneous temperatures of quenching. Experiments were performed in triplicate. Final values given with error calculated at a 90% confidence interval.

Quenching Solution	Actual Bath Temperature (°C)	Quenching Solution Temperature (°C)	Instantaneous Temperature of Mixing (°C)	Time to 0°C (s)
100% Methanol	-77	-74	-5.1 ± 1.6	N/A
100% Methanol	-50	-48	2.4 ± 2.5	16 ± 8
100% Methanol	-17	-17	9.6 ± 1.5	66 ± 18
Partially Frozen Normal Saline (9 g/L)	-4	-0.6	2.4 ± 1.1	243 ± 35
0% Frozen Normal Saline (9 g/L)	-4	-0.6	4.8 ± 0.5	>300

Methanol chilled in a dry ice/ethanol bath (-74°C) was the only quenching method tested that reduced the temperature of the solution below 0°C immediately. Despite the temperature of the quenching solution chilled in the dry ice/acetonitrile bath (-48°C) being significantly colder than the partially frozen normal saline solution (-0.6°C), we found instantaneous temperatures of mixing to be similar. The heat consumed by melting the partially frozen saline solution overcame a nearly 50°C temperature difference in the two quenching solutions. However, the colder surrounding bath temperature greatly reduced the time needed for the mixed methanol solution to reach 0°C.

Due to the heat generated when mixing the aqueous culture sample with 100% methanol, cell samples were not immediately brought below 0°C by addition to methanol at -20°C. A saline quenching solution that is partially frozen by 15% is theoretically sufficient to instantaneously reduce the temperature of the solution below 0°C (Table 2), and the partially frozen quenching solution we produced in this experiment reduced the temperature of the mixture to below 4°C. From results in Table 3 and predictions in Table 2, our visibly slushy saline solution was likely only 10% frozen. While we did not explore the option for this analysis, it is certainly plausible that a secondary cold bath at a lower temperature than the quenching solution could be used to reduce the time needed to bring

the cell mixture to 0°C or lower, with caution taken not to freeze the quenched sample. One such example is given in Abernathy et al. using liquid nitrogen to sustain the cold temperature immediately after quenching[58].

3.2 Metabolic Engineering in Cyanobacteria

The main purpose of metabolic engineering in microorganisms is to develop strains better suited to the industrial production of chemicals, like ethanol by yeast, or penicillin by *Penicillium chrysogenum*. To engineer metabolism and redirect fluxes toward desired products, synthetic biology tools are applied to cells to alter gene expression, knock-in new proteins, knock-out competing pathways, etc. In cyanobacteria, many synthetic biology tools have already been developed to elucidate the mechanisms of photosynthesis and carbon metabolism. This information helps us to better understand how to engineer these microorganisms for the sustainable production of chemicals from atmospheric CO_2 and sunlight. In this section I provide context for achievements made in the field and detail the methods I have developed and validated to accelerate the production of industrially relevant cyanobacterial production strains.

3.2.1 Synthetic Biology Toolkit in Cyanobacteria

The ultimate goal of synthetic biology is to create fully interchangeable parts that perform as expected across a variety of organisms, much like what Henry Ford did for car manufacturing. While still underdeveloped compared to model organisms like *E. coli* and yeast, much progress has been made in recent years to provide the field with enhanced tools for genomic and metabolic manipulation in cyanobacteria. A confounding issue is that cyanobacterial strains are quite divergent, so some tools that work well in some strains of cyanobacteria may be completely ineffective in others. This has slowed the pace of development of tools in these photosynthetic organisms, as tools and techniques need to be validated in a strain before we can have confidence in their performance.

One major advance in the synthetic toolbox is the development of the CyanoGate kit (Kit 1000000146)[59]. In the study of Vasudevan et al. a large compilation of tools were consolidated from the literature and validated in the cyanobacterial strains *Synechococcus* 7002, *Synechocystis* sp. PCC 6803 (hereafter *Syenchocystis* 6803), *Synechococcus elongatus* PCC 7942 (herafter *Synechococcus elongatus* 7942), and a fast growing relative of *Synechococcus elongatus* 7942 named *Synechococcus elongatus* UTEX 2973 (herafter UTEX 2973). These tools include replicating and integrative vectors, promoters, neutral site target sequences, terminators, and many more. All tools were designed to be compatible with the modular cloning (MoClo) system, using golden gate cloning to ligate together standard and custom parts into more and more complex constructs for insertion into cyanobacteria. The CyanoGate kit uses the pre-established infrastructure of the Moclo Kit (Kit 1000000044)[60][61] designed for modular construction of vectors in plants. All vectors designed in these kits are available from repositories, and represent a streamlined method for designing and executing the construction of vectors for nearly any purpose.

This MoClo system uses golden gate cloning techniques with restriction endonucleases (RE). REs are naturally found in microbes, and provide immunity to foreign deoxyribonucleic acids (DNA) by cleaving at specific, usually palindromic, recognition sites on double stranded DNA that are not present in the host DNA, effectively inactivating all foreign DNA with that specific sequence[62]. Thousands of REs have been discovered, cleaving DNA in various manners to produce blunt ends or DNA overhangs of different sizes. Type II REs are a class that are capable of cleaving DNA outside of the recognition sequence, and thousands have been discovered to date [63]. This allows for tunable overhangs and modular, unidirectional construction of individual DNA sequences. The Type II REs BpiI and BsaI are used in the CyanoGate and MoClo kit to cleave modular parts into linear DNA strands that can be ligated back together using a DNA ligase into a product vector. Figure 3.1 compares the recognition and cleavage sites between BpiI, BsaI, and other commonly used REs, HindIII and BamHI. The application of modular cloning

techniques to cyanobacteria has the potential to rapidly increase our understanding of cyanobacterial metabolism by allowing the field to more efficiently and rapidly create new strains, learn from the new phenotypes, and accelerate the existing design-build-test-learn cycle.

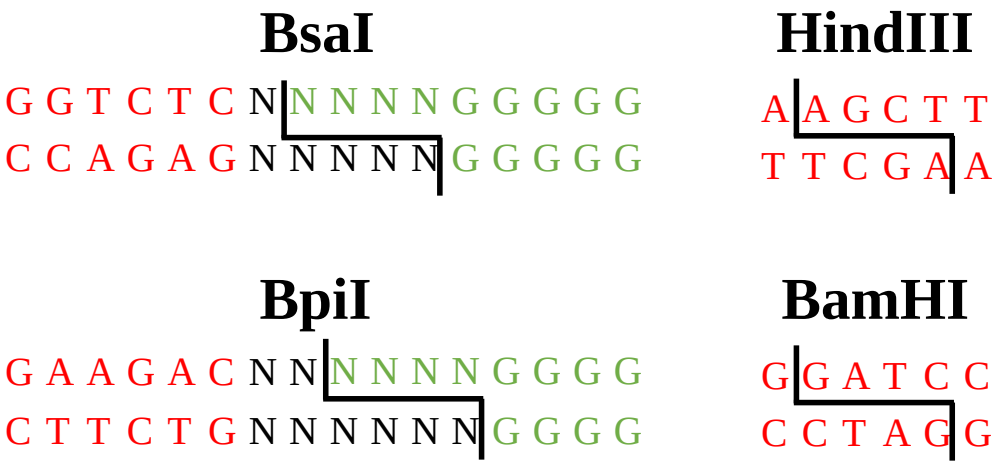

Figure 3.1 Action of restriction endonucleases. BsaI and BpiI are type II REs that bind to a recognition site (red) that is removed from the cleavage site, depicted by black lines. This allows the resulting four base pair overhangs to be tunable, with any combination of the four DNA basepairs possible. An example four basepair overhang of a modular part of all G nucleotides created by the action of BsaI or BpiI is shown as green. By contrast, the overhangs resulting from HindIII and BamHI are fixed because the recognition site and cleavage site overlap. N represents a basepair that could be any of the four nucleotides.

Many other notable achievements have been made in the field to compliment the vast amount of data collected to create the CyanoGate kit. One such achievement is the development of Ribosome Binding Site (RBS) libraries in *Synechococcus* 7002 for finer control of expression[64]. Another is harnessing small regulatory RNA (sRNA) molecules to control expression in cyanobacterial hosts. In *Synechococcus* 7002, Zess et al. demonstrated the use of sRNA molecules under an inducible promoter for the attenuation of target genes[65]. Similarly, it has been demonstrated that CRISPRi repression of

transcripts can be achieved in *Synechococcus* 7002[66].

CRISPRi application using the dCas9 protein is effective in cyanobacteria for the repression of target genes[59]. With concurrent expression of a small guiding RNA (sgRNA) sequence, the dCas9 protein and sgRNA sequence bind, identifying and binding to sequences on the genome of an organism to block transcription by an RNA polymerase, effectively repressing transcript abundance and gene expression, as shown in Figure 3.2. The dCas9 system requires homology between the sgRNA sequence and a target gene directly following a protospacer adjacent motif (PAM) sequence, NGG for the dCas9 protein [67]. This allows selective binding and repression of a single gene in an entire genome of a cyanobacterial host[68].

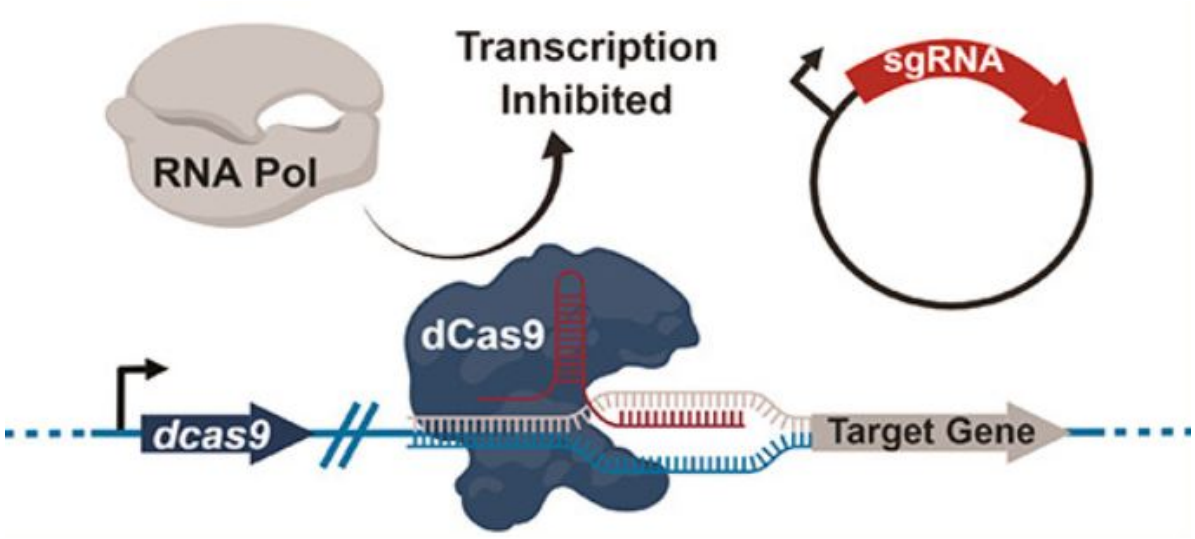

Figure 3.2 Function of the CRISPRi system in vivo. The dCas9 protein (blue), along with an sgRNA strand (red), containing sequence homology to a target gene, identify and reversibly bind to double stranded DNA of a target gene, repressing transcription of the gene by RNA polymerases. Copyright permission in Figure C.3.

Using the CyanoGate toolbox, I designed, optimized, and executed the necessary techniques in our lab for DNA manipulation and vector construction. These techniques, along with rational engineering strategies resulted in new phenotypes by designing final plasmids for gene overexpressions, gene knockouts, and inducible expression and inducible

transcript repression using the CRISPR/dCas9 system. All of these were applied to develop methods for gleaning useful information about the complex metabolism of these microorganisms.

3.2.2 Vector Construction and Transformations in *E. coli*

Golden gate cloning techniques were used to construct vectors in cell free restriction-ligation reactions, and transformed into the *E. coli* DH5α strain, engineered for cloning appications. The CyanoGate and MoClo modular cloning kits were used in conjunction with custom made parts and standard *E. coli* cloning procedures. Experimental procedures used for the design, cloning, purification, and transformation of DNA vectors referred to in this section can be found in Appendix A, along with *E. coli* growth conditions.

I used restriction-ligation polymerase chain reaction (PCR) protocols adapted from Gale et al. [69] to cut and ligate level 0 parts together to form level 1 constructs (Figure A.1) using the BsaI type II restriction enzyme. Next, level 1 constructs were assembled together with linker sequences using the BpiI type II restriction enzyme into acceptor vectors compatible with cyanobacteria (Figure A.1). I use a one pot restriction-ligation system that is made possible by the Type II restriction enzymes. Figure 3.3 describes how two modular parts can be joined together in a single PCR reaction in the presence of the appropriate restriction enzyme, in this case BsaI, and a DNA ligase. The ligation of parts in this fashion is referred to as seamless cloning, because the product vector no longer contains the restriction sites used to prepare the modular parts for ligation.

All acceptor vectors used in this modular construction workflow were compatible with blue-white screening as described in Gale et al.[69], a method for screening *E. coli* colonies for the desired product vector among population of transformants. After each restriction-ligation reaction, the PCR product was electroporated into *E. coli* DH5α and plated on LB plates with 5-Bromo-4-Chloro-3-Indolyl -D-Galactopyranoside (X-gal) for selection of positive transformants. LB plates were made with a range of antibiotic

concentrations. The full protocols for plating and selection procedures are detailed in Figure A.2.

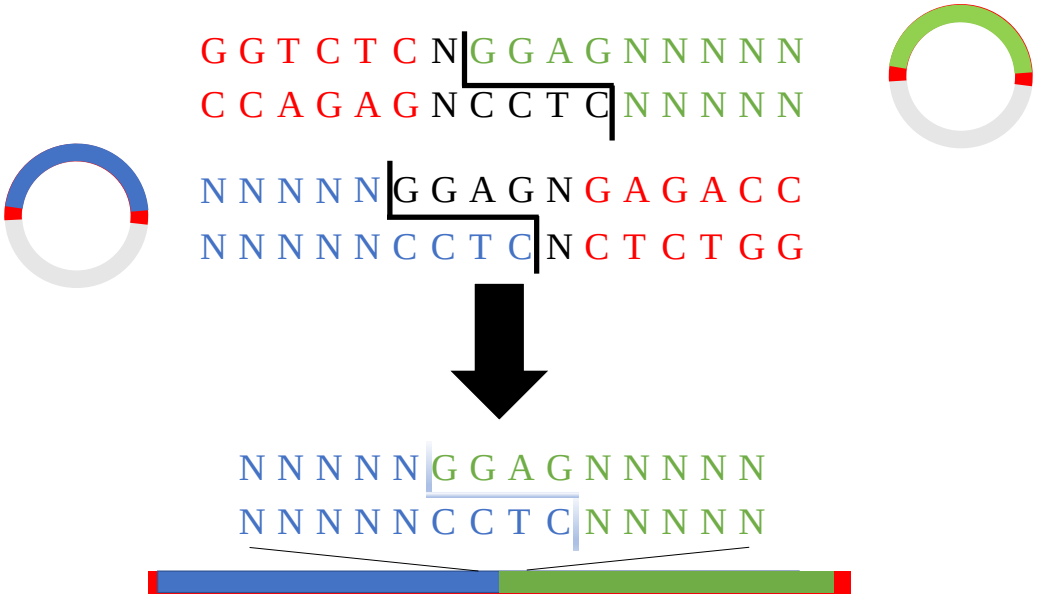

Figure 3.3 Restriction-Ligation reaction unidirectionally ligating two parts (blue and green) seamlessly, while destroying the BsaI recognition site (red), permanently conjoining the two strands of DNA because of their matching sticky ends. The restriction sites on either end of the conjoined blue-green DNA strand can now find and ligate to their respective matching sticky ends, creating a new circular product vector.

Prospective positive transformant colonies (white) were picked from agar plates after a 12-16 hour incubation, and grown in liquid media with the appropriate antibiotic concentrations overnight. The plasmids were isolated the next day using the QIAprep Spin Miniprep Kit (Qiagen), following all manufacturers instructions and always using the maximum allowable volume of cell culture for maximum DNA recovery. All plasmids were first confirmed for expected size using restriction reactions to cleave DNA into known sizes, and gel electrophoresis to visualize the DNA and confirm approximate size. Next, plasmids were sent in for sequencing by Eurofins using the appropriate sequencing primers provided in the appendix, Table B.3.

3.2.3 Cyanobacterial Transformations

Cyanobacterial transformation of the resultant level T constructs was achieved by three different techniques throughout the course of these works. The first is electroporation, the application of electrical pulses to create temporary pores in the membrane of a microorganism, allowing plasmids to pass through to the intracellular cytoplasm. Another is conjugation, or tri-parental mating. Some cyanobacteria, such as *Synechocystis 6803* are capable of exchanging DNA with *E. coli* through direct cell to cell contact using complimentary extracellular machinery [70]. The last transformation technique used in these works is natural transformation, the uptake of DNA directly from the extracellular medium.

Bacterial conjugation from *E. coli* DH5α to *Synechocystis* 6803 was achieved for constructs built into the self-replicating pCAT.000 level T acceptor vector. The level T vectors contained the desired expression cassette along with a mobilization gene required for direct DNA exchange between the *E. coli* strain carrying the plasmid and *Synechocystis* 6803. The full conjugation protocol was adapted from Gale et al. [69] and can be found in Figure A.6.

Electroporation of *Synechocystis* 6803 was performed with limited success (Protocol in Figure A.5). Despite low efficiency of electroporation, this method was needed to transform *Synechocystis* 6803 with integrative vectors, as the acceptor vector (pCAT.334) from the CyanoGate kit did not contain the necessary mobilization gene required for conjugation between *E. coli* DH5α and *Synechocystis* 6803. For the self-replicating vectors (those assembled with the pCAT.000 acceptor vector), which did include the mobilization gene necessary for conjugation between species, I adapted the the conjugation protocol to our lab from the protocol described in Gale et al. [69].

Synechococcus 7002 is capable of natural transformation [71], meaning the cell can uptake DNA, linear or circular, directly from the extracellular medium without the need for electroporation or conjugation between another organism. Integrative vectors were

introduced to *Synechococcus* 7002 through natural transformation by the protocol provided in Figure A.4.

3.3 Promoter Characterization

I conducted a promoter characterization study to assess the performance of two promoters provided by the CyanoGate kit, the NirA nitrogen inducible promoter and the J23119 synthetic promoter. The NirA promoter is native to cyanobacteria, where it controls nitrogen metabolism by promoting gene expression in the presence of nitrate(NO_3), and repressing expression in the presence of ammonium(NH_4). For control of the NirA promoter, I grew strains in modified BG-11 media, containing either 17.6 millimolar (mM) NH_4 as the sole nitrogen source, or an equal molar amount of NO_3 as the sole nitrogen source. Qi et al. produced a nitrogen free basal media for BG-11, to which either NH_4 or NO_3 could be supplied separately to either induce or repress the NirA promoter [72]. The wild type strain of *Synechocystis* 6803 exhibited similar growth characteristics overall in the NH_4 and NO_3 containing media, as well as an equally split molar ratio media containing 8.8 mM of each nitrogen source (Figure 3.4). I measured a slightly slower growth rate but slightly higher steady state biomass accumulation for cultures grown in NO_3, as expected in this organism [73].

To test the level of expression control in different nitrogen media I constructed promoter characterization strains in which the NirA promoter was used to promote a codon optimized yellow fluorescent protein (eYFP) gene in one strain, and the J23119_TSS promoter outfitted with the same RBS sequence as the NirA promoter was used to promote eYFP in another strain (Figure 3.5). The eYFP expression can be quantitatively measured by fluorescence assays in a plate reader, emitting fluorescence at a light wave length of 530 nanometers (nm) when excited by light at a wavelength of 515 nm [74]. The constructs were placed in a self-replicating plasmid and transformed into *Synechocystis* 6803 by electroporation. The resulting phenotypes were confirmed by a 96 hour growth curve to show similar growth characteristics to the wild type strain (Figure 3.6).

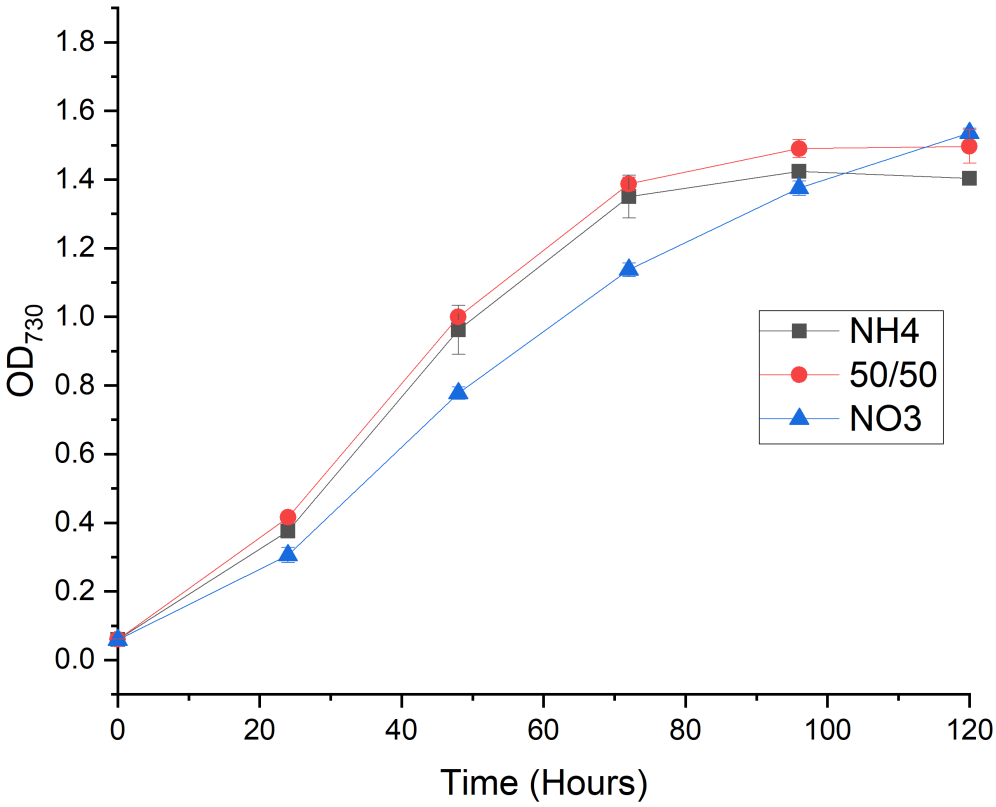

Figure 3.4 Growth of *Synechocystis* 6803 in BG-11 media altered to contain either only NH_4 or only NO_3, as well as an equally split molar ratio of both nitrogen sources. Cultures were grown at 1% CO_2 at the conditions described in. Error bars represent standard deviation of biological replicates(n=3).

The florescence emitted by expression of the eYFP gene of each resulting strain was measured every 24 hours for a four day period. To test the repression of the NirA promoter in the presence of NH_4, this experiment was repeated in triplicate for three media conditions: 17.6 mM NH_4, 17.6 mM NO_3, and an evenly split molar ratio of media with 8.8 mM of both NH_4 and NO_3. The strain expressing eYFP under the NirA promoter shows higher florescence in NO_3 than NH_4, verifying the function of the NirA promoter to differentially express genes of interest when grown in media containing different nitrogen (Figure 3.7). The florescence in the split ratio media was similar to the florescence in NH_4,

showing that the presence of NH_4 in any concentration is the driver for repression and that the promoter is not titrable. I also confirmed that at every timepoint and in every media the J23119 promoter outperformed the NirA promoter in terms of relative florescence units normalized to optical density at 730 nm (Figure 3.7).

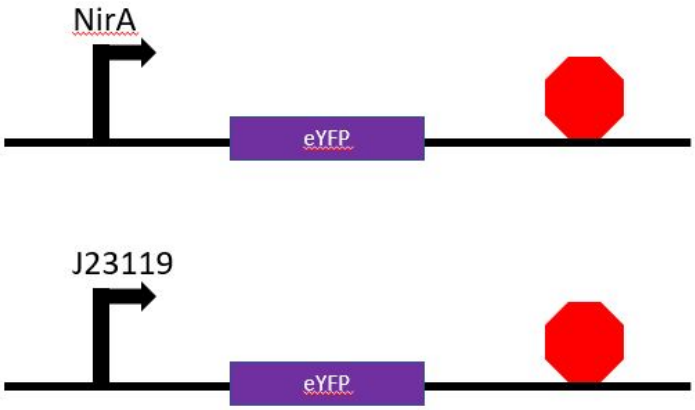

Figure 3.5 Self-replicating plasmid expressing the eYFP gene promoted by either the inducible NirA promoter, or the synthetic J23119 promoter outfitted with the same RBS sequence as nirA.

The characterized NirA promoter was then used to test the essentiality of *dxr* in *Synechocystis* 6803. I used the NirA promoter in conjunction with CRISPRi to develop a method for inducible repression of a target gene, in this case *dxr* from the MEP pathway. If a gene is essential, it will not be possible to knock it out; due to the failure of transformation, is not possible to distinguish if the transformation was bad or the gene was essential, therefore a different approach has to be taken. The gene of interest (*dxr*) has to be expressed on a plasmid, knocked out on the genome and then the plasmid can be cured from the organism. Both approaches to test the essentiality of *dxr* are now described.

The CRISPRi repression system developed is modeled after the system validated in Vasudevan et al.[59] for successful repression of eYFP. The J23119 promoter, truncated to the transcription start site (TSS), is used in Vasudevan et al. to promote small guiding

RNA (sgRNA). In Vasudevan et al., the cpc560 promoter was used to promote the dCas9.

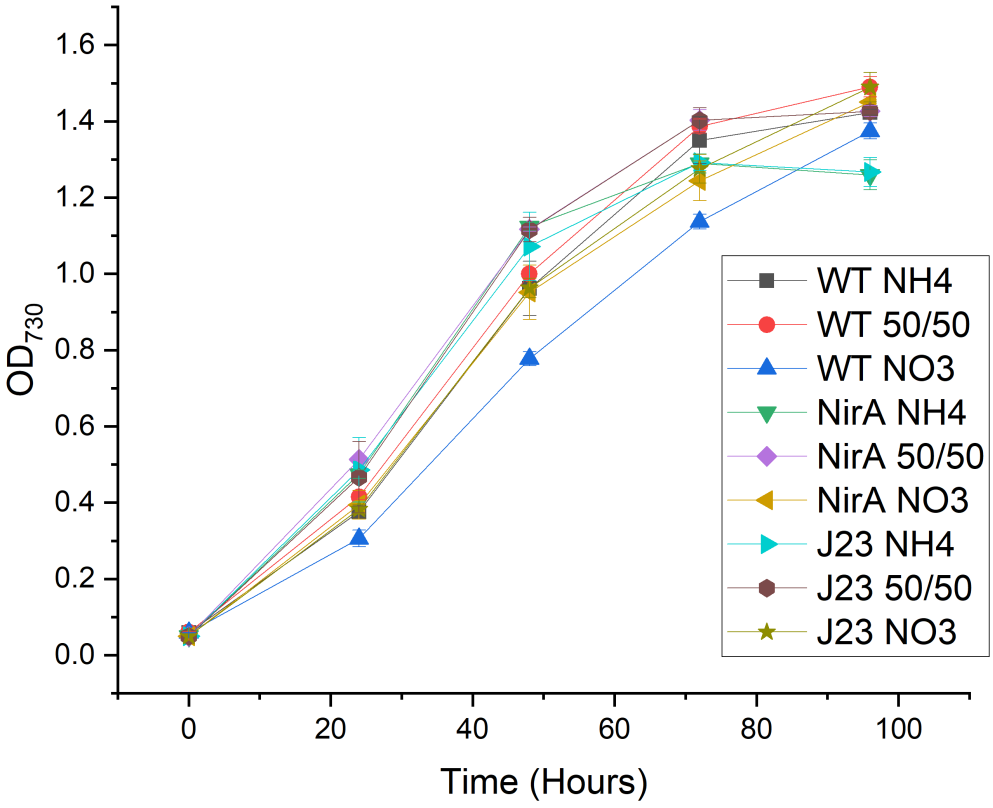

Figure 3.6 Growth of *Synechocystis* 6803 mutant strains expressing the eYFP protein behind either the NirA or J23119 promoter. Both strains in all three nitrogen conditions are graphed with the WT strain for comparison. Cultures were grown at 1% CO_2. Error bars represent standard deviation of biological replicates(n=3).

The system I designed replaced the cpc560 promoter with the NirA promoter to provide inducible expression of dCas9. This requires validation that the J23119 promoter able to supply enough sgRNA in every nitrogen condition when paired with the NirA promoter. I observed higher fluorescence intensity at every time point and in every condition by the J23119 eYFP expression compared to NirA eYFP expression (Figure 3.7). These results confirm that expression by the NirA promoter limits the presence of dCas9 inside the cell, and consequently the action of CRISPRi repression. Additionally, I tested the promoting

strength of each promoter in an environment with both NH_4 and NO_3, to test the NirA promoter for titratable action, or whether the amount of NH_4 available to the cell influences the strength of repression.

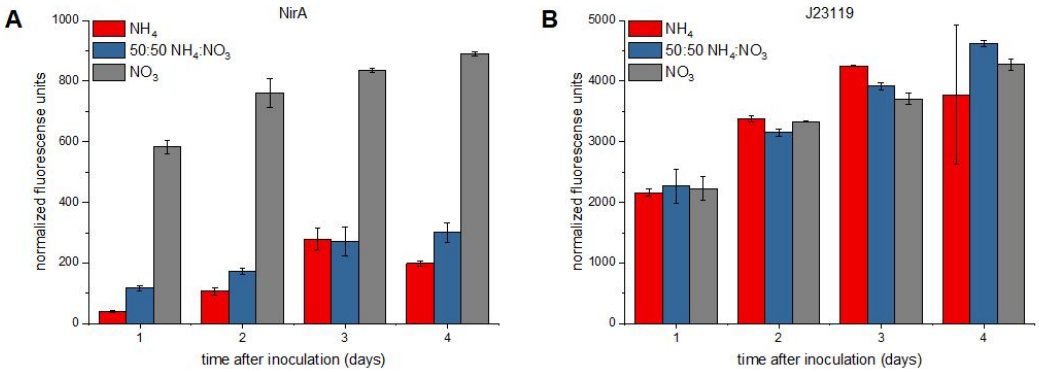

Figure 3.7 Promoter characterization of the inducible NirA and J23119 synthetic promoter in *Synechocystis* 6803. Promoter strength was quantified as a function of fluorescence (normalized to culture optical density at 730 nm) by the eYFP protein under three different nitrogen environments. Only NH_4, only NO_3, and a split molar ratio of the two nitrogen compounds were used to test the inducibility of the NirA promoter, and verify that the J23119 synthetic promoter is unaffected by nitrogen content in the media. Error bars represent standard deviation of biological replicates(n=3) and technical replicates (n=2).

3.4 CRISPRi Repression of *dxr*

I designed an inducible CRISPRi repression system targeting *dxr* for repression only in NO_3 media. The CyanoGate kit provided me with the necessary DNA for dCas9 expression in cyanobacteria, as well as a scaffold for the sgRNA that accompanies the dCas9 protein. I designed the short sgRNA sequence with homology to *dxr* next to the appropriate PAM sequence for dCas9 (NGG). The dCas9 gene is promoted by the NirA inducible promoter, giving the vector 'inducible repression' capabilities. The sgRNA sequence is promoted by the J23119 synthetic promoter, truncated to the transcription start site (TSS). Figure 3.8 details the construct.

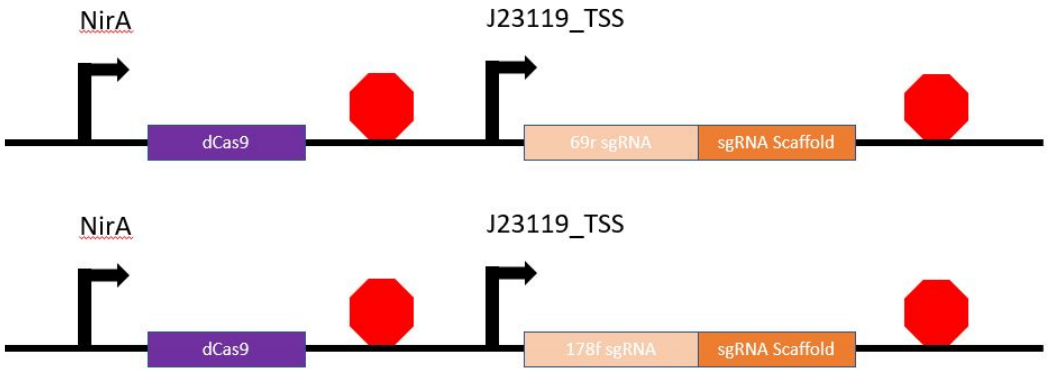

Figure 3.8 Self-replicating plasmid expressing the dCas9 protein and sgRNA sequence specific to *dxr* for transcript repression. The two constructs targeted either the 69th or 178th base pair from the beginning of the open reading frame of *dxr*.

Synechocystis 6803 was transformed with these plasmids via conjugation with a self-replicating plasmid, resulting in two mutant strains, Cr178 and Cr69. The strain targeting *dxr* with homology to the 178th base pair (*Synechocystis* 6803 Cr178) was successfully transformed, while the other strain (*Synechocystis* 6803 Cr69) was not. Preliminary growth curve data shows no significant reduction in growth in the NO_3 media that induces dCas9 expression (Figure 3.9). More experiments are needed to validate the repression of *dxr* transcripts by the CRISPRi system. Once we validate the decreased *dxr* transcript abundance, this system can be used to test the essentiality of other genes as well by repressing transcripts without completely knocking out the enzyme function in the cell system.

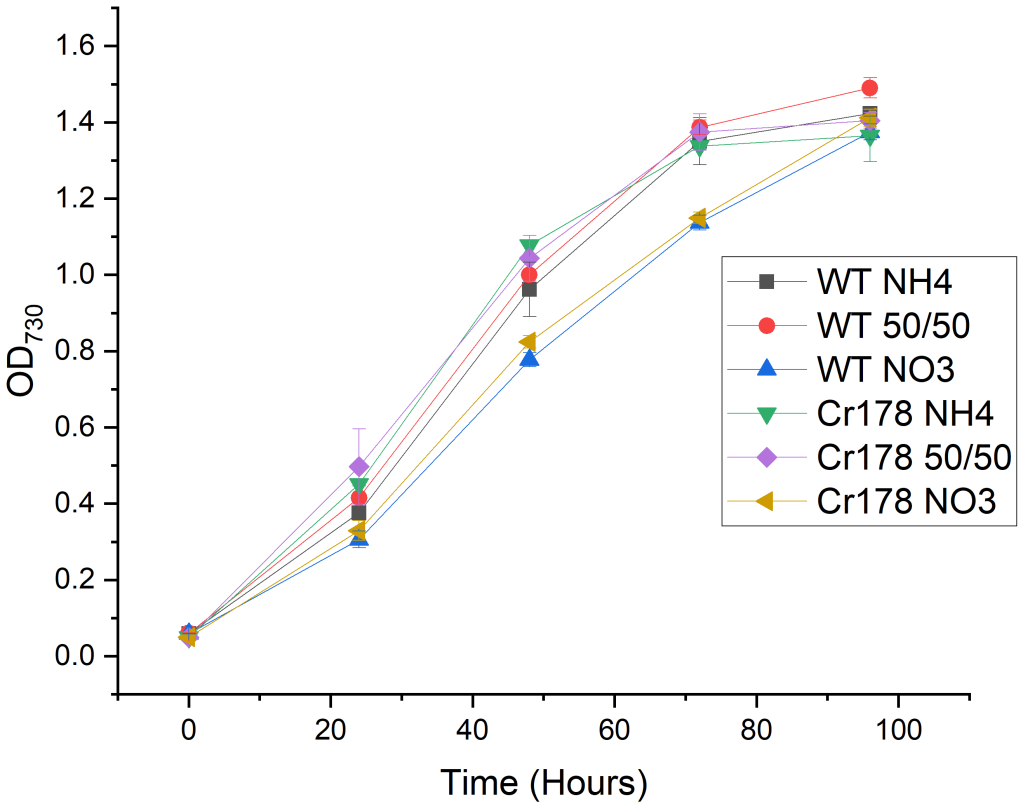

Figure 3.9 Growth of *Synechocystis* 6803 Cr178 strain in different nitrogen conditions, compared to growth of the WT strain. The strain expressing CRISPRi repression of the *dxr* transcript displayed similar growth characteristics compared to the WT strain, even in NO_3 when dCas9 was fully exressed. All cultures were grown at 1% CO_2. Error bars represent standard deviation of biological replicates(n=3).

3.5 Overexpression of Native Genes

3.5.0.1 *dxr* Overexpression and Knockout

Along with the CRISPRi system for *dxr* repression, I designed a separate set of constructs with a knockout cassette and a self-replicating vector with an extra copy of *dxr* on separate plasmids. The self-replicating vector uses the NirA inducible promoter to control expression of the *dxr* open reading frame (ORF), amplified from the genomic DNA of *Synechocystis* 6803 and outfitted with the appropriate restriction sites and four base pair overhangs for integration into the CyanoGate infrastructure. I used the primers listed in the appendix, Table B.3. This inducible extra copy of *dxr* was placed next to the *sacB* sequence provided by CyanoGate, for counterselection of the plasmid after knocking out the genomic copy of *dxr* (Figure 3.10). Including *sacB* in the self-replicating vector required a custom linker sequence (Table B.4), synthesized with the correct four base pair overhangs using overlapping oligonucleotide primers that anneal together (Table B.3).

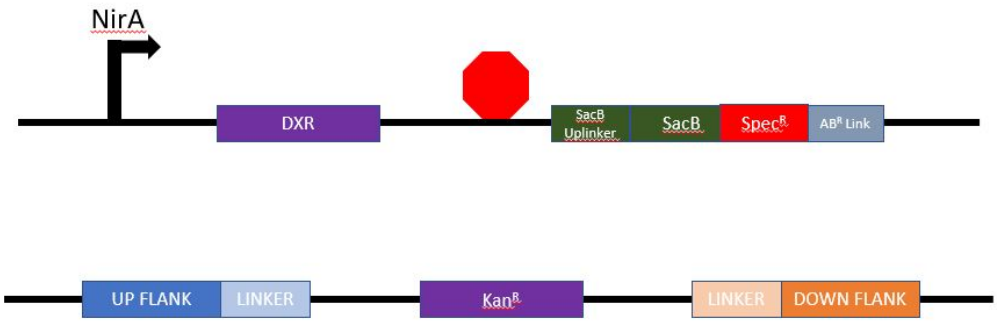

Figure 3.10 Two vector system for the inducible expression of an extra copy of *dxr* on a self-replicating plasmid, followed by a knockout of the genomic copy. A *sacB* counterselection gene was included in the self-replicating vector for counterselection

The self-replicating plasmid has been successfully conjugated into *Syenchocystis* 6803, and the integrative *dxr* knockout cassette has been electroporated in for double homologous recombination. The transformants have been replated weekly for segregation

of the recombinant DNA through all copies of genomic DNA. Colony PCR (Figure A.3) using verification primers listed in Table B.3 is used to visualize the knockout insertion site and verify segregation. To date, complete segregation has not been achieved, and full segregation of the knockout cassette into every copy of the genomic DNA is necessary before the essentiality of *dxr* can be tested.

dxr under the control of the NirA promoter will be used to test the impact of lowering expression of *dxr* on growth. This presents a platform for testing the effect of the *dxr* gene on product formation, such as limonene, in the future. Additionally, I have confirmed in partially segregated mutants that the *sacB* method of counter-selection of a self-replicating plasmid is a feasible route to counterselection of the plasmid.

The strain overexpressing *dxr* in (*Synechocystis* 6803 DXR) under the NirA promoter was characterized by growth curves in all three nitrogen conditions (Figure 3.11). Similar growth characteristics are displayed in relation to the WT strain. When comparing both the Cr178 and overexpression strains to the WT, evidence suggests that the abundance of *dxr* has little to no impact on *Synechocystis* 6803 growth. Alternatively, these results could be due to ineffective repression or overexpression of the enzyme. Measuring transcript abundances in these mutant strains and comparing it to the transcript abundance of *dxr* in the WT strain will shed light on the extent of *dxr* repression and overexpression.

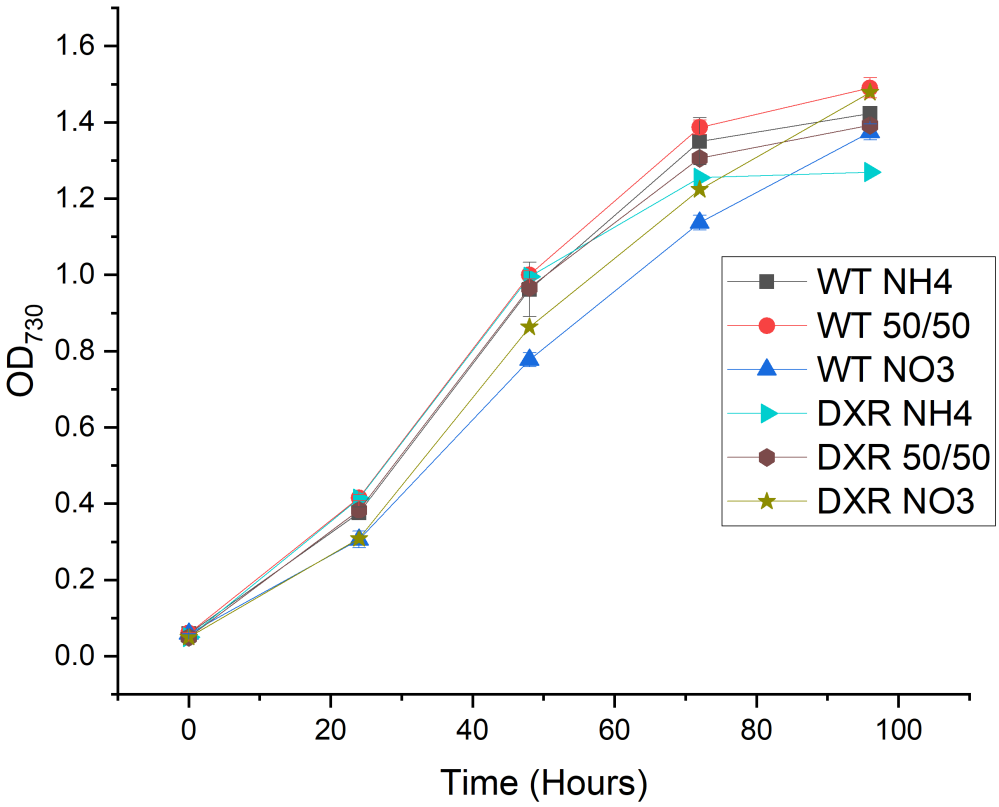

Figure 3.11 Growth of *Synechocystis* 6803 DXR overexpressing strain in different nitrogen conditions, compared to growth of the WT strain. The strain overexpressing *dxr*. All cultures were grown at 1% CO_2. Error bars represent standard deviation of biological replicates(n=3).

3.5.0.2 Overexpression of bifunctional fructose-1,6-biphosphatase/Sedoheptulose-1,7-Bisphosphatase enzyme (SBPase) in *Synechococcus* 7002

The SBPase enzyme in cyanobacteria is responsible for cleaving the phosphate group from SBP and FBP to produce S7P and F6P, respectively. This reaction occurs in the Calvin-Benson-Bassham (CBB) cycle and is responsible for redirecting carbon in the form of DHAP, GAP and E4P back into the CBB cycle for carbon fixation. Overexpression of *fbp1* in photoautotrophic microorganisms has previously been shown to increase

photosynthetic efficiency, growth rate, cell size, and oxygen evolution rate [75][76]. Here, we hypothesize that the overexpression of *fbp1* in limonene producing *Synechococcus* 7002 will result in increased growth and increased limonene titers. These mutant strains will provide evidence as to the feasibility of altering central carbon metabolism in cyanobacteria for the purpose of increased secondary metabolite production. Secondarily, this approach will investigate the potential alternative source of terpenoid precursor molecules, that may originate from the pentose phosphate pathway (PPP) in cyanobacteria, as detailed in the previous section.

I designed integrative constructs with three distinct promoter strengths in order to test the effect of SBPase overexpression on cellular metabolism. The synthetic promoters J23119, J23109, and J23108 were previously characterized in *Syenchococcus* 7002 [64]. In this study, the J23108 promoter was shown to promote at a strength of approximately 10% the strength of the J23119, while the J23109 promoter strength was about 1% of the J23119 promoter. This difference of one order of magnitude was ideal for evaluting the impact on growth. The same synthetic RBS used in Markley et al. [64] to characterize the synthetic promoters was used in the promoters in this study as well, the full sequences ordered for each promoter part, outfitted with the correct restriction sites and four base pair overhangs, can be found in Table B.4.

The CyanoGate kit provided up and down flanking sequences for the Neutral Site 1 (NS1) insertion region (next to the SYNPCC7002_A0159 gene)[71], as well as a kanamycin resistance cassette with the required up- and down-stream linkers. The *fbp1* expression cassette was amplified from the genome of *Synechococcus* 7002 using primers in Table B.3, which provided the sequence with the correct four base pair overhangs and restriction sites for integration into the CyanoGate infrastructure. Figure 3.12 depicts the plasmid structures that were introduced into NS1 by natural transformation and homologous recombination. Note that NS1 as named by Vasudevan et al. [59] in the CyanoGate kit was originally found and validated by Vogel et al.[71]. This NS1, in the A0159 gene

position, should not be confused with the NS1 used in Davies et al.[31], which describes the neutral site between genes A0935 and A0936 as NS1.

Figure 3.12 Overexpression of *fbp1* amplified from 7002 genomic DNA. The same open reading frame was promoted by three different synthetic promoters for expression at different strengths J23119, J23209, and J23108 and inserted into NS1 as named in the CyanoGate kit [59] in the region of the *Synechococcus* 7002 A0159 genomic DNA region.

These three constructs were transformed into the *Synechococcus* 7002 WT strain to produce three distinct mutant strains (*Synechococcus* 7002 SBP_J23119, *Synechococcus* 7002 SBP_J23109, *Synechococcus* 7002 SBP_J23108) each overexpressing *fbp1* at different levels. The transformants were re-plated weekly for segregation of the recombinant DNA through all copies of genomic DNA. Colony PCR (Figure A.3) using verification primers listed in Table B.3 were used to visualize the neutral site and verify segregation. Once NS1 was confirmed by colony PCR and gel electrophoresis to contain only the desired DNA sequence in the NS1 site, the transformants were grown in liquid media for long-term storage by freezer stocks and additional experimentation. Strains were grown in the appropriate antibiotics in liquid media and agar as described in Appendix A.

I found clear phenotypic differences between the three strains (Figure 3.13) when grown at ambient levels of CO_2, evidenced by drastically different coloring of the cultures. None of the strains outgrew the WT strain at ambient CO_2 levels. I hypothesize that high CO_2

levels (5

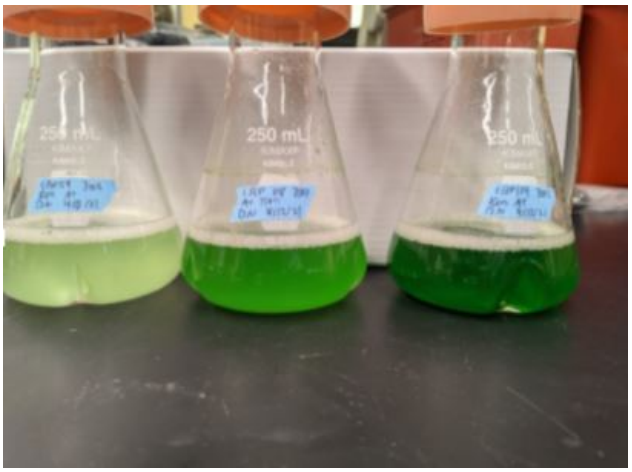

Figure 3.13 Phenotypic differences between the three *fbp1* overexpressing strains. From left to right are cultures of *Synechococcus* 7002 SBPJ23108, *Synechococcus* 7002 SBPJ23109, then *Synechococcus* 7002 SBPJ23119.

The same protocols for transformation and segregation were used to introduce each of the three *fbp1* overexpressing cassettes into *Synechococcus* 7002 LS, but complete segregation has not yet occurred to date. In an effort place further pressure on the LS strains to fully segregate, kanamycin concentrations were steadily increased up to 500μg/mL antibiotic, 10x the effective dosage. Still full segregation was not achieved. This provides evidence of competing pressures in the double mutant strains, with the antibiotic pressure pushing toward full segregation, and an opposite pressure against the expression of *fbp1*. This could be an issue of energy balancing within the cell, as limonene and *fbp1* both require valuable energy to be synthesized and take away from the energy devoted to growth and maintenance in the cell. CRISPR editing techniques may be required to produce double mutants that both over express SBPase and express the LS enzyme. These mutants will be used to test the hypothesis that increasing flux through the CBB cycle can increase titers of terpenoid products such as limonene.

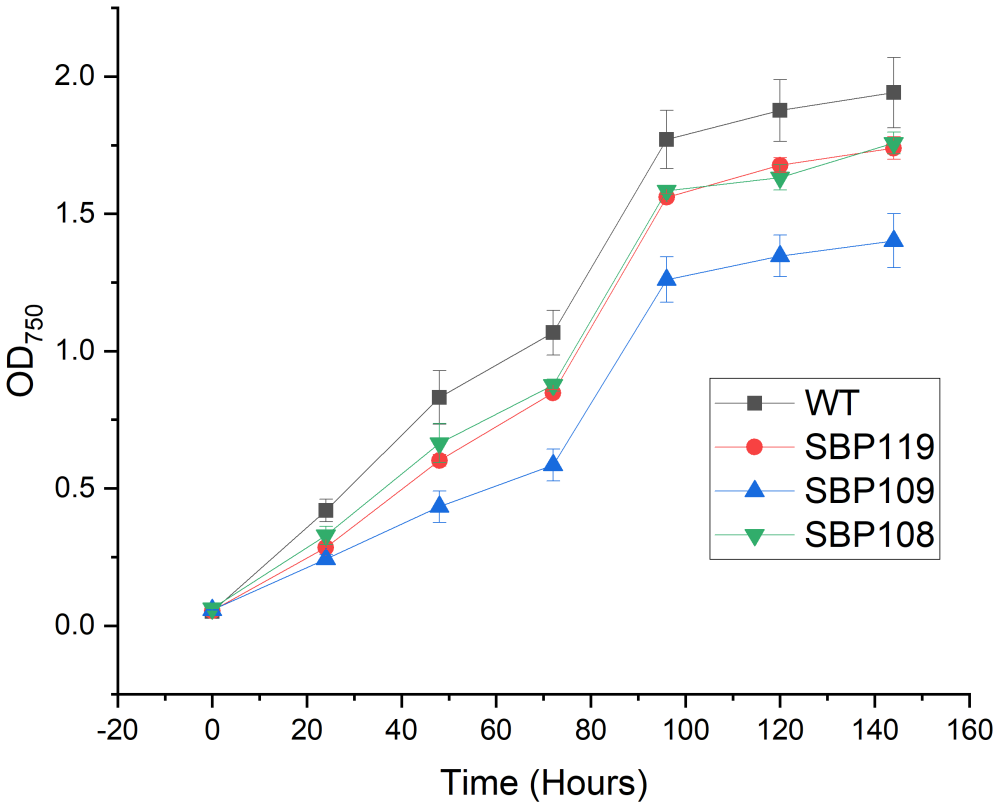

Figure 3.14 Growth of the *Synechococcus* 7002 SBPJ23119, *Synechococcus* 7002 SBPJ23109 and *Synechococcus* 7002 SBPJ23108 strains compared to the WT strain. Lower growth rates and final biomass accumulation are observed in all *fbp1* overexpressing strains. All cultures were grown at 1% CO_2 at the conditions described in Appendix A. Error bars represent standard deviation of biological replicates(n=3).

CHAPTER 4

QUANTIFICATION OF THE CENTRAL METABOLISM OF A LIMONENE PRODUCING *SYNECHOCOCCUS* SP. PCC 7002

In this chapter, I focus on the cyanobacterium *Synechococcus* 7002. Previously, Davies et. al. isolated a limonene producing mutant strain, expressing the *Mentha spicata* limonene synthase (LS) protein that was introduced into the *Synechococcus* 7002 genome by double homologous recombination [31]. This proof-of-concept strain provided evidence that *Synechococcus* 7002 is capable of producing limonene, a molecule of the terpenoid class and a promising biofuel precursor, albeit at the low titer of 4 mg/L over a four day incubation period. This titer must be drastically increased for commercialization of this product from cyanobacteria. I will provide context to cyanobacterial production of molecules such as limonene, describe work done to characterize the central metabolism of the limonene producing *Synechococcus* 7002 strain (hereafter referred to as *Synechococcus* 7002 LS), and provide direction for future experiments to increase limonene titers in cyanobacteria such as *Synechococcus* 7002.

4.1 Background

4.1.1 Isotopically Non-stationary ^{13}C Metabolic Flux Analysis (INST-^{13}CMFA)

INST-^{13}CMFA is a state of the art technique for the determination of intracellular fluxes. This procedure relies on heavy isotopes, or atoms containing extra neutrons in the nucleus that increase the atomic weight of the atom. Heavy isotopes are found in nature at low abundance, such as ^{13}C carbon, ^{18}O oxygen, or ^{15}N nitrogen. Before it was possible to isolate heavy isotopes for use in metabolomics studies, only extracellular fluxes could be directly measured, with information on intracellular metabolites unquantifiable. This technique utilizes experimental, analytical chemistry and computational tools in tandem

solve flux maps for heterorophic, mixotrophic, and autotrophic organisms to better understand the characteristics of their metabolism. The full experimental workflow of INST-^{13}CMFA shown in detail in Figure 4.1.

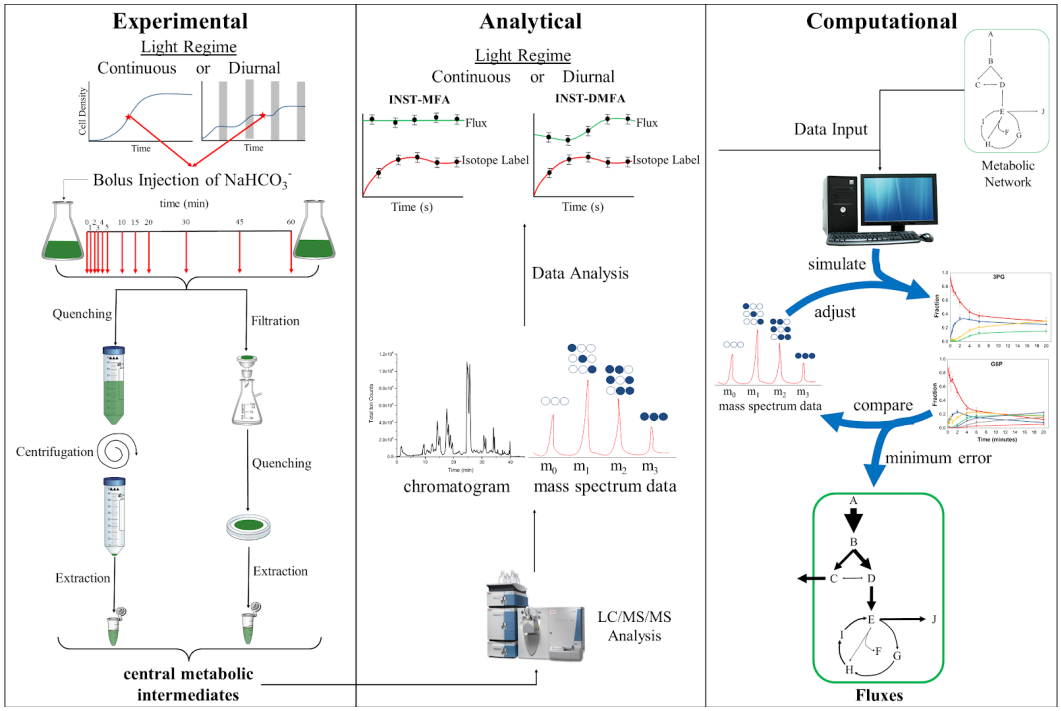

Figure 4.1 Complete workflow for INST-^{13}CMFA in cyanobacteria. Cyanobacterial cultures are injected with a bolus of $H^{13}CO_3^-$ and quenched at different times over a 60 minute experiment. Intracellular metabolites are extracted from the quenched sample and analyzed by LC-MS/MS. Data from LC-MS/MS is supplied to a computational model describing central metabolism and atom transitions between reactions, and used to iteratively solve for the final fluxes through central metabolic pathways. Copyright Permission in Figure C.2[77].

^{13}CMFA begins with the addition of isotopically labeled carbon substrates into a metabolically active culture. Within seconds, cells uptake the heavy carbon containing substrates and incorporate them into intracellular metabolites, just as they do for the most abundant form of carbon in nature (^{12}C). In cyanobacteria, isotopically labeled carbon is supplied in the form of ^{13}C-labeled bicarbonate($H^{13}CO_3^-$), which is readily taken up by cells and fixed in the Calvin-Benson-Bassham (CBB) cycle. This process is different than Metabolic Flux analysis (MFA) developed for heterotrophic organisms such as *E. coli* [78],

yeast [79], and mammalian cells [80]

Heterotrophic cells are fed isotopically labeled cocktails of reduced carbon substrates such as glucose, glutamine or acetate, and analytical chemistry techniques are used to measure the incorporation of carbon labels in downstream metabolites. A reduced carbon cocktail of labeled substrates can be tuned to produce useful results, for example by adding uniformly labeled glucose, unlabeled glucose, and glucose-1-^{13}C, the dynamics of intracellular metabolism can be resolved by analyzing the labeling patterns of downstream metabolite pools (Figure 4.2). Downstream pools are composed of different isotopomers, the same molecular structure with different molecular masses due to varying amounts of heavy carbon labels.

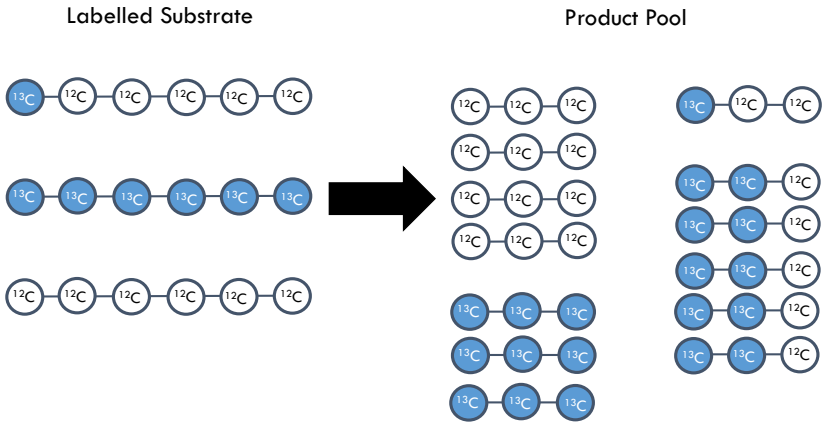

Figure 4.2 Example of metabolite pool labeling of a three carbon intracellular metabolite when fed a cocktail of unlabeled, uniformly labeled, and a 1-^{13}C labeled six carbon substrate.

Cyanobacteria, such as *Synechococcus* 7002 are incapable of growth on reduced carbon as obligate photoautotrophs, so they must incorporate $^{13}CO_2$ into their metabolic pathways. This process does not produce useful final product pool labeling patterns such as those produced by incorporation of reduced carbon substrates like in Figure 4.2. Rather, the final result is a fully labeled product pool, from which no useful information can be

gleaned (Figure 4.3). The non-trivial results in INST-^{13}CMFA lie in the transient labeling patterns prior to complete labeling. This requirement introduces new challenges to traditional MFA procedures, including a quenching step. Quenching is usually accomplished in microorganisms by plunging samples of a culture into a cold quenching solution, such as methanol or saline solution. Sufficiently cold temperatures arrest all metabolic activity in the sample, effectively taking a snapshot of the isotopomer pools from the time of quenching.

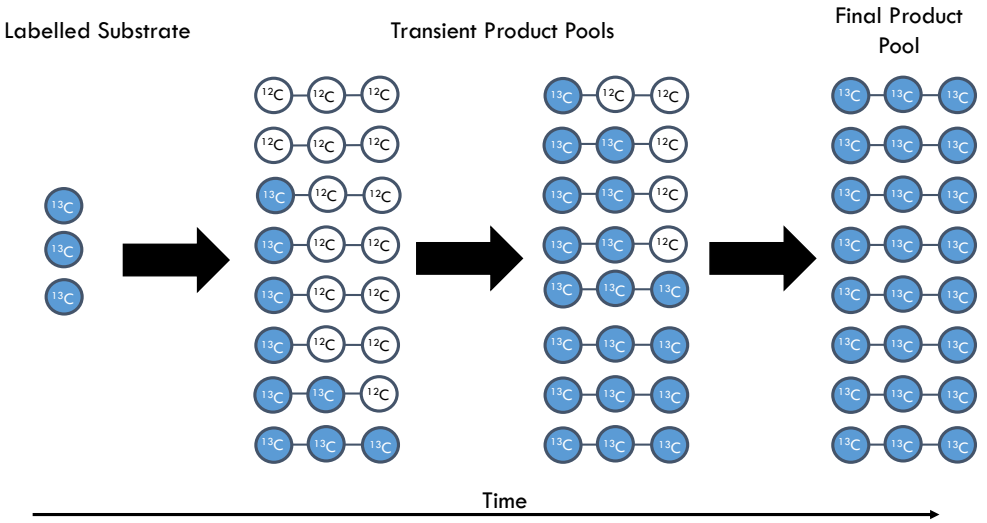

Figure 4.3 Example of transient metabolite pool labeling of a three carbon intracellular metabolite when fed a single carbon ^{13}C labeled substrate.

Labeling patterns of extracted intracellular metabolites are quantified by analytical chemistry techniques such as liquid chromatography with tandem mass spectrometry (LC-MS/MS) or gas chromatrography with mass spectrometry (GC/MS) to precisely determine the ratios of isotopomers in a given metabolite pool. These isotopomer ratios change over time as pools become more enriched with the heavy carbon label. Transient labeling patterns are supplied to computation models as Mass Isotopomer Distributions (MIDs). A MID provides information on transient labeling patterns by consolidating labeling patterns at different time points into a single vector. Figure 4.4 shows the changes

in labeling over a 60 minute experiment for the intracellular metabolites 3PG and fumarate (FUM). Depending on the proximity of a metabolite to the carbon-fixation reaction, and the reactions flowing in to and out of the metabolite pool, the MID can have different characteristics. 3PG is the direct product of the carbon-fixation reaction in cyanobacteria, so labeling occurs fast. In contrast, FUM, a product of the tricarboxylic acid (TCA) shows very little labeling over the course of a 60 minute quenching experiment. The TCA cycle is utilized at low carbon fluxes in cyanobacteria[81], and is reflected by MIDs obtained in these works.

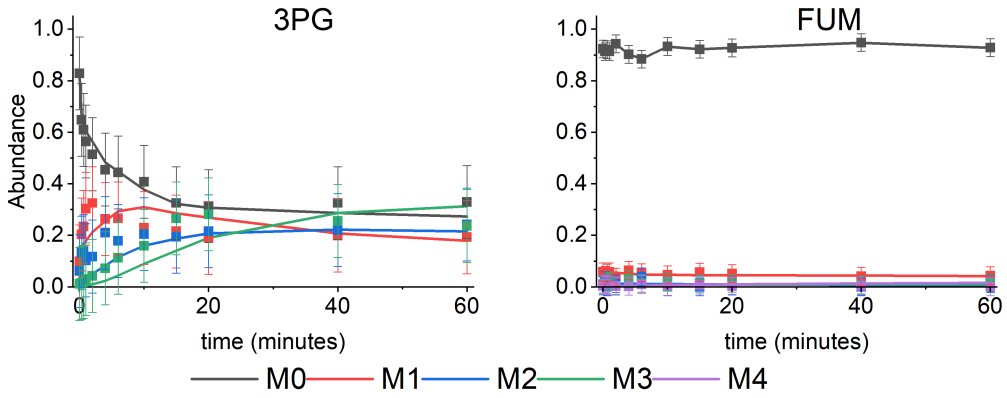

Figure 4.4 MIDs for the intracellular metabolites 3PG and FUM describing the change in labeling over time as cells incorporated more isotopically labeled ^{13}C into metabolite pools. Symbols and error bars represent experimental data standard error (n=3), and lines represent simulation fits. An M0 isotopomer contains zero labeled carbon atoms, with M1 containing one labeled carbon atom, M2 containing two labeled carbon atoms, M3 containing three labeled carbon atoms, and M4 containing four labeled carbon atoms. Since 3PG is only a three carbon molecule, the M4 isotopomer is not measurable and not shown.

Using MIDs from key metabolites we can solve flux maps for obligate photoautotrophs such as *Synechococcus* 7002. Young et al. have developed a computational framework to

solve flux maps in autotrophs with a MATLAB-based tool called INCA[82]. INCA accepts MID vectors for intracellular metabolites, along with a metabolic network describing the reactions taking place in a cell. The metabolic network provides information on atom transitions, or how atoms rearrangements occur when enzymes form new metabolites. INCA iteratively solves the flux map describing metabolic fluxes by comparing computational results to experimental data. The end result of INST-^{13}CMFA is a flux map, a single solution to the network of reactions which describes the fluxes of carbon through individual reactions. Figure 4.5 is an example of a flux map of the CBB cycle, with the weights of arrows from one metabolite to another representing the magnitude of the flux between the metabolites.

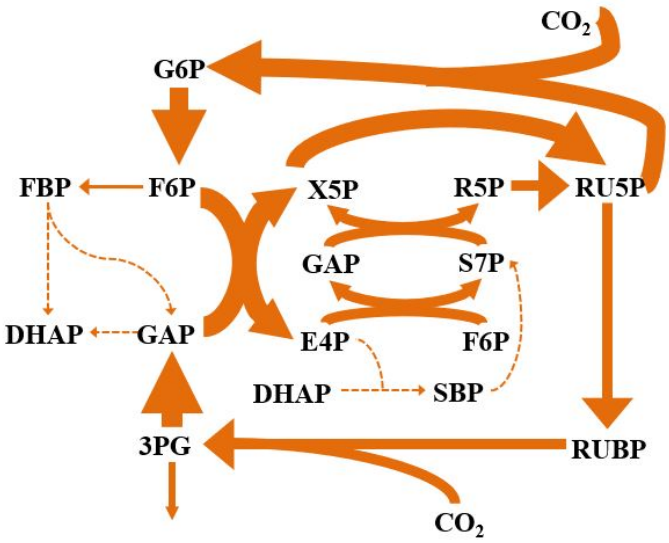

Figure 4.5 Example flux map of the CBB cycle depicting carbon flow through reactions from metabolite to metabolite. The thickness of the arrow indicates the magnitude of the flux through a reaction, and dotted lines indicate no flux.

4.2 Isotopically Non-stationary ^{13}C Metabolic Flux Analysis (INST-^{13}CMFA) on Limonene Producing *Synechococcus* sp. PCC 7002

Darrian M. Newman[5], Cara L. Sake[5], Alex J. Metcalf[5], Fiona K. Davies[6], *Nanette R. Boyle[5]

*Corresponding Author

Manuscript in preparation

4.2.1 Abstract

Synechococcus sp. PCC 7002 is a unicellular cyanobacterium capable of fast growth, even under high light intensity and high salinity. These attributes along with genetic tractability make *Synechococcus* sp. PCC 7002 an attractive candidate for industrial scale production of specialty and commodity chemicals. One such strain, engineered previously by Davies et al. produces limonene, an energy dense diesel jet fuel precursor, at a titer of 4 mg/L over a four day incubation period. In this study, we use the state of the art whole-cell characterization tool, isotopically non-stationary ^{13}C metabolic flux analysis (INST-^{13}CMFA) to determine intracellular fluxes through the pathways of central metabolism for the limonene producing strain and wild type strain of *Synechococcus* sp. PCC 7002. We find similar flux distribution in the Calvin-Benson-Bassham cycle, photorespiration, oxidative pentose phosphate pathway, and reductive tricarboxylic acid cycle. The key difference between strains emerges in the production of pyruvate. The limonene producing strain displays significantly higher flux through the amphibolic pathways of phosphoenolpyruvate carboxylase and the malic enzyme to synthesize pyruvate, while the wild type strain uses pyruvate kinase in a single step. We hypothesize that this adjustment in flux distribution is a product of energy balancing regulatory action. The upregulation of this amphibolic pathway may act to restore the physiological $NADP^+$/NADPH ratio in response to the synthesis of the energy-dense limonene molecule.

[5]Department of Chemical and Biological Engineering, Colorado School of Mines, Golden, CO 80401, USA
[6]Living Ink Technologies, Commerce City, CO 80022, USA

This amphibolic loop is known to cycle NADH to NADPH. These findings provide evidence that energy reactions may play a role in limonene production, and provide new avenues for engineering increased titers of energy dense molecules in cyanobacteria.

4.2.2 Introduction

Amid growing concerns over climate change and increasing anthropogenic carbon emissions, cyanobacteria have emerged as a promising platform for the sustainable production of a wide range of specialty and commodity chemicals. Cyanobacteria utilize the Calvin-Benson-Bassham (CBB) cycle to fix atmospheric carbon dioxide. The CBB cycle accounts for 99% of global primary biomass production and is one of nature's primary tools for carbon recycling[83]. However, natural carbon recycling cannot keep pace with anthropogenic carbon emissions, as a result of global dependence on fossil fuels for energy and petrochemically derived products (rubber, lubricants, plastics, etc.). Cyanobacteria can help alleviate this dependence on fossil fuels through the carbon negative production of structural materials and the carbon neutral production of liquid fuel, recycling atmospheric carbon dioxide and closing the carbon loop.

Cyanobacterial cell factories fix atmospheric carbon dioxide into a variety of valuable chemicals: sugars, alcohols, acids, alkanes, alkenes, ketones, fatty acids, and terpenoids [84]. This variety of end products can be achieved using only the inputs of light, atmospheric carbon dioxide, and trace minerals. The potential efficacy of cyanobacteria as carbon neutral producers of specialty and commodity chemicals is strengthened by their genetic tractability as well as higher photosynthetic efficiency and growth rate when compared to plants [9][10]. *Synechococcus* sp. PCC 7002 (hereafter *Synechococcus* 7002) is an attractive candidate for production of industrially relevant chemicals to displace petrochemicals due to a short doubling time of only 2.6 h when provided reduced nitrogen[85]. *Synechococcus* 7002 can also tolerate high salinity and light intensity[11][12].

Two strains are studied here, the wild type (WT) *Synechococcus* 7002 strain and a limonene producing (LS) strain, engineered by Davies et al.[31]. The *Synechococcus* 7002

LS strain produces 4 mg L-1 L-limonene over a 96 hour growth period [31]. Briefly, L-limonene is synthesized in cyanobacterial cells via the methylerythritol 4-phosphate (MEP) pathway, a linear seven step pathway beginning with the condensation of glyceraldehyde 3-phosphate (GAP) and pyruvate (PYR), and ending with the production of either isopentenyl diphosphate (IPP) or dimethylallyl diphosphate (DMAPP). In cyanobacteria, many attempts have been made to increase flux through the MEP pathway toward valuable end products through the overexpression of bottlenecks[86][33] and by alleviating competition for carbon with sinks such as glycogen[31][87]. *Synechococcus* 7002 LS titers need to be increased to produce economically feasible amounts of limonene.

Allocation of carbon throughout cyanobacterial metabolism must be understood if we are to rationally redirect carbon flux on a whole cell scale toward the MEP pathway and terpenoids, and isotopically nonstationary 13C metabolic flux analysis (INST-13CMFA) has emerged as a valuable tool in cyanobacterial synthetic biology to directly quantify metabolic phenotypes. INST-13CMFA uses isotopically labeled carbon to produce time-dependent mass isotopomer distributions (MIDs) of key metabolites in central metabolism, from which flux values can be estimated for an entire network of reactions. INST-MFA has been utilized in *Synechococcus* 7002 [87][88][89], as well as the model cyanobacterial species *Synechocystis* sp. PCC 6803.

In this study, we use INST-13CMFA to characterize the central metabolism of both the *Synechococcus* 7002 WT and LS strains to glean information about phenotypic differences induced by the production of L-limonene. We find redirection of carbon from the PEP node, with the WT strain sending a higher proportion of flux directly to pyruvate, and the LS strain redirecting flux through the amphibolic reactions of PEPc and the malic enzyme. This redistribution of carbon flux could be evidence of the mutant strain utilizing the reductive TCA cycle for NADPH production to alleviate the stress induced by synthesizing the energy dense limonene molecule. Additionally, the mutant strain could be using the malic enzyme cycle as a less energy intensive route to synthesizing pyruvate from PEP.

4.2.3 Methods

Chemicals supplied by Sigma-Aldrich, unless otherwise noted.

4.2.3.1 Strains and Cultivation Conditions

Synechococcus 7002 cultures were grown in A+ medium [90] supplemented with 8.26 mM Trisma base buffer (pH 8.2) and maintained on 1.5% (w/v) plates. Cultures of the limonene producing strain were supplemented with a final concentration of 50 µg/mL spectinomycin. Liquid cultures were propagated and grown in 250 mL and 500 mL beveled Erlenmeyer flasks with 100 mL and 200 mL of media, respectively. Flasks were shaken at 180 rpm in an INFORS HT Minitron shake plate incubator at ambient CO2 conditions (¡0.1%), and 37 °C. The approximate light intensity was 80 µmol photons m-2 s-1 in continuous illumination by white fluorescent bulbs. Cell growth was monitored using spectrophotometric optical density (OD730).

4.2.3.2 Dynamic Labeling and Quenching Experiment

The labeling experiment was performed on a benchtop flask shaker under 20 µmol photon m-2 s-1 light from white fluorescent lights. The cultures were first grown up to mid-exponential phase (OD730 0.5) at the conditions previously described. Before the addition of label, 15 mL of culture was pipetted out and immediately quenched in 30 mL of partially frozen saline quench solution in a 50 mL conical centrifuge tube, as described in Sake et al.[56]. This sample corresponded to the zero timepoint sample (t=0). Then a 5 mL bolus of 0.8 M 13C sodium bicarbonate (98 atom % 13C, 99% purity, Sigma-Aldrich, USA) was injected into the flask at time t=0. 15 mL Samples were rapidly quenched at 20s, 40s, 1 min, 2min, 4min, 6min, 10min, 15min, 20min, 40min, 60min. The quenched samples were centrifuged in an Eppendorf 5810R swinging bucket centrifuge at 4,000 rpm for 15 minutes at -2°C, and the supernatant was decanted. The pellet was washed in 2 mL in water, transferred to a 2 mL microcentrifuge tube, and centrifuged again at 8,000xg on a tabletop centrifuge at -2°C. The pellet was stored at -20°C for later extraction.

4.2.3.3 Metabolite Extraction

Intracellular metabolites were extracted from the frozen cell pellets using a methanol extraction [56]. Cell pellets were resuspended in 500 µL pure methanol and spiked with ribitol and PIPES internal standards for final concentrations of 150 ppb and 50 ppb, respectively. Samples were frozen in liquid nitrogen, thawed on ice, and vortexed at 0°C for 5 minutes and 1000 rpm. This freeze/thaw/vortex cycle was repeated twice more, and samples were centrifuged at 8000xg for 5 minutes at -9°C in a Sorvall Legend Micro 17R (Thermo Scientific). The supernatant (extract) was collected in a new tube and stored at -20°C. The extraction process was repeated twice more with 500 µL of 50% methanol, each time adding the collected extract to the first portion. All samples were then dried overnight under vacuum at 45°C in a Savant SPD131DDA SpeedVac (Thermo Scientific). Dried extracts were resuspended in 150 µL optima water and filtered with nylon filter tubes (Spin-X, Costar). Filters were rinsed with an additional 50 µL optima water for a total concentrated extract volume of 200 µL. Finally, the samples were filtered through a 3 kilodalton filter (Spin Filter 3K, VWR) and collected for LC-MS/MS analysis.

4.2.3.4 LC/MS-MS Quantitation of Metabolites

Metabolite extracts were analyzed using an LC-MS/MS method adapted from Young et al. [82]. Analysis was performed using a Phenomenex 150 mm x 2 mm Synergi Hydro-RP column connected to an Agilent 1200 Series HPLC system and autosampler in tandem with the AB Sciex 5500 QTrap MS/MS system. LC was performed with an injection volume of 20 µL, using gradient elution of 10 mM tributylamine and 15 mM acetic acid (aqueous phase) with acetonitrile (organic phase) at a constant flow of 0.3 mL/min. The gradient profile of the organic phase is as follows: 0% B (0 min), 8% B (8 min), 16% B (15 min), 30% B (16.5 min), 30% B (19 min), 90% B (21.5 min), 90% B (26.5 min), 0% B (26.6 min), and 0% B (30.5 min). MS analysis was performed in negative ionization mode using a multiple reaction monitoring (MRM) acquisition method. Data acquisition was performed

on the Sciex Analyst 1.7 software. Metabolite pool sizes were quantified using Sciex MultiQuant 3.0.3 software. MSConvert was used to process data files into an open-source format, and isotope labeling profiles were processed using a combination of pyOpenMS and SciPy packages in Python.

4.2.3.5 Isotopically Non-stationary 13C Metabolic Flux Analysis

The flux network and atom transitions for this study was modeled based on previous studies on *Synechococcus* 7002[87][88], including in the network the Calvin-Benson-Bassham(CBB) cycle, photorespiration pathway, oxidative pentose phosphate pathway, tricarboxylic acid (TCA) cycle, and amphibolic reactions. The full metabolic network and atom transitions can be found in Table S. The MEP condensed pathway to limonene was constructed based on gene annotations from the KEGG database. We used the lumped biomass equation constructed Abernathy et al.[88]. from biomass composition analysis. The MATLAB-based INCA toolbox[91] was used to construct the network, and INST-MFA simulations were run to estimate reaction fluxes and metabolite pool sizes by minimizing the difference between simulated and measured Mass Isotopomer Distributions (MIDs) provided to the model, as well as biomass accumulation rates estimated from growth rate (Table S). The parameter continuation method provided by INCA estimated 95% confidence intervals around each estimated parameter. Dilution parameters were set as needed to account for labeling dilutions from metabolically inactive pools[92] (Table S).

4.2.4 Results and Discussion

We constructed the central metabolic network of *Synechococcus* 7002 based on similar studies performed on *Synechococcus* 7002 [87][88][58][93]. Both networks were constrained to the same biomass formation equation, determined by composition analysis from a study conducted by Abernathy et al. on *Synechococcus* 7002 in photoautotrophic conditions [88]. We assumed the biomass formation equation to remain constant between strains, given the

low limonene titers (4 mg/L) found by Davies et al. [31]. We constrained each network to the biomass accumulation rate expected during the time of the experiment (1 hour) (Figure S4). In order to correct for incomplete labeling in some metabolites in the network, dilution pools were used for 3PG, RU5P, PEP, GAP, and DHAP. The active percentage of each pool for both flux maps can be found in Table S2, along with tabulated flux values for every reaction.

The WT flux map was solved by the INCA package in Matlab to an acceptable SSR of 482.1, within the range of 472.8 to 601.0. Likewise, the LS flux map was solved to an acceptable SSR of 538.4 within the range of 435.2 to 558.5. The resulting flux maps were assigned 95% confidence intervals for each individual reaction in the network (Table S2). The general distribution of flux throughout central metabolism concurs with previous INST-MFA studies on *Synechococcus* 7002 and similar cyanobacterial strains [87][88][58][93], with a large proportion of flux directed through the CBB cycle for carbon fixation, and relatively low flux through the TCA cycle. We allowed photorespiration pathway to be active in the model, but the flux was determined to be negligible based on labelling. This is likely due to the high bicarbonate concentration accumulated inside the cells after a bolus of 13C bicarbonate was added at the zero timepoint. Cyanobacteria are able to rapidly transport available bicarbonate into the cell [94], validating both the suppression of photorespiration as well as the establishment of an intracellular dissolved inorganic carbon (DIC) pool dominated by 13C. Both 13C and 12C CO2 pools were made available to the cell for transport in simulations, and we determined that practically all fixed CO2 during the experiment was isotopically labeled (Table S2). Cyanobacteria use a bifurcated TCA cycle [38], typically with low flux through the carbon inefficient reductive branch and more flux supplying oxaloacetate and malate through the oxidative branch, additionally supplemented by fumarate through purine synthesis[95]. As expected, we see low fluxes in Figure 4.6 for the reductive TCA cycle, mainly utilized by both strains for the production of biomass precursors (ie. AKG).

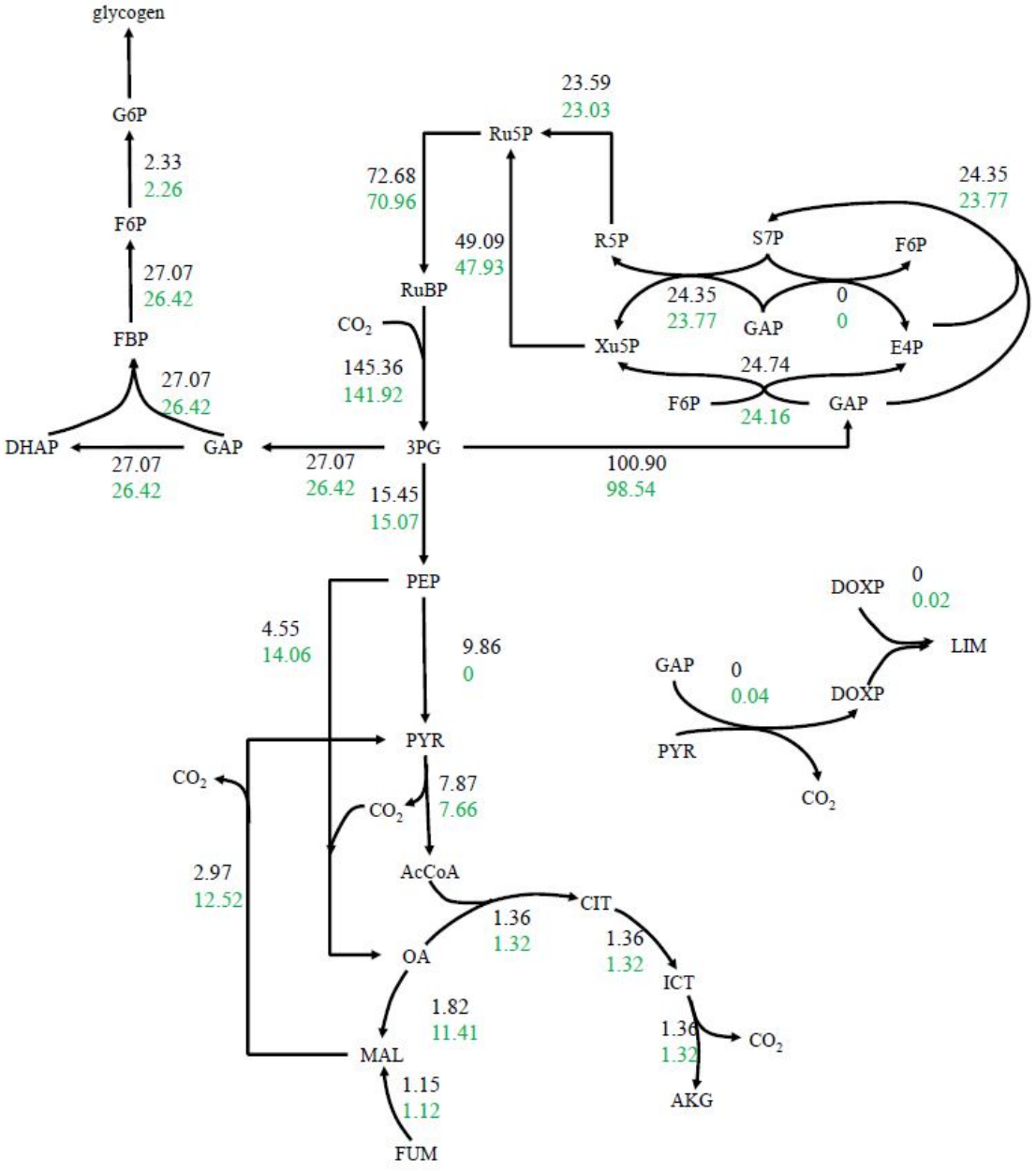

Figure 4.6 *Synechococcus* 7002 WT and LS solved flux maps. Flux values for the WT strain are presented for each reaction in black, with corresponding fluxes for the LS strain in green. The thickness of arrows represents relative flux through the reaction. Both networks use the same biomass accumulation equation, constrained by different biomass accumulation rates as determined by growth rate at the approximate time of the experiment (Figure S2). Dilution pools were applied to 3PG, RU5P, GAP, DHAP and PEP in only the LS strain to account for lower than expected enrichment.

The flux maps reveal significant differences in the oxidative TCA cycle between the WT and LS strains. In the WT strain, PEPc fixes 4.55 umol/gDW/hr CO2 into oxaloacetate, of which only 2.97 umol/gDW/hr is cycled through the malic enzyme, resulting in the production of pyruvate from PEP. The limonene strain fixes 14.06 umol/gDW/hr of CO2 by PEPc activity, ultimately sending higher flux through the malic enzyme as well, 12.52 umol/gDW/hr. This significant difference in flux distribution is the result of differential labeling in measured metabolites, mainly in PEP Figure 4.7, as removing the condensed MEP pathway and specifying the same growth rate in the LS strain as the WT strain does not return PEPc activity to the WT levels in simulations.

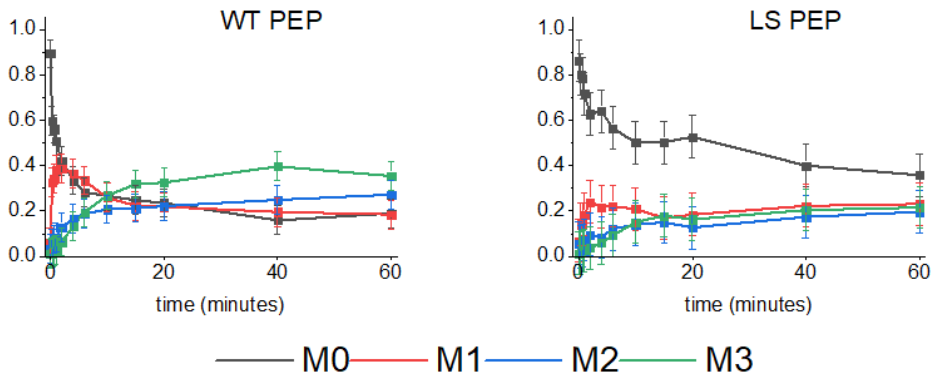

Figure 4.7 Transient labeling patterns for PEP. Significantly lower labeling in the LS PEP mass isotopomer distribution necessitated a dilution pool applied to the PEP pool. Symbols and error bars represent experimental data standard error (n=3), and lines represent simulation fits.

In the WT strain we measured the steady state PEP enrichment to be nearly 60%. In identical experimental conditions, we measured the LS steady state PEP enrichment to be only 42%. This difference necessitated the use of a dilution pool for the LS PEP pool in the INCA model to account for the low labeling, and was needed for the SSR of the solved flux map to fall within the accepted error range.

The differences in labeling patterns (Figure 4.7) along with simulation predictions of increased PEPc activity (Figure 4.6) indicate that metabolite channeling is present in the

amphibolic loop utilized by the LS strain. Evidence of metabolite channeling already exists in bacterial cells[96][97], and more recently INST -13C-MFA has been used to characterize the disruption of subcellular organization and provide evidence of metabolite channeling on metabolite labeling patterns in *Synechococcus* 7002 [88]. In this study we see evidence of metabolite channeling suppressing the enrichment of PEP due to redistribution of flux through the three enzyme amphibolic loop to make pyruvate, as opposed to the single enzyme step of pyruvate kinase utilized by the WT strain.

Limonene is an energy dense molecule, with a molecular formula of C10H16, including two double bonds. Therefore, the cell must spend valuable NADPH to synthesize each limonene, skewing the ratio of NADPH to NADP+ from the WT strains baseline. The malic enzyme reaction is a known route in bacteria and archaea as an NADPH generating reaction[98][99][100]. By upregulating this pathway in response to the limonene energy sink, cells would be able to restore their physiological optimal ratio of NADPH/NADP+. This is accomplished through an energy molecule currency exchange from NADH to NADPH through the reduction and oxidation components of each reaction in the amphibolic loop (Figure 4.8). By redirecting carbon at the PEP node toward OAA through the PEPc enzyme, the limonene strain spends an ATP, rather than producing an ATP with pyruvate kinase. Although forfeiting the production of an ATP, cells gain NADPH in the process. After PEPc fixes a carbon atom to PEP to form OAA, the backward function of the malate dehydrogenase enzyme oxidizes an NADH to NAD^+ with the malate dehydrogenase, before releasing the carbon to form PYR from MAL and reducing $NADP^+$ to NADPH with the malic enzyme.

To synthesize one limonene molecule, the cell must supply approximately 28 NADPH as well as 36 ATP. The increase in flux through the malic enzyme, a difference of 9.55 $\pm$ 1.72 umol/gDW/hr between strains produces an equivalent difference of NADPH, consuming one ATP and one NADH in the process. This production of NADPH is more than enough to account for the production of 0.02 umol/gDW/hr limonene, requiring only 0.56

umol/gDW/hr NADPH to fix the carbon.

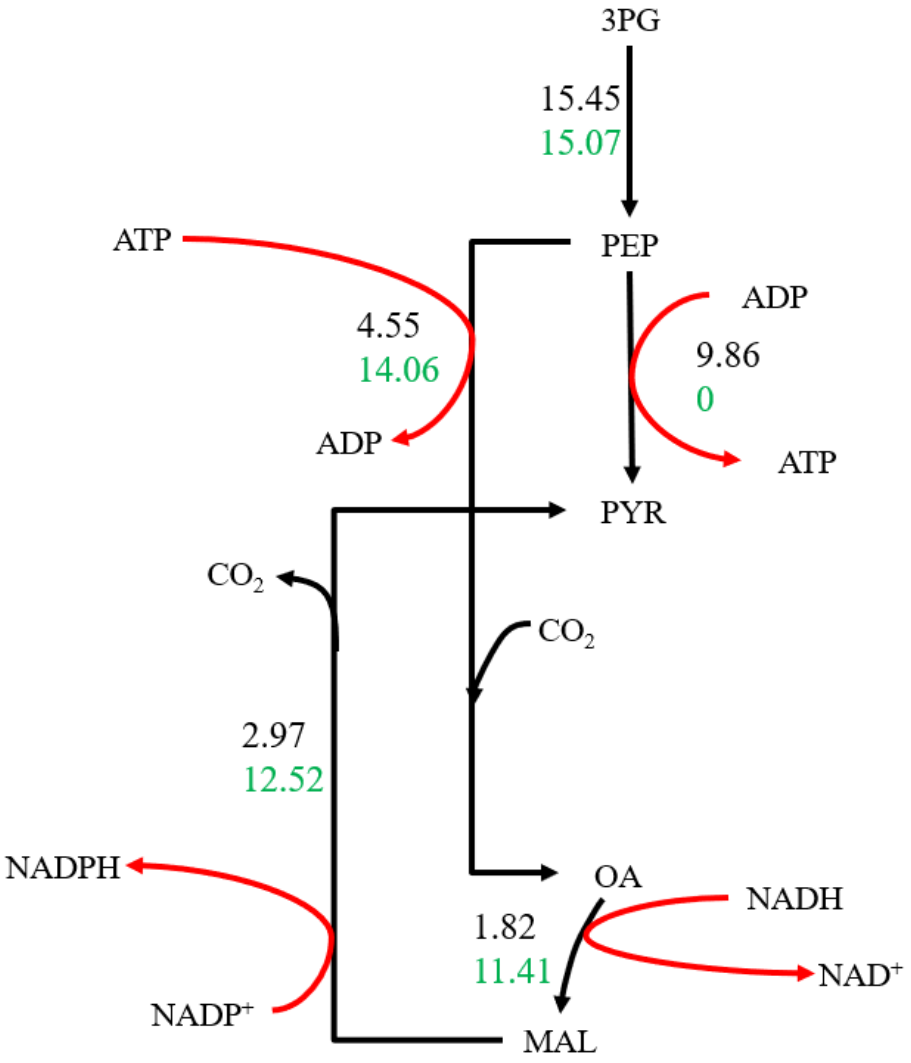

Figure 4.8 Associated energy and reducing power transfer reactions (red) accompanying the two reaction pathways cyanobacteria use to synthesize PYR from PEP. The one step pathway uses pyruvate kinase to synthesize PYR directly from GAP, forming an ATP in the process. The amphibolic reaction uses PEP carboxylase to fix a carbon onto PEP, forming OA at the expense of one ATP. OA is then reduced to MAL, oxidizing NADH to NAD^+ in the process. In a final step the malic enzyme decarboxylates MAL into PYR, reducing an $NADP^+$ to NADPH.

4.2.5 Conclusions

To characterize the phenotype of a limonene producing strain of *Synechococcus* 7002, INST-13C-MFA was performed on the LS strain, and compared to the results of the WT strain. Results were very similar in the CBB cycle, gluconeogenesis, and the reductive TCA cycle, however flux maps revealed differential flux through the amphibolic reaction, from PEP carboxylase to the malic enzyme. The LS strain redirects carbon flux from PEP to the oxidative TCA cycle rather than directly to pyruvate. This redistribution could be linked to NADPH generation through the malic enzyme, needed to rebalance the NADPH/NADP+ ratio within the cell since valuable NADPH is consumed for the production of limonene. Additionally, we provide further evidence of metabolite channeling in *Synechococcus* 7002, specifically in the amphibolic loop including PEP carboxylase, malate dehydrogenase, and the malic enzyme. This study provides a new avenue for increasing titers of terpenoid products in the amphibolic reactions by proposing NADPH as an important limiting factor in the production of energy dense terpenoid derived molecules. We also highlight the advantages of INST-13C-MFA as an essential analytical tool for characterizing and understanding cyanobacterial phenotypes from a whole-cell perspective.

CHAPTER 5

THE EFFECT OF CHANGING BIOMASS COMPOSITION ON THE OUTCOME OF CONSTRAINT BASED METABOLIC MODELS

Darrian M. Newman, Alex J. Metcalf, Michelle F. Meagher, Nanette R. Boyle

5.1 Abstract

Constraint based metabolic models can be extremely useful in metabolic engineering studies, but care must be taken in their construction in order to produce accurate predictions of both growth and intracellular fluxes. Here, we collected experimentally determined biomass composition data from published metabolic models of 4 different photosynthetic microbes in different growth conditions from different laboratories. From this data, we constructed biomass formation equations corresponding to each composition and then used that as the objective function in the iCRE1355 model of *Chlamydomonas reinhardtii*, finding errors in growth rate of up to 40% compared to the experimentally determined growth rate. Unsurprisingly, the biomass formation equation that most accurately predicts growth rate is data collected for the same species in the same growth condition modeled. The same organism grown in a different laboratory with slightly different growth conditions results in a larger error; when data from a related species are used, the error becomes even larger. Model predictions of biomass yield on light as well as sensitivity to changes in macromolecular composition were highly variable across data sets, further highlighting the importance of accuracy in the biomass formation equation to the predictive capabilities of a given model. Therefore, we argue that extreme care must be taken in assuming biomass compositions from literature instead of measuring them directly. We also provide some guidance on how best to select data when it is not possible to perform experiments for composition analysis.

5.2 Introduction

The most common usage of the term biomass refers to plant matter that can be processed to yield fuels such as the industrial production of ethanol corn grains and corn stover. However, the practice of producing valuable, biologically based specialty and commodity chemicals extends far beyond the fermentation of plant biomass. Advances in biotechnology and genetic engineering have allowed us to direct engineering efforts inside the cell. We are now able to optimize biological systems for the production of biomass and/or diverse specialty and commodity chemicals by manipulating complex metabolic networks to reroute carbon. The availability of metabolic models has streamlined editing these complex networks because thousands of simulations changing environmental conditions or genetic background can be completed in a fraction of the time it would take to perform similar experiments in a lab environment. As with all computational tools, the accuracy of the prediction made by metabolic models relies heavily on the accuracy of the information used to build the model.

A critical aspect of building a metabolic model, especially a constraint based model such as flux balance analysis (FBA), is the development of the biomass formation equation, which defines the sink of metabolites to form biomass. FBA is based on linear programming that simulates the ability of a cell to optimize a specific objective under a set of associated constraints[101]; often times the objective function is to maximize biomass. In this case, the biomass formation equation serves as the reaction subject to optimization. Measuring the biomass composition for the creation of a biomass objective function is a labor-intensive process, and some analysis methods are highly error prone. As such, many published metabolic models develop their biomass equations from literature values on biomass composition. Of the reviewed metabolic models of algae, only models with experimental data are compared (Figure 5.1). The remaining models assume biomass composition data from the literature to partly[102], [103][104][105] or completely[106][107][95][108][109][110][111] construct their biomass formation. The

assumption that biomass composition is generally consistent among the same or similar species can be a dangerous one. As is evident in Figure 5.1, even in the same species grown in different laboratories or different growth conditions the biomass composition can be different. In the absence of suitable literature data for the species under investigation, data from phylogenetically close species is sometimes used to construct the biomass objective function[95][108]. However, phylogenetic closeness does not necessarily correlate to similarities in biomass composition.

In this study, we use a genome scale metabolic model of the green alga *Chlamydomonas reinhardtii*[112] to investigate how changing the biomass composition effects the accuracy of model predictions. We use FBA to predict growth rates with the objective of maximum biomass under several different biomass compositions reported in literature for the same species, a closely related algal species and cyanobacteria. We also use the model to determine the change in uptake fluxes for important nutrients, such as nitrogen and phosphorus when we perturb biomass compositions.

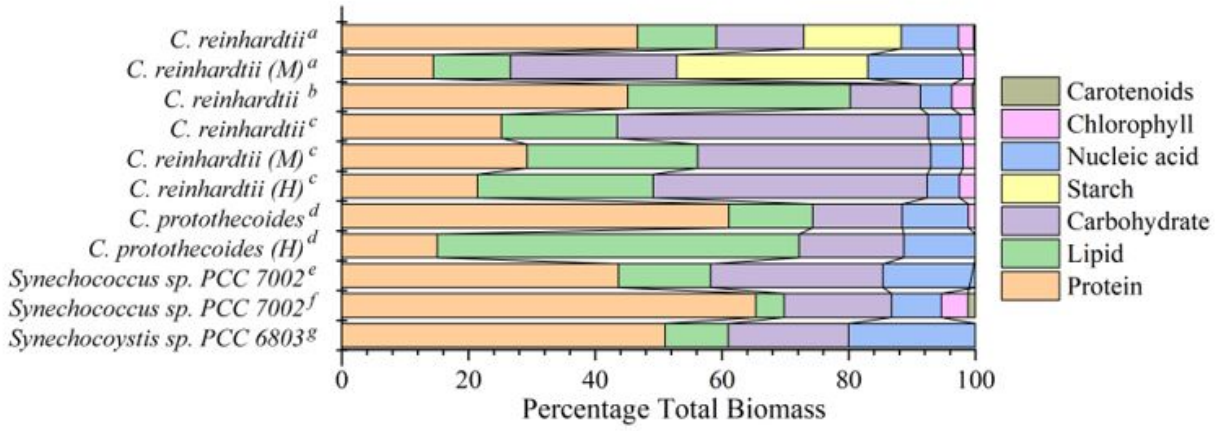

Figure 5.1 Comparison of published, experimentally determined biomass composition for a variety of algae and cyanobacteria species. Even for the same strain, different growth conditions lead to dramatically different biomass compositions. All are for photoautotrophic growth unless noted by (M) or (H) which indicates mixotrophic or heterotrophic growth respectively. Data is sourced from the following: a[112], b[102], c[113], d[101], e[114], f[115], g[116].

5.3 Materials and Methods

5.3.1 Metabolic Model

The iCRE1355 model of *Chlamydomonas reinhardtii*[112] was used for our analysis. For each simulation performed in this study we used the photoautotrophic model constrained by phototrophic conditions reported by Imam et al. and maximum biomass was the objective function. The specific constraints used for the simulations were: 1.7635 mmol gDW^{-1} hr^{-1} dissolved inorganic carbon (DIC) , 0.50 mmol gDW^{-1} hr^{-1} ammonia, and 0.0255 mmol gDW^{-1} hr^{-1} phosphate.

5.3.2 Biomass Formation Equations

The only parameter in the model we changed between simulations were the proportions of macromolecules diverted to biomass through the biomass formation equation. We grouped every molecule identified and included in the original biomass equation by Imam et al. into 7 macromolecule categories: carotenoids, chlorophyll, nucleic acids, starch, carbohydrates, lipids, and proteins. We adjusted the macromolecule groups to match composition fractions taken from the mixotrophic and heterotrophic biomass equations from the same study, as well as composition fractions of biomass equations taken from similar studies of *Chlamydomonas*, *Chlorella*, and the cyanobacterial species *Synechococcus* sp. PCC 7002 (*Synechococcus*) and *Synechocystis* sp. PCC 6803 (*Synechocystis*). Each biomass equation constructed was normalized by total mass flux to the original phototrophic biomass equation using the molecular mass of each component. In cases where data for a macromolecule group was unavailable, we left the original stoichiometry of the metabolite unchanged. The exact stoichiometric coefficients calculated for each of the biomass formation equations can be found in Supplemental Table 1. Negative coefficients indicate that the metabolite is consumed in the reaction, while positive coefficients indicate the production of the metabolite by the reaction.

5.3.3 Biomass Yield on Light Calculations

Biomass yield on light (Ybiomass/photons) was calculated using 5.1 shown below.

$$Y_{biomass/photons} = \frac{X}{E_{max}}(\frac{mmol}{gDWhr}) \tag{5.1}$$

Where X is the growth rate in hr-1 and Emax is the saturation photon flux (mmole gDW^{-1} hr^{-1}). We define the saturation photon flux as the value at which any further increase in photon flux results in no additional biomass being generated; this indicates that growth above this photon value is carbon limited.

5.3.4 Sensitivity Analysis

We determined the sensitivity of carbon dioxide, ammonium and inorganic phosphate in response to changes in macromolecular composition in each simulation. The growth rate was fixed at the experimental value of 0.042 hr-1 and we allowed unlimited exchange of the three substrates. Each of the macromolecule groups were perturbed 20 percent from the original value and the overall composition was renormalized. Then we calculated the percent error between the perturbed flux value and unperturbed flux value. Every sensitivity value in this study is reported as a percent error from the unperturbed flux over a constant perturbation range of 20 percent.

5.4 Results

To determine the effect of using different biomass compositions on the accuracy of model predictions of growth, we used the iCre1355 metabolic model of *Chlamydomonas reinhardtii*[112]. We compared the predicted growth rate of the original model published by Imam et al.[112] to predictions made when the biomass formation equation was swapped with studies of the same organisms in different laboratories and the same organism in different conditions (mixo- and heterotrophic growth). We also compared the effect of assuming biomass composition from a closely related species, *Chlorella protothecoides*, or a

more distant class (Cyanophyceae). The biomass compositions of the studies we considered (see Figure 5.1) covered a wide range of compositions: protein, lipid, and carbohydrate compositions ranged from 14 – 61%, 4 – 53%, and 11 – 51% respectively. Compared to the experimentally determined growth rate of 0.042 h-1, the biomass equation native to iCre1355 predicted growth withing 5% error and therefore was accepted by Imam et al.[112] The model was further validated by accurate predictions of triacylglycerol (TAG) accumulation under nitrogen starvation and maximum theoretical yields of TAGs on both carbon dioxide and light[112]. However, predictive capabilities of the model using alternative objective functions proved highly variable, with an average error in predicted growth rate of 18% across all trials compared to the error accepted by Imam et al. of 6% (see Figure 5.2). The biomass formation equations constructed from three different Chlamydomonas studies[112], [102][113] (shown in Figure 5.1) for autotrophic growth produced an average absolute error of 9.8% compared to 15.4% for all growth conditions (auto-, mixo- and heterotrophic). When the biomass formation equation is assumed to be another alga, Chlorella[101], the error is 12.6% and when assumed to be that of a cyanobacterium[114][115][116], the average absolute error is 24.0%. Similar variability was found for the yield of biomass on light (see Figure 5.2), with photon saturation (Emax) ranging from 24 to 35 mmol gDW^{-1} hr^{-1} to fulfill the energy requirements of the cell.

Next, we evaluated the effect of using different biomass compositions on nutrient requirements. To do this, we fixed the growth rate to 0.042 hr-1 and allowed unlimited uptake of extracellular CO2, ammonium and inorganic phosphate. For each macromolecule, we increased/decreased the respective macromolecule by 10 and 20% while maintaining the relative composition of other biomass. As expected, the response for each macromolecule was linear, so we have chosen to present the data for a 20% increase in the four major macromolecules (Figure 5.3); changes in carotenoid or chlorophyll content have little to no effect on exchange fluxes.

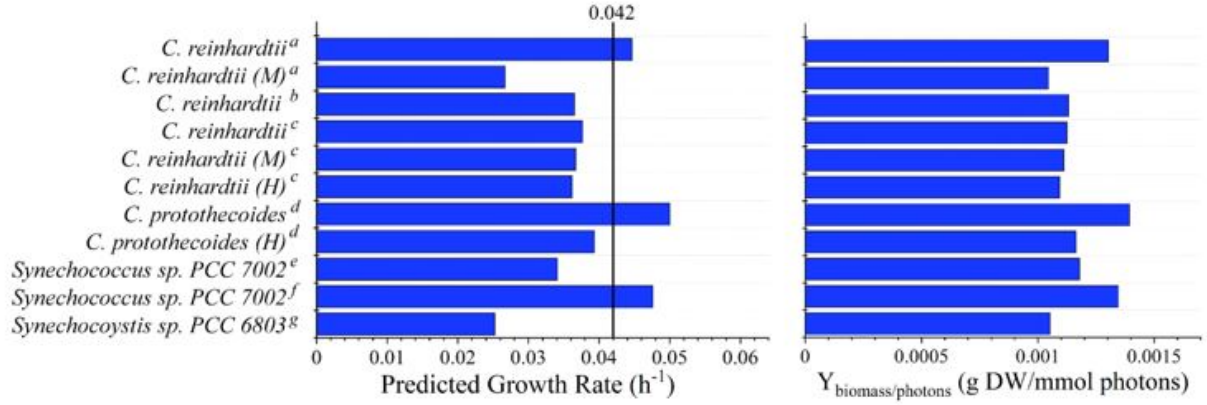

Figure 5.2 Comparison of growth rate and yield predictions for the Imam et al. *Chlamydomonas reinhardtii* genome scale model[112] using several different biomass formation equations. Unless indicated by a (M) for mixotrophic or (H) for heterotrophic, all growth conditions shown are for photoautotrophic growth. Biomass formation equations used in each simulation are obtained from the following: a[112], b[102], c[113], d[101], e[114], f[115], g[116]. The absolute error in predicting growth rate varies widely, even for the same organism in the same growth conditions.

5.5 Discussion

The formulation of an accurate biomass formation equation is an extremely important step in the construction of a constraint based metabolic model, especially when this is used as the objective function. Here, we used the previously published genome scale model of Chlamydomonas rienhardtii[112] to investigate the effect of assuming other published biomass compositions on the accuracy of the model. As a base case, we used the biomass composition that was measured specifically for the model created by Imam et al.[112] and compared both the predicted growth rate and yield on light when other biomass compositions were assumed; we used published biomass compositions for the same organism in the same growth mode (photoautotrophic), the same organism in a different growth mode (mixo- or heterotrophic), another green alga and two different cyanobacteria species (see Figure 5.2). Compared to the 6% error accepted by Imam et al.[112] the error increases approximately 50% to 9.8% by using other measured biomass compositions from Chlamydomonas grown in photoautotrophic conditions in other laboratories[102][101].

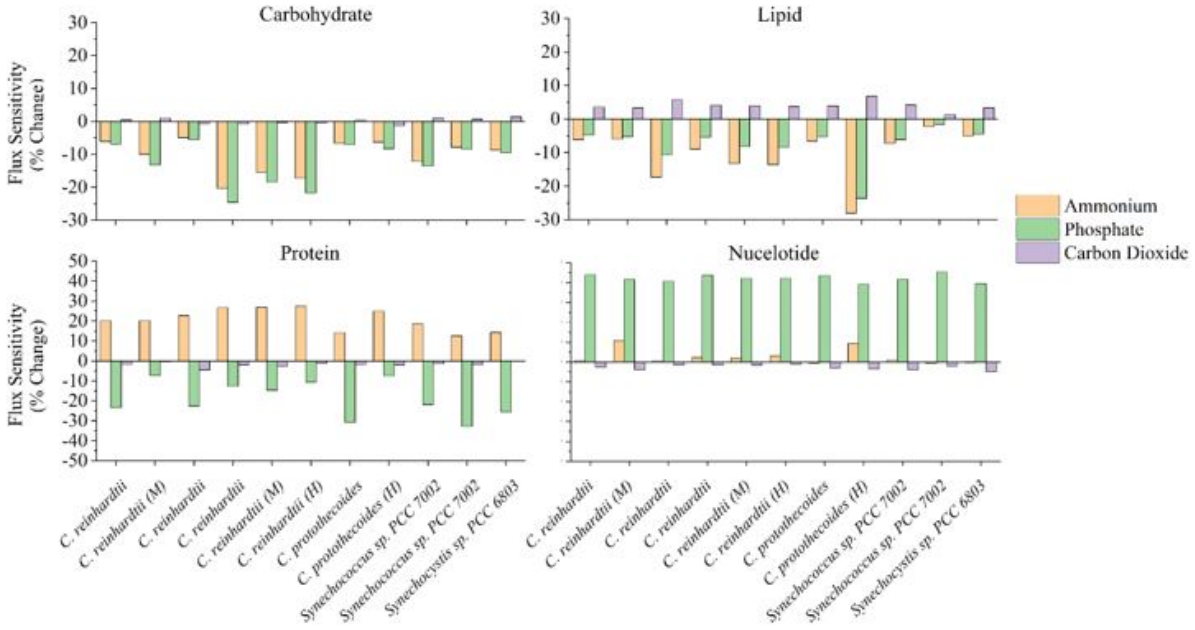

Figure 5.3 Flux sensitivity analysis for changing biomass compositions. The sensitivity of each model to changes in relative contribution of the four major macromolecular groups to the biomass formation equation. Changes in the uptake/excretion rates of three important nutrients, ammonium, phosphate, and carbon dioxide are presented as a percent change of the perturbed value of uptake relative to the unperturbed value of uptake. The changes in uptake are simulated in response to a twenty percent increase in relative contribution of the macromolecule, after renormalizing the biomass equation in each case. Each uptake varied linearly over a 20% perturbation range from 80% to 120% of the original value of uptake.

Comparing the growth conditions between these three studies, the major differences are: growth mode (continuous growth in a photobioreactor[112][102] versus batch growth in flasks[113]), growth medium composition, light intensity, and carbon dioxide availability (ambient conditions[102][113] versus high carbon dioxide environment[112]). The specific growth conditions used in the study conducted by Cogne et al.[102] are described in detail in Pottier et al.[117]. Much larger errors in growth rate, an average of 15.4%, are found when other growth modes are considered, such as mixotrophic growth or heterotrophic growth. If we assume a biomass composition from another green alga, *Chlorella protothecoides*, we have a smaller error than for all growth modes in Chlamydomonas. This is counter intuitive, as we expected that using biomass composition from another organism

would result in larger error; this is likely due to a lack of data because there are not many experimentally measured biomass compositions for algae. Actually, the growth rate predicted by the model using the biomass for photoautotrophic growth of Chlorella has an error of 19.0% and 6.3% for heterotrophic growth; this indicates that the biomass composition of heterotrophic Chlorella is closer to autotrophic Chlamydomonas. As expected, the highest average error, 24.0%, comes from assuming a biomass composition from cyanobacteria. These results indicate that the best option for accurate modeling is to measure the biomass composition of the modeled organism in the same conditions being modeled; if that is not possible, the then next best option would be to assume a published literature value from the same organism in the same growth mode. If the same species isn't possible, then the closest phylogenetically related species is the next best option. The large errors associated with using biomass compositions from different growth conditions or different species can render a model useless, therefore it is important to carefully consider the data used to craft the biomass formation equation and the conditions under which is it used for modeling.

We also investigated how changing biomass compositions effects nutrient needs. To do this, we fixed the growth rate to match the experimentally determined rate and perturbed the biomass composition of each major component (carotenoids, chlorophyll, starch, protein, lipid, carbohydrates, and nucleotides) individually while allowing unlimited uptake of external nutrients (see Figure 5.3). Pigments, such as chlorophyll and carotenoids, are very small components of biomass and have little to no effect on nutrient uptakes rates (data not shown). Of the flux sensitivities shown in Figure 5.3, that for changes in nucleotide composition are relatively stable across all the different biomass composition tested. Changes in composition of carbohydrates, proteins and lipids are more variable across the different compositions tested. Given the atomic composition of these molecules, it is not surprising that a 20% increase in protein results in an increased uptake or ammonium or higher nucleotide content results in increased demand for phosphate. In the

same way, an increased carbohydrate or lipid content results in decreased uptake of ammonium and phosphate. In a similar study, Beck et al.[114] arbitrarily altered the contributions of five macromolecule groups (DNA, RNA, protein, lipid, and poly-saccharide) in a stoichiometric model of Alicyclobacillus acidocaldarius. The ten alternative biomass compositions created produced notable variability in model predictions, including changes in biomass yield on electron acceptor of up to 70%, changes in growth associated maintenance (GAM) of 40%, and changes in biomass yield on nitrogen of 35%. The authors found that the overall capability of the model to predict a range of important characteristics like nitrogen uptake, energy generation reaction fluxes, and growth associated maintenance values are all be hindered by inaccuracies in the biomass formation equation. The non-uniform response of fluxes to changes in biomass across difference compositions indicates how important it is to ensure that the biomass composition used in a constraint based model be as accurate as possible to maximize the utility of the model.

5.6 Conclusions

Constraint based metabolic modeling has proven to be an extremely useful tool for metabolic engineers when designing and testing new strains. Like all computational tools, the models are only as good as the data that is used to create them. Here, our analysis shows the importance of performing detailed biomass composition analysis for each strain and growth condition to be modeled. This is not a trivial task, especially for research groups whose main expertise lies in computational approaches; it requires adapting and optimizing protocols for each new species studied. It is understandable that experimentally determining the biomass composition of every growth condition for each species modeled is not possible. Since extreme care must be taken in assuming biomass composition data from the literature, whether it be the same species under different growth conditions or a separate species with phylogenetic similarity in order to minimize error, we suggest the development of a database of biomass compositions along with metadata. This will not only help researchers choose the most accurate biomass data available, it also would enable

data analysis to identify clear trends in biomass compositions. Another option would be to develop transient, flexible biomass formation equations which would mimic what the cell actually does in nature, optimizing the storage or usage of metabolites based on current conditions. This is computationally much harder but would give models more flexibility for modeling varied growth conditions. Our analysis here indicates that the choice of biomass composition used to formulate the biomass formation equation in constraint based metabolic modeling has a significant influence on the accuracy of predictions. While some models do use experimentally determined biomass compositions for their given growth conditions, others assume literature values. We argue here that more care needs to be taken when doing this in order to have more robust and predictive models.

5.7 Conflicts of Interest

None declared

CHAPTER 6
CONCLUSION

Cyanobacteria have the potential to play a large role in sustainable energy and chemical production. We can use cyanobacteria to simultaneously produce valuable chemicals and lower atmospheric carbon dioxide levels, reversing the damage caused by anthropogenic climate change. The reason these strategies have not already been employed already is due to economic feasibility. The titers of chemicals produced by cyanobacterial strains are altogether too low to compete with existing feedstocks of chemicals, especially petrochemically derived feedstocks. In this thesis I contribute to accelerating the design-build-test-learn cycle in photosynthetic microorganisms to accelerate the production of high-titer, industrially relevant strains. Using metabolic engineering I construct new strains with new phenotypes to test hypotheses regarding the function of the MEP pathway, and use analytical chemistry and computational biology techniques to characterize existing phenotypes to gain a deeper understanding of the mechanisms behind cyanobacterial metabolism.

The rate of production of new tools for both altering and analyzing cyanobacterial metabolism is promising, with large milestones crossed in just the last few decades. Tools like the CRISPRi transcript repression validated in this thesis will play integral roles in deepening our understanding of pathway relationships and gene essentiality, providing new avenues for research and development in these microorganisms. When combined with analytical chemistry techniques such as INST-13CMFA, the far-reaching consequences of metabolic perturbations can be captured and studied from a whole-cell perspective. In this thesis I demonstrate the combined use of metabolic engineering and characterization using analytical chemistry coupled with computational biology on the limonene producing strain, Synechococcus 7002.

INST-13CMFA revealed significant flux redistribution in central metabolism in the limonene producing strain. With the addition of the limonene synthase gene, acting far downstream in the MEP pathway, significant changes in intracellular flux were estimated for the phosphoenolpyruvate carboxylase and malic enzymes. Whether this change in flux is a consequence of precursor availability or energy balancing in the cell, it provides the field with new targets to increase the production of terpenoid products from the MEP pathway.

6.1 Future Works

Elucidating the mechanisms behind low MEP pathway flux should be of utmost importance in the field of cyanobacterial metabolic engineering. Inconsistency in the literature highlights our lack of understanding of the MEP pathway, both in function and in regulation. Are native regulatory elements responsible for low fluxes? Is the architecture of the MEP pathway in cyanobacteria truly the same as in E. coli and other heterotrophic microorganisms? Resources must be devoted to answering these questions in depth before any significant progress can be made toward the production of industrially relevant cyanobacterial strains.

To address this problem, I have designed constructs to probe the MEP pathway and test the essentiality of the DXR gene. By measuring transcript abundance of the DXR gene in CRISPRi strains, and a knockout mutant a selectively inducible DXR gene, the effect of DXR abundance on cell growth and eventually terpenoid production can be tested. reverse transcription quantitative PCR (RT-qPCR) is an important tool to be added to this experimental framework for testing these hypotheses. With information of DXR transcript abundance and phenotypic behavior, the relationship between DXR and growth and product formation can be elucidated.

If the MEP pathway proves non-essential in cyanobacteria, the evidence suggests the pentose phosphate pathway as the supplier of carbon compounds for terpenoid production. The SBPase overexpressing Synechococcus 7002 strains can help direct future research efforts because these mutants increase carbon flux to pentose phosphate pathway

compounds. In combination with RT-qPCR and INST-13CMFA, these mutants will be able to test whether increased flux toward pentose phosphate compounds contribute to higher terpenoid production. One major roadblock to the testing of these hypotheses is the segregation of cyanobacterial mutants. Competing selection pressures in double homologous recombination transformants prevent full segregation of the heterologous sequence into genomic DNA. To resolve this issue, future works should focus on the adaptation of CRISPR systems to cyanobacterial species for more efficient engineering of genomic DNA.

If the field is to collect sufficient information that terpenoid production by cyanobacteria cannot compete with production by heterotrophic organisms, there is still hope for cyanobacterial contribution to sustainable biotechnology. Cyanobacterial central metabolism is dominated by carbohydrate production, with high flux consistently running through sugar phosphates for carbon fixation and glycogen storage. If cyanobacteria are unable to be rewired for production of terpenoids, the knowledge gained from the research conducted can still be applied to sugar production for conversion to valuable chemicals by heterotrophic organisms. Photosynthesis is still a powerful tool that has transformed nature, and has the power to transform modern society as well.

REFERENCES

[1] Myles R Allen, Opha Pauline Dube, William Solecki, Fernando Aragón-Durand, Wolfgang Cramer, Stephen Humphreys, Mikiko Kainuma, Jatin Kala, Natalie Mahowald, and Yacob Mulugetta. Global warming of 1.5°c. *Global warming of*, 1(5), 2018.

[2] Zhu Liu, Philippe Ciais, Zhu Deng, Ruixue Lei, Steven J. Davis, Sha Feng, Bo Zheng, Duo Cui, Xinyu Dou, Biqing Zhu, Rui Guo, Piyu Ke, Taochun Sun, Chenxi Lu, Pan He, Yuan Wang, Xu Yue, Yilong Wang, Yadong Lei, Hao Zhou, Zhaonan Cai, Yuhui Wu, Runtao Guo, Tingxuan Han, Jinjun Xue, Olivier Boucher, Eulalie Boucher, Frédéric Chevallier, Katsumasa Tanaka, Yiming Wei, Haiwang Zhong, Chongqing Kang, Ning Zhang, Bin Chen, Fengming Xi, Miaomiao Liu, François-Marie Bréon, Yonglong Lu, Qiang Zhang, Dabo Guan, Peng Gong, Daniel M. Kammen, Kebin He, and Hans Joachim Schellnhuber. Near-real-time monitoring of global co2 emissions reveals the effects of the covid-19 pandemic. *Nature Communications*, 11(1), 2020. ISSN 2041-1723. doi: 10.1038/s41467-020-18922-7.

[3] Haradhan Mohajan. Greenhouse gas emissions increase global warming. 2011.

[4] R Lindsey. Climate change: Atmospheric carbon dioxide, 2021. URL https://www.climate.gov/news-features/understanding-climate/climate-change-atmospheric-carbon-dioxide.

[5] Belinda Gallardo and David C. Aldridge. Evaluating the combined threat of climate change and biological invasions on endangered species. *Biological Conservation*, 160: 225–233, 2013. ISSN 0006-3207. doi: 10.1016/j.biocon.2013.02.001.

[6] Sikandar Khan and Pengcheng Fu. Biotechnological perspectives on algae: a viable option for next generation biofuels. *Current Opinion in Biotechnology*, 62:146–152, 2020. ISSN 0958-1669. doi: 10.1016/j.copbio.2019.09.020.

[7] Ni Wan, Mary Abernathy, Joseph Kuo-Hsiang Tang, Yinjie J. Tang, and Le You. Cyanobacterial photo-driven mixotrophic metabolism and its advantages for biosynthesis. *Frontiers of Chemical Science and Engineering*, 9(3):308–316, 2015. ISSN 2095-0179. doi: 10.1007/s11705-015-1521-7.

[8] Tylor J. Johnson, Jaimie L. Gibbons, Liping Gu, Ruanbao Zhou, and William R. Gibbons. Molecular genetic improvements of cyanobacteria to enhance the industrial potential of the microbe: A review. *Biotechnology Progress*, 32(6):1357–1371, 2016. ISSN 8756-7938. doi: 10.1002/btpr.2358. URL https://doi.org/10.1002/btpr.2358. OA status: bronze.

[9] Daniel C. Ducat, Jeffrey C. Way, and Pamela A. Silver. Engineering cyanobacteria to generate high-value products. *Trends in Biotechnology*, 29(2):95–103, 2011. ISSN 0167-7799. doi: 10.1016/j.tibtech.2010.12.003.

[10] Bertram M. Berla, Rajib Saha, Cheryl M. Immethun, Costas D. Maranas, Tae Seok Moon, and Himadri B. Pakrasi. Synthetic biology of cyanobacteria: unique challenges and opportunities. *Frontiers in Microbiology*, 4, 2013. ISSN 1664-302X. doi: 10.3389/fmicb.2013.00246. URL https://doi.org/10.3389/fmicb.2013.00246.

[11] John C. Batterton and C. Baalen. Growth responses of blue-green algae to sodium chloride concentration. *Archiv fr Mikrobiologie*, 76(2):151–165, 1971. ISSN 0302-8933. doi: 10.1007/bf00411789.

[12] C. T. Nomura, T. Sakamoto, and D. A. Bryant. Roles for heme-copper oxidases in extreme high-light and oxidative stress response in the cyanobacterium synechococcus sp. pcc 7002. *Arch Microbiol*, 185(6):471–9, 2006. ISSN 0302-8933 (Print) 0302-8933 (Linking). doi: 10.1007/s00203-006-0107-7. URL https://www.ncbi.nlm.nih.gov/pubmed/16775753. Nomura, Christopher T Sakamoto, Toshio Bryant, Donald A eng Research Support, U.S. Gov't, Non-P.H.S. Germany Arch Microbiol. 2006 Jun;185(6):471-9. doi: 10.1007/s00203-006-0107-7. Epub 2006 Apr 27.

[13] Jiří Komárek and Jeffrey R Johansen. *Filamentous cyanobacteria*, pages 135–235. Elsevier, 2015.

[14] A. Ludwiczuk, K. Skalicka-Woźniak, and M.I. Georgiev. *Terpenoids*, pages 233–266. Elsevier, 2017. doi: 10.1016/b978-0-12-802104-0.00011-1.

[15] Po Cheng Lin and Himadri B. Pakrasi. Engineering cyanobacteria for production of terpenoids. *Planta*, 249(1):145–154, 2019. ISSN 0042501830. doi: 10.1007/s00425-018-3047-y. URL https://doi.org/10.1007/s00425-018-3047-y.

[16] Jörg Bohlmann and Christopher I. Keeling. Terpenoid biomaterials. *The Plant Journal*, 54(4):656–669, 2008. ISSN 0960-7412. doi: 10.1111/j.1365-313x.2008.03449.x.

[17] Elizabeth Cordoba, Mari Salmi, and Patricia León. Unravelling the regulatory mechanisms that modulate the mep pathway in higher plants. *Journal of Experimental Botany*, 60(10):2933–2943, 2009. doi: 10.1093/jxb/erp190.

[18] W. Eisenreich, A. Bacher, D. Arigoni, and F. Rohdich. Biosynthesis of isoprenoids via the non-mevalonate pathway. *Cellular and Molecular Life Sciences*, 61(12), 2004. ISSN 1420-682X. doi: 10.1007/s00018-004-3381-z.

[19] Bagmi Pattanaik and Pia Lindberg. Terpenoids and their biosynthesis in cyanobacteria. *Life*, 5(1):269–293, 2015. doi: 10.3390/life5010269.

[20] Julie E. Chaves and Anastasios Melis. Engineering isoprene synthesis in cyanobacteria. *FEBS Letters*, 592(12):2059–2069, 2018. ISSN 0014-5793. doi: 10.1002/1873-3468.13052. URL https://febs.onlinelibrary.wiley.com/doi/pdf/10.1002/1873-3468.13052. OA status: bronze.

[21] Julie E. Chaves, Paloma Rueda Romero, Henning Kirst, and Anastasios Melis. Role of isopentenyl-diphosphate isomerase in heterologous cyanobacterial (synechocystis) isoprene production. *Photosynthesis Research*, 130(1-3), 2016. doi: 10.1007/s11120-016-0293-3.

[22] Lishan Zhao, Wei-chen Chang, Youli Xiao, Hung-wen Liu, and Pinghua Liu. Methylerythritol phosphate pathway of isoprenoid biosynthesis. 2013. doi: 10.1146/annurev-biochem-052010-100934.

[23] Rosaria Ciriminna, Monica Lomeli-Rodriguez, Piera Demma Carà, Jose A. Lopez-Sanchez, and Mario Pagliaro. Limonene: a versatile chemical of the bioeconomy. *Chem. Commun.*, 50(97):15288–15296, 2014. ISSN 1359-7345. doi: 10.1039/c4cc06147k.

[24] Wenzhao Wu and Christos T. Maravelias. Synthesis and techno-economic assessment of microbial-based processes for terpenes production. *Biotechnology for Biofuels*, 11 (1), 2018. ISSN 1754-6834. doi: 10.1186/s13068-018-1285-7. URL https://www.ncbi.nlm.nih.gov/pmc/articles/PMC6203976. OA status: green$_p$*ublished*.

[25] Chenhao Sun, Constantinos Theodoropoulos, and Nigel S. Scrutton. Techno-economic assessment of microbial limonene production. *Bioresource Technology*, 300:122666, 2020. ISSN 0960-8524. doi: 10.1016/j.biortech.2019.122666.

[26] C. C. Burke, M. R. Wildung, and R. Croteau. Geranyl diphosphate synthase: Cloning, expression, and characterization of this prenyltransferase as a heterodimer. *Proceedings of the National Academy of Sciences*, 96(23):13062–13067, 1999. ISSN 0027-8424. doi: 10.1073/pnas.96.23.13062. URL http://europepmc.org/articles/pmc23900?pdf=render. OA status: green$_p$*ublished*.

[27] Jihua Wu, Si Cheng, Jiayu Cao, Jianjun Qiao, and Guang-Rong Zhao. Systematic optimization of limonene production in engineered escherichia coli. *Journal of Agricultural and Food Chemistry*, 67(25):7087–7097, 2019. ISSN 0021-8561. doi: 10.1021/acs.jafc.9b01427.

[28] Xuan Cao, Yu-Bei Lv, Jun Chen, Tadayuki Imanaka, Liu-Jing Wei, and Qiang Hua. Metabolic engineering of oleaginous yeast yarrowia lipolytica for limonene overproduction. *Biotechnology for Biofuels*, 9(1), 2016. ISSN 1754-6834. doi: 10.1186/s13068-016-0626-7. URL http://europepmc.org/articles/pmc5057495?pdf=render. OA status: green$_p$*ublished*.

[29] Aparajita Banerjee, Yan Wu, Rahul Banerjee, Yue Li, Honggao Yan, and Thomas D. Sharkey. Feedback inhibition of deoxy-d-xylulose-5-phosphate synthase regulates the methylerythritol 4-phosphate pathway. *Journal of Biological Chemistry*, 288(23): 16926–16936, 2013. doi: 10.1074/jbc.M113.464636.

[30] Cinzia Formighieri and Anastasios Melis. Sustainable heterologous production of terpene hydrocarbons in cyanobacteria. *Photosynthesis Research*, 130(1-3):123–135, 2016. ISSN 0166-8595. doi: 10.1007/s11120-016-0233-2.

[31] Fiona K. Davies, Victoria H. Work, Alexander S. Beliaev, and Matthew C. Posewitz. Engineering limonene and bisabolene production in wild type and a glycogen-deficient mutant of synechococc us. 2(June):1–11, 2014. doi: 10.3389/fbioe.2014.00021.

[32] Xin Wang, Wei Liu, Changpeng Xin, Yi Zheng, Yanbing Cheng, Su Sun, Runze Li, Xin-Guang Zhu, Susie Y. Dai, Peter M. Rentzepis, and Joshua S. Yuan. Enhanced limonene production in cyanobacteria reveals photosynthesis limitations. *Proceedings of the National Academy of Sciences*, 113(50):14225–14230, 2016. ISSN 0027-8424. doi: 10.1073/pnas.1613340113. URL http://europepmc.org/articles/pmc5167140?pdf=render. OA status: green$_p$*ublished*.

[33] Xiang Gao, Fang Gao, Deng Liu, Hao Zhang, Xiaoqun Nie, and Chen Yang. Engineering the methylerythritol phosphate pathway in cyanobacteria for photosynthetic isoprene production from co2. *Energy Environmental Science*, 9(4):1400–1411, 2016. ISSN 1754-5692. doi: 10.1039/c5ee03102h.

[34] Sun Young Choi, Hyun Jeong Lee, Jaeyeon Choi, Jiye Kim, Sang Jun Sim, Youngsoon Um, Yunje Kim, Taek Soon Lee, Jay D. Keasling, and Han Min Woo. Photosynthetic conversion of co2 to farnesyl diphosphate-derived phytochemicals (amorpha-4,11-diene and squalene) by engineered cyanobacteria. *Biotechnology for Biofuels*, 9(1), 2016. ISSN 1754-6834. doi: 10.1186/s13068-016-0617-8. URL https://biotechnologyforbiofuels.biomedcentral.com/track/pdf/10.1186/s13068-016-0617-8.

[35] Johannes Zeidler, Jörg Schwender, Christian Müller, Jochen Wiesner, Claus Weidemeyer, Ewald Beck, Hassan Jomaa, and Hartmut K. Lichtenthaler. Inhibition of the non-mevalonate 1-deoxy--xylulose-5-phosphate pathway of plant isoprenoid biosynthesis by fosmidomycin. *Zeitschrift für Naturforschung C*, 53(11-12):980–986, 1998. doi: 10.1515/znc-1998-11-1208.

[36] Nidhi Singh, Gweneal Cheve, Mitchell Avery, and Christopher McCurdy. Targeting the methyl erythritol phosphate (mep) pathway for novel antimalarial, antibacterial and herbicidal drug discovery: Inhibition of 1-deoxy-d-xylulose-5-phosphate reductoisomerase (dxr) enzyme. *Current Pharmaceutical Design*, 13(11):1161–1177, 2007. doi: 10.2174/138161207780618939.

[37] Yuru Tong, Ping Su, Yujun Zhao, Meng Zhang, Xiujuan Wang, Yujia Liu, Xianan Zhang, Wei Gao, and Luqi Huang. Molecular cloning and characterization of dxs and dxr genes in the terpenoid biosynthetic pathway of tripterygium wilfordii. *International Journal of Molecular Sciences*, 16(10):25516–25535, 2015. ISSN 1422-0067. doi: 10.3390/ijms161025516. URL https://doi.org/10.3390/ijms161025516.

[38] Wei Xiong, Melissa Cano, Bo Wang, and Damien Douchi. The plasticity of cyanobacterial carbon metabolism. *Current Opinion in Chemical Biology*, 41:12–19, 2017. doi: 10.1016/j.cbpa.2017.09.004. URL http://dx.doi.org/10.1016/j.cbpa.2017.09.004.

[39] Hiroshi Kiyota, Yukiko Okuda, Michiho Ito, Masami Yokota Hirai, and Masahiko Ikeuchi. Engineering of cyanobacteria for the photosynthetic production of limonene from co2. *Journal of Biotechnology*, 185:1–7, 2014. ISSN 0168-1656. doi: 10.1016/j.jbiotec.2014.05.025. URL https://manuscript.elsevier.com/S0168165614002715/pdf/S0168165614002715.pdf. OA status: gold$_o$*ther*.

[40] T. Kaneko, S. Sato, H. Kotani, A. Tanaka, E. Asamizu, Y. Nakamura, N. Miyajima, M. Hirosawa, M. Sugiura, S. Sasamoto, T. Kimura, T. Hosouchi, A. Matsuno, A. Muraki, N. Nakazaki, K. Naruo, S. Okumura, S. Shimpo, C. Takeuchi, T. Wada, A. Watanabe, M. Yamada, M. Yasuda, and S. Tabata. Sequence analysis of the genome of the unicellular cyanobacterium synechocystis sp. strain pcc6803. ii. sequence determination of the entire genome and assignment of potential protein-coding regions. *DNA Research*, 3(3):109–136, 1996. ISSN 1340-2838. doi: 10.1093/dnares/3.3.109.

[41] AV Hill. The possible effects of the aggregation of the molecules of haemoglobin on its oxygen dissociation. *J Physiol*, 40:iv–vii, 1910.

[42] Yuri V. Ershov, R. Raymond Gantt, Francis X. Cunningham, and Elisabeth Gantt. Isoprenoid biosynthesis in synechocystis sp. strain pcc6803 is stimulated by compounds of the pentose phosphate cycle but not by pyruvate or deoxyxylulose-5-phosphate. *Journal of Bacteriology*, 184(18):5045–5051, 2002. doi: 10.1128/JB.184.18.5045-5051.2002.

[43] Kelly Poliquin, Yuri V. Ershov, Francis X. Cunningham, Tinsay T. Woreta, R. Raymond Gantt, and Elisabeth Gantt. Inactivation ofsll1556insynechocystisstrain pcc 6803 impairs isoprenoid biosynthesis from pentose phosphate cycle substrates in vitro. *Journal of Bacteriology*, 186(14):4685–4693, 2004. ISSN 0021-9193. doi: 10.1128/jb.186.14.4685-4693.2004.

[44] Po-Cheng Lin, Fuzhong Zhang, and Himadri B. Pakrasi. Enhanced limonene production in a fast-growing cyanobacterium through combinatorial metabolic engineering. *Metabolic Engineering Communications*, 12:e00164, 2021. ISSN 2214-0301. doi: 10.1016/j.mec.2021.e00164.

[45] Po Cheng Lin, Rajib Saha, Fuzhong Zhang, and Himadri B. Pakrasi. Metabolic engineering of the pentose phosphate pathway for enhanced limonene production in the cyanobacterium synechocysti s sp. pcc. *Scientific Reports*, 7(1):1–10, 2017. doi: 10.1038/s41598-017-17831-y. URL http://dx.doi.org/10.1038/s41598-017-17831-y.

[46] Hsin-ho Huang, Daniel Camsund, Peter Lindblad, and Thorsten Heidorn. Design and characterization of molecular tools for a synthetic biology approach towards developing cyanobacterial biotechnology. 38(8):2577–2593, 2010. doi: 10.1093/nar/gkq164.

[47] Catherine L Winder, Warwick B Dunn, Stephanie Schuler, David Broadhurst, Roger Jarvis, Gillian M Stephens, and Royston Goodacre. Global metabolic profiling of escherichia coli cultures: an evaluation of methods for quenching and extraction of intracellular metabolites. *Analytical Chemistry*, 80(8):2939–2948, 2008. ISSN 0003-2700.

[48] André B Canelas, Cor Ras, Angela Ten Pierick, Jan C van Dam, Joseph J Heijnen, and Walter M Van Gulik. Leakage-free rapid quenching technique for yeast metabolomics. *Metabolomics*, 4(3):226–239, 2008. ISSN 1573-3890.

[49] Wim de Koning and Karel van Dam. A method for the determination of changes of glycolytic metabolites in yeast on a subsecond time scale using extraction at neutral ph. *Analytical biochemistry*, 204(1):118–123, 1992. ISSN 0003-2697.

[50] Lodewijk P. De Jonge, Rutger D. Douma, Joseph J. Heijnen, and Walter M. Van Gulik. Optimization of cold methanol quenching for quantitative metabolomics of penicillium chrysogenum. *Metabolomics*, 8(4):727–735, 2012. ISSN 1573-3882. doi: 10.1007/s11306-011-0367-3. URL https://repository.tudelft.nl/islandora/object/uuid%3A2d4ef227-e75f-4e57-8675-8969509329e6/datastream/OBJ/download.

[51] Christoph Wittmann, Jens O Krömer, Patrick Kiefer, Tina Binz, and Elmar Heinzle. Impact of the cold shock phenomenon on quantification of intracellular metabolites in bacteria. *Analytical biochemistry*, 327(1):135–139, 2004. ISSN 0003-2697.

[52] Silas G. Villas-Bôas and Per Bruheim. Cold glycerol–saline: The promising quenching solution for accurate intracellular metabolite analysis of microbial cells. *Analytical Biochemistry*, 370(1):87–97, 2007. ISSN 0003-2697. doi: 10.1016/j.ab.2007.06.028.

[53] Christopher A Sellick, Rasmus Hansen, Gill M Stephens, Royston Goodacre, and Alan J Dickson. Metabolite extraction from suspension-cultured mammalian cells for global metabolite profiling. *Nature protocols*, 6(8):1241–1249, 2011. ISSN 1750-2799.

[54] María J. Sáez and Rosario Lagunas. Determination of intermediary metabolites in yeast. critical examination of the effect of sampling conditions and recommendations for obtaining true levels. *Molecular and Cellular Biochemistry*, 13(2):73–78, 1976. ISSN 0300-8177. doi: 10.1007/bf01837056.

[55] Walter M Van Gulik. Fast sampling for quantitative microbial metabolomics. *Current Opinion in Biotechnology*, 21(1):27–34, 2010. ISSN 0958-1669. doi: 10.1016/j.copbio.2010.01.008.

[56] Cara L. Sake, Darrian M. Newman, and Nanette R. Boyle. Evaluation of quenching methods for metabolite recovery in photoautotrophic synechococcus sp. pcc 7002. *Biotechnology Progress*, 36(5), 2020. ISSN 8756-7938. doi: 10.1002/btpr.3015.

[57] Qin Yang, Rui Tao, Bo Yang, Hao Zhang, Yong Q. Chen, Haiqin Chen, and Wei Chen. Optimization of the quenching and extraction procedures for a metabolomic analysis of lactobacillus plantarum. *Analytical Biochemistry*, 557:62–68, 2018. ISSN 0003-2697. doi: 10.1016/j.ab.2017.12.005.

[58] Mary H. Abernathy, Jingjie Yu, Fangfang Ma, Michelle Liberton, Justin Ungerer, Whitney D. Hollinshead, Saratram Gopalakrishnan, Lian He, Costas D. Maranas, Himadri B. Pakrasi, Doug K. Allen, and Yinjie J. Tang. Deciphering cyanobacterial phenotypes for fast photoautotrophic growth via isotopically nonstationary metabolic flux analysis. *Biotechnology for Biofuels*, 10(1):1–13, 2017. doi: 10.1186/s13068-017-0958-y.

[59] Ravendran Vasudevan, Grant A. R. Gale, Alejandra A. Schiavon, Anton Puzorjov, and John Malin. Cyanogate : A modular cloning suite for engineering cyanobacteria based on the plant moclo syntax 1 [open]. *Plant Physiology*, 180(May):39–55, 2019. ISSN 0000000191951. doi: 10.1104/pp.18.01401.

[60] Ernst Weber, Carola Engler, Ramona Gruetzner, Stefan Werner, and Sylvestre Marillonnet. A modular cloning system for standardized assembly of multigene constructs. *PLoS ONE*, 6(2):e16765, 2011. ISSN 1932-6203. doi: 10.1371/journal.pone.0016765. URL https://journals.plos.org/plosone/article/file?id=10.1371/journal.pone.0016765&type=printable.

[61] Stefan Werner, Carola Engler, Ernst Weber, Ramona Gruetzner, and Sylvestre Marillonnet. Fast track assembly of multigene constructs using golden gate cloning and the moclo system. *Bioengineered*, 3(1):38–43, 2012. ISSN 2165-5979. doi: 10.4161/bbug.3.1.18223. URL https://www.tandfonline.com/doi/pdf/10.4161/bbug.3.1.18223?needAccess=true. OA status: bronze.

[62] Aneel K. Aggarwal. Structure and function of restriction endonucleases. *Current Opinion in Structural Biology*, 5(1):11–19, 1995. ISSN 0959-440X. doi: 10.1016/0959-440x(95)80004-k.

[63] A. Pingoud. Structure and function of type ii restriction endonucleases. *Nucleic Acids Research*, 29(18):3705–3727, 2001. ISSN 1362-4962. doi: 10.1093/nar/29.18.3705.

[64] Andrew L. Markley, Matthew B. Begemann, Ryan E. Clarke, Gina C. Gordon, and F. P. Brian. Synthetic biology toolbox for controlling gene expression in the cyanobacterium synechococcus sp. strain pcc 7002. 2015.

[65] Erin K. Zess, Matthew B. Begemann, and Brian F. Pfleger. Construction of new synthetic biology tools for the control of gene expression in the cyanobacteriumsynechococcussp. strain pcc 7002. *Biotechnology and Bioengineering*, 113(2):424–432, 2016. ISSN 0006-3592. doi: 10.1002/bit.25713.

[66] Gina C. Gordon, Travis C. Korosh, Jeffrey C. Cameron, Andrew L. Markley, Matthew B. Begemann, and F. P. Brian. Crispr interference as a titratable , trans -acting regulatory tool for metabolic engineering in the cyanobacterium synechococcus sp . strain pcc 7002. 38:170–179, 2016. doi: 10.1016/j.ymben.2016.07.007.

[67] Francisco JM Mojica, César Díez-Villaseñor, Jesús García-Martínez, and Cristóbal Almendros. Short motif sequences determine the targets of the prokaryotic crispr defence system. *Microbiology*, 155(3):733–740, 2009. ISSN 1350-0872.

[68] Andrew M. Hogan, A. S. M. Zisanur Rahman, Tasia J. Lightly, and Silvia T. Cardona. A broad-host-range crispri toolkit for silencing gene expression in burkholderia. *ACS Synthetic Biology*, 8(10):2372–2384, 2019. ISSN 2161-5063. doi: 10.1021/acssynbio.9b00232. URL https://doi.org/10.1101/618413.

[69] Grant A. R. Gale, Alejandra A. Schiavon Osorio, Anton Puzorjov, Baojun Wang, and Alistair J. McCormick. Genetic modification of cyanobacteria by conjugation using the cyanogate modular cloning toolkit. (October):1–17, 2019. doi: 10.3791/60451.

[70] Jeff Elhai and C Peter Wolk. [83] conjugal transfer of dna to cyanobacteria. *Methods in enzymology*, 167:747–754, 1988. ISSN 0076-6879.

[71] Anne Ilse Maria Vogel, Rahmi Lale, and Martin Frank Hohmann-Marriott. Streamlining recombination-mediated genetic engineering by validating three neutral integration sites in synechococcus sp. pcc 7002. *Journal of Biological Engineering*, 11(1), 2017. ISSN 1754-1611. doi: 10.1186/s13036-017-0061-8. URL https://doi.org/10.1186/s13036-017-0061-8.

[72] Qungang Qi, Ming Hao, Wing-on Ng, Steven C. Slater, Susan R. Baszis, James D. Weiss, and Henry E. Valentin. Application of the synechococcus nira promoter to establish an inducible expression system for engineering the synechocystis tocopherol pathway. *Applied and Environmental Microbiology*, 71(10):5678–5684, 2005. doi: 10.1128/AEM.71.10.5678.

[73] Yoshitake Ohashi, Wei Shi, Nobuyuki Takatani, Makiko Aichi, Shin-Ichi Maeda, Satoru Watanabe, Hirofumi Yoshikawa, and Tatsuo Omata. Regulation of nitrate assimilation in cyanobacteria. *Journal of Experimental Botany*, 62(4):1411–1424, 2011. ISSN 1460-2431. doi: 10.1093/jxb/erq427. URL https://academic.oup.com/jxb/article-pdf/62/4/1411/16929254/erq427.pdf. OA status: bronze.

[74] Eberhard Spiess, Felix Bestvater, Anna HECKEL-POMPEY, Katalin Toth, Martin Hacker, Gregor Stobrawa, Thomas Feurer, Christoph Wotzlaw, Utta BERCHNER-PFANNSCHMIDT, and Torsten Porwol. Two-photon excitation and emission spectra of the green fluorescent protein variants ecfp, egfp and eyfp. *Journal of Microscopy*, 217(3):200–204, 2005. ISSN 0022-2720.

[75] Alexander Hammel, Frederik Sommer, David Zimmer, Mark Stitt, Timo Mühlhaus, and Michael Schroda. Overexpression of sedoheptulose-1,7-bisphosphatase enhances photosynthesis in chlamydomonas reinhardtii and has no effect on the abundance of other calvin-benson cycle enzymes. *Frontiers in Plant Science*, 11(868), 2020. ISSN 1664-462X. doi: 10.3389/fpls.2020.00868. URL https://www.frontiersin.org/article/10.3389/fpls.2020.00868.

[76] Alice Jara De Porcellinis, Hanne Nørgaard, Laura Maria Furelos Brey, Simon Matthé Erstad, Patrik R. Jones, Joshua L. Heazlewood, and Yumiko Sakuragi. Overexpression of bifunctional fructose-1,6-bisphosphatase/sedoheptulose-1,7-bisphosphatase leads to enhanced photosynthesis and global reprogramming of carbon metabolism in synechococcus sp. pcc 7002. *Metabolic Engineering*, 47:170–183, 2018. ISSN 1096-7176. doi: 10.1016/j.ymben.2018.03.001. URL http://spiral.imperial.ac.uk/bitstream/10044/1/60613/6/MBE_2017_311_Revision.pdf.

[77] Cara L. Sake, Alexander J. Metcalf, and Nanette R. Boyle. The challenge and potential of photosynthesis : unique considerations for metabolic flux measurements in photosynthetic microorganisms. *Biotechnology Letters*, 41(1):35–45, 2019. ISSN 0123456789. doi: 10.1007/s10529-018-2622-4. URL https://doi.org/10.1007/s10529-018-2622-4.

[78] Robert W. Leighty and Maciek R. Antoniewicz. Parallel labeling experiments with [u-13c]glucose validate e. coli metabolic network model for 13c metabolic flux analysis. *Metabolic Engineering*, 14(5):533–541, 2012. ISSN 1096-7176. doi: 10.1016/j.ymben.2012.06.003.

[79] Henrique C. T. Veras, Christiane G. Campos, Igor F. Nascimento, Patrícia V. Abdelnur, João R. M. Almeida, and Nádia S. Parachin. Metabolic flux analysis for metabolome data validation of naturally xylose-fermenting yeasts. *BMC Biotechnology*, 19(1), 2019. ISSN 1472-6750. doi: 10.1186/s12896-019-0548-0. URL https://doi.org/10.1186/s12896-019-0548-0.

[80] Lake-Ee Quek, Stefanie Dietmair, Jens O. Krömer, and Lars K. Nielsen. Metabolic flux analysis in mammalian cell culture. *Metabolic Engineering*, 12(2):161–171, 2010. ISSN 1096-7176. doi: 10.1016/j.ymben.2009.09.002.

[81] Shuyi Zhang and Donald A Bryant. The tricarboxylic acid cycle in cyanobacteria. *Science*, 334(6062):1551–1553, 2011. ISSN 0036-8075.

[82] J. D. Young, A. A. Shastri, G. Stephanopoulos, and J. A. Morgan. Mapping photoautotrophic metabolism with isotopically nonstationary (13)c flux analysis. *Metab Eng*, 13(6):656–65, 2011. ISSN 1096-7184 (Electronic) 1096-7176 (Linking). doi: 10.1016/j.ymben.2011.08.002. URL https://www.ncbi.nlm.nih.gov/pubmed/21907300. Young, Jamey D Shastri, Avantika A Stephanopoulos, Gregory Morgan, John A eng R01 DK075850-05/DK/NIDDK NIH HHS/ F32DK072856/DK/NIDDK NIH HHS/ F32 DK072856/DK/NIDDK NIH HHS/ R01 DK075850/DK/NIDDK NIH HHS/ R01DK075850/DK/NIDDK NIH HHS/ F32 DK072856-03/DK/NIDDK NIH HHS/ Research Support, N.I.H., Extramural Research Support, U.S. Gov't, Non-P.H.S. Belgium Metab Eng. 2011 Nov;13(6):656-65. doi: 10.1016/j.ymben.2011.08.002. Epub 2011 Sep 1.

[83] J. Overmann Garica-Pichel and F. *The Phototrophic Way of Life*, volume 3, pages 32–85. 2006. doi: 10.1007/0-387-30742-7_3.

[84] Aqib Zafar Khan, Muhammad Bilal, Shahid Mehmood, Ashutosh Sharma, and Hafiz M. N. Iqbal. State-of-the-art genetic modalities to engineer cyanobacteria for sustainable biosynthesis of biofuel and fine-chemicals to meet bio–economy challenges. *Life*, 9(3):1–22, 2019. doi: 10.3390/life9030054.

[85] Marcus Ludwig and Donald A. Bryant. Acclimation of the global transcriptome of the cyanobacterium synechococcus sp. strain pcc 7002 to nutrient limitations and different nitrogen sources. *Frontiers in Microbiology*, 3, 2012. ISSN 1664-302X. doi: 10.3389/fmicb.2012.00145. URL https://www.frontiersin.org/articles/10.3389/fmicb.2012.00145/pdf. OA status: $\text{gold}_{d}oaj$.

[86] Elias Englund, Kiyan Shabestary, Elton P. Hudson, and Pia Lindberg. Systematic overexpression study to find target enzymes enhancing production of terpenes in synechocystis pcc 6803, using isoprene as a model compound. *Metabolic Engineering*, 49: 164–177, 2018. ISSN 1096-7176. doi: 10.1016/j.ymben.2018.07.004. URL http://uu.diva-portal.org/smash/get/diva2:1248892/FULLTEXT01. OA status: $\text{green}_{p}ublished$.

[87] John I. Hendry, Charulata Prasannan, Fangfang Ma, K. Benedikt Möllers, Damini Jaiswal, Madhuri Digmurti, Doug K. Allen, Niels Ulrik Frigaard, Santanu Dasgupta, and Pramod P. Wangikar. Rerouting of carbon flux in a glycogen mutant of cyanobacteria assessed via isotopically non-stationary 13c metabolic flux analysis. *Biotechnology and Bioengineering*, 114(10):2298–2308, 2017. doi: 10.1002/bit.26350.

[88] Mary H. Abernathy, J. Czajka, Douglas K. Allen, Nicholas C. Hill, C. Cameron, and Yinjie J. Tang. Cyanobacterial carboxysome mutant analysis reveals the in fl uence of enzyme compartmentalization on cellular metabolism and metabolic network rigidity. 54 (February):222–231, 2019. doi: 10.1016/j.ymben.2019.04.010.

[89] Xiao Qian, Yuan Zhang, Desmond S. Lun, and G. Charles Dismukes. Rerouting of metabolism into desired cellular products by nutrient stress: Fluxes reveal the selected pathways in cyanobacterial photosynthesis. *ACS Synthetic Biology*, 7(5):1465–1476, 2018. doi: 10.1021/acssynbio.8b00116.

[90] Jack Myers S. E. Stevens Jr., C. O. Pat Patterson. The production of hydrogen peroxide by blue-green algae: A survey. *Journal of Phycology*, 9(4):427–430, 1973. doi: doi:10.1111/j.0022-3646.1973.00427.x.

[91] Jamey D. Young. Inca: A computational platform for isotopically non-stationary metabolic flux analysis. *Bioinformatics*, 30(9):1333–1335, 2014. doi: 10.1093/bioinformatics/btu015.

[92] Lara J Jazmin, Yao Xu, Yi Ern Cheah, Adeola O Adebiyi, Carl Hirschie Johnson, and Jamey D Young. Isotopically nonstationary 13c flux analysis of cyanobacterial isobutyraldehyde production. *Metabolic engineering*, 42:9–18, 2017. ISSN 1096-7176.

[93] Adeola O. Adebiyi, Lara J. Jazmin, and Jamey D. Young. 13c flux analysis of cyanobacterial metabolism. *Photosynthesis Research*, 126(1):19–32, 2015. doi: 10.1007/s11120-014-0045-1.

[94] Brian Colman. Photosynthetic carbon assimilation and the suppression of photorespiration in the cyanobacteria. *Aquatic Botany*, 34(1-3):211–231, 1989. ISSN 0304-3770. doi: 10.1016/0304-3770(89)90057-0.

[95] H. Knoop, Y. Zilliges, W. Lockau, and R. Steuer. The metabolic network of synechocystis sp. pcc 6803: systemic properties of autotrophic growth. *Plant Physiol*, 154(1):410–22, 2010. ISSN 1532-2548 (Electronic) 0032-0889 (Linking). doi: 10.1104/pp.110.157198. URL https://www.ncbi.nlm.nih.gov/pubmed/20616194. Knoop, Henning Zilliges, Yvonne Lockau, Wolfgang Steuer, Ralf eng Research Support, Non-U.S. Gov't Plant Physiol. 2010 Sep;154(1):410-22. doi: 10.1104/pp.110.157198. Epub 2010 Jul 8.

[96] Momoyo Ishikawa, Daisuke Tsuchiya, Takuji Oyama, Yasuo Tsunaka, and Kosuke Morikawa. Structural basis for channelling mechanism of a fatty acid -oxidation multienzyme complex. *The EMBO Journal*, 23(14):2745–2754, 2004. ISSN 0261-4189. doi: 10.1038/sj.emboj.7600298. URL https://www.ncbi.nlm.nih.gov/pmc/articles/PMC514956. OA status: green$_p$*ublished*.

[97] Jared T. Broddrick, Benjamin E. Rubin, David G. Welkie, Niu Du, Nathan Mih, Spencer Diamond, Jenny J. Lee, Susan S. Golden, and Bernhard O. Palsson. Unique attributes of cyanobacterial metabolism revealed by improved genome-scale metabolic modeling and essential gene analysis. *Proceedings of the National Academy of Sciences*, 113(51): E8344–E8353, 2016. ISSN 0027-8424. doi: 10.1073/pnas.1613446113. URL https://www.pnas.org/content/pnas/113/51/E8344.full.pdf. OA status: bronze.

[98] Sebastiaan Spaans, Ruud Weusthuis, John Van Der Oost, and Servé Kengen. Nadph-generating systems in bacteria and archaea. *Frontiers in Microbiology*, 6(742), 2015. ISSN 1664-302X. doi: 10.3389/fmicb.2015.00742. URL https://www.frontiersin.org/article/10.3389/fmicb.2015.00742.

[99] Ranji Singh, Joseph Lemire, Ryan J. Mailloux, and Vasu D. Appanna. A novel strategy involved anti-oxidative defense: The conversion of nadh into nadph by a metabolic network. *PLoS ONE*, 3(7):e2682, 2008. ISSN 1932-6203. doi: 10.1371/journal.pone.0002682. URL https://doi.org/10.1371/journal.pone.0002682.

[100] Sangeeta Negi, Amanda N. Barry, Natalia Friedland, Nilusha Sudasinghe, Sowmya Subramanian, Shayani Pieris, F. Omar Holguin, Barry Dungan, Tanner Schaub, and Richard Sayre. Impact of nitrogen limitation on biomass, photosynthesis, and lipid accumulation in chlorella sorokiniana. *Journal of Applied Phycology*, 28(2):803–812, 2015. ISSN 0921-8971 1573-5176. doi: 10.1007/s10811-015-0652-z.

[101] C. Wu, W. Xiong, J. Dai, and Q. Wu. Genome-based metabolic mapping and 13c flux analysis reveal systematic properties of an oleaginous microalga chlorella protothecoides. *Plant Physiol*, 167(2):586–99, 2015. ISSN 1532-2548 (Electronic) 0032-0889 (Linking). doi: 10.1104/pp.114.250688. URL https://www.ncbi.nlm.nih.gov/pubmed/25511434. Wu, Chao Xiong, Wei Dai, Junbiao Wu, Qingyu eng Research Support, Non-U.S. Gov't Plant Physiol. 2015 Feb;167(2):586-99. doi: 10.1104/pp.114.250688. Epub 2014 Dec 15.

[102] G. Cogne, M. Rugen, A. Bockmayr, M. Titica, C. G. Dussap, J. F. Cornet, and J. Legrand. A model-based method for investigating bioenergetic processes in autotrophically growing eukaryotic microalgae: application to the green algae chlamydomonas reinhardtii. *Biotechnol Prog*, 27(3):631–40, 2011. ISSN 1520-6033 (Electronic) 1520-6033 (Linking). doi: 10.1002/btpr.596. URL https://www.ncbi.nlm.nih.gov/pubmed/21567987. Cogne, Guillaume Rugen, Marco Bockmayr, Alexander Titica, Mariana Dussap, Claude-Gilles Cornet, Jean-Francois Legrand, Jack eng Research Support, Non-U.S. Gov't Biotechnol Prog. 2011 May-Jun;27(3):631-40. doi: 10.1002/btpr.596. Epub 2011 May 12.

[103] Y. Hirokawa, S. Matsuo, H. Hamada, F. Matsuda, and T. Hanai. Metabolic engineering of synechococcus elongatus pcc 7942 for improvement of 1,3-propanediol and glycerol production based on in silico simulation of metabolic flux distribution. *Microb Cell Fact*, 16(1):212, 2017. ISSN 1475-2859 (Electronic) 1475-2859 (Linking). doi: 10.1186/s12934-017-0824-4. URL https://www.ncbi.nlm.nih.gov/pubmed/29178875. Hirokawa, Yasutaka Matsuo, Shingo Hamada, Hiroyuki Matsuda, Fumio Hanai, Taizo eng England Microb Cell Fact. 2017 Nov 25;16(1):212. doi: 10.1186/s12934-017-0824-4.

[104] A. M. Kliphuis, A. J. Klok, D. E. Martens, P. P. Lamers, M. Janssen, and R. H. Wijffels. Metabolic modeling of chlamydomonas reinhardtii: energy requirements for photoautotrophic growth and maintenance. *J Appl Phycol*, 24(2):253–266, 2012. ISSN 0921-8971 (Print) 0921-8971 (Linking). doi: 10.1007/s10811-011-9674-3. URL https://www.ncbi.nlm.nih.gov/pubmed/22427720. Kliphuis, Anna M J Klok, Anne J Martens, Dirk E Lamers, Packo P Janssen, Marcel Wijffels, Rene H eng Netherlands J Appl Phycol. 2012 Apr;24(2):253-266. doi: 10.1007/s10811-011-9674-3. Epub 2011 Apr 15.

[105] C. Zuniga, C. T. Li, T. Huelsman, J. Levering, D. C. Zielinski, B. O. McConnell, C. P. Long, E. P. Knoshaug, M. T. Guarnieri, M. R. Antoniewicz, M. J. Betenbaugh, and K. Zengler. Genome-scale metabolic model for the green alga chlorella vulgaris utex 395 accurately predicts phenotypes under autotrophic, heterotrophic, and mixotrophic growth conditions. *Plant Physiol*, 172(1):589–602, 2016. ISSN 1532-2548 (Electronic) 0032-0889 (Linking). doi: 10.1104/pp.16.00593. URL https://www.ncbi.nlm.nih.gov/pubmed/27372244. Zuniga, Cristal Li, Chien-Ting Huelsman, Tyler Levering, Jennifer Zielinski, Daniel C McConnell, Brian O Long, Christopher P Knoshaug, Eric P Guarnieri, Michael T Antoniewicz, Maciek R Betenbaugh, Michael J Zengler, Karsten eng Research Support, U.S. Gov't, Non-P.H.S. Research Support, Non-U.S. Gov't Plant Physiol. 2016 Sep;172(1):589-602. doi: 10.1104/pp.16.00593. Epub 2016 Jul 2.

[106] R. L. Chang, L. Ghamsari, A. Manichaikul, E. F. Hom, S. Balaji, W. Fu, Y. Shen, T. Hao, B. O. Palsson, K. Salehi-Ashtiani, and J. A. Papin. Metabolic network reconstruction of chlamydomonas offers insight into light-driven algal metabolism. *Mol Syst Biol*, 7:518, 2011. ISSN 1744-4292 (Electronic) 1744-4292 (Linking). doi: 10.1038/msb.2011.52. URL https://www.ncbi.nlm.nih.gov/pubmed/21811229. Chang, Roger L Ghamsari, Lila Manichaikul, Ani Hom, Erik F Y Balaji, Santhanam Fu, Weiqi Shen, Yun Hao, Tong Palsson, Bernhard O Salehi-Ashtiani, Kourosh Papin, Jason A eng Research Support, Non-U.S. Gov't Research Support, U.S. Gov't, Non-P.H.S. England Mol Syst Biol. 2011 Aug 2;7:518. doi: 10.1038/msb.2011.52.

[107] C. Gomes de Oliveira Dal'Molin, L.E. Quek, R. W. Palfreyman, and L. K. Nielsen. Algagem – a genome-scale metabolic reconstruction of algae based on the chlamydomonas reinhardtii genome¡algagem.pdf¿. *BMC Genomics*, 12(S4), 2011. doi: 10.1186/1471-2164-12-S4-S5.

[108] N. Loira, S. Mendoza, M. Paz Cortes, N. Rojas, D. Travisany, A. D. Genova, N. Gajardo, N. Ehrenfeld, and A. Maass. Reconstruction of the microalga nannochloropsis salina genome-scale metabolic model with applications to lipid production. *BMC Syst Biol*, 11(1): 66, 2017. ISSN 1752-0509 (Electronic) 1752-0509 (Linking). doi: 10.1186/s12918-017-0441-1. URL https://www.ncbi.nlm.nih.gov/pubmed/28676050. Loira, Nicolas Mendoza, Sebastian Paz Cortes, Maria Rojas, Natalia Travisany, Dante Genova, Alex Di Gajardo, Natalia Ehrenfeld, Nicole Maass, Alejandro eng England BMC Syst Biol. 2017 Jul 4;11(1):66. doi: 10.1186/s12918-017-0441-1.

[109] A. Montagud, E. Navarro, P. Fernández de Córdoba, J. F. Urchueguía, and K. R. Patil. Reconstruction and analysis of a genome-scale metabolic model of a photosynthetic bacterium. *BMC Systems Biology*, 4, 2010. doi: 10.1186/1752-0509-4-156.

[110] Ab Rauf Shah, Ahmad Ahmad, Shireesh Srivastava, and B. M. Jaffar Ali. Reconstruction and analysis of a genome-scale metabolic model of nannochloropsis gaditana. *Algal Research*, 26:354–364, 2017. ISSN 22119264. doi: 10.1016/j.algal.2017.08.014.

[111] K. Yoshikawa, Y. Kojima, T. Nakajima, C. Furusawa, T. Hirasawa, and H. Shimizu. Reconstruction and verification of a genome-scale metabolic model for synechocystis sp. pcc6803. *Appl Microbiol Biotechnol*, 92(2):347–58, 2011. ISSN 1432-0614 (Electronic) 0175-7598 (Linking). doi: 10.1007/s00253-011-3559-x. URL https://www.ncbi.nlm.nih.gov/pubmed/21881889. Yoshikawa, Katsunori Kojima, Yuta Nakajima, Tsubasa Furusawa, Chikara Hirasawa, Takashi Shimizu, Hiroshi eng Research Support, Non-U.S. Gov't Germany Appl Microbiol Biotechnol. 2011 Oct;92(2):347-58. doi: 10.1007/s00253-011-3559-x. Epub 2011 Sep 1.

[112] S. Imam, S. Schauble, J. Valenzuela, A. Lopez Garcia de Lomana, W. Carter, N. D. Price, and N. S. Baliga. A refined genome-scale reconstruction of chlamydomonas metabolism provides a platform for systems-level analyses. *Plant J*, 84(6):1239–56, 2015. ISSN 1365-313X (Electronic) 0960-7412 (Linking). doi: 10.1111/tpj.13059. URL https://www.ncbi.nlm.nih.gov/pubmed/26485611. Imam, Saheed Schauble, Sascha Valenzuela, Jacob Lopez Garcia de Lomana, Adrian Carter, Warren Price, Nathan D Baliga, Nitin S eng P50 GM076547/GM/NIGMS NIH HHS/ 2P50 GM076547/GM/NIGMS NIH HHS/ Research Support, N.I.H., Extramural Research Support, Non-U.S. Gov't Research Support, U.S. Gov't, Non-P.H.S. England Plant J. 2015 Dec;84(6):1239-56. doi: 10.1111/tpj.13059. Epub 2015 Nov 30.

[113] N. R. Boyle and J. A. Morgan. Flux balance analysis of primary metabolism in chlamydomonas reinhardtii. *BMC Syst Biol*, 3:4, 2009. ISSN 1752-0509 (Electronic) 1752-0509 (Linking). doi: 10.1186/1752-0509-3-4. URL https://www.ncbi.nlm.nih.gov/pubmed/19128495. Boyle, Nanette R Morgan, John A eng Research Support, U.S. Gov't, Non-P.H.S. England BMC Syst Biol. 2009 Jan 7;3:4. doi: 10.1186/1752-0509-3-4.

[114] Ashley Beck, Kristopher Hunt, and Ross Carlson. Measuring cellular biomass composition for computational biology applications. *Processes*, 6(5), 2018. ISSN 2227-9717. doi: 10.3390/pr6050038.

[115] J. I. Hendry, C. B. Prasannan, A. Joshi, S. Dasgupta, and P. P. Wangikar. Metabolic model of synechococcus sp. pcc 7002: Prediction of flux distribution and network modification for enhanced biofuel production. *Bioresour Technol*, 213:190–197, 2016. ISSN 1873-2976 (Electronic) 0960-8524 (Linking). doi: 10.1016/j.biortech.2016.02.128. URL https://www.ncbi.nlm.nih.gov/pubmed/27036328. Hendry, John I Prasannan, Charulata B Joshi, Aditi Dasgupta, Santanu Wangikar, Pramod P eng England Bioresour Technol. 2016 Aug;213:190-197. doi: 10.1016/j.biortech.2016.02.128. Epub 2016 Mar 9.

[116] A. A. Shastri and J. A. Morgan. Flux balance analysis of photoautotrophic metabolism. *Biotechnology Progress*, 21:1617–1626, 2005.

[117] L. Pottier, J. Pruvost, J. Deremetz, J. F. Cornet, J. Legrand, and C. G. Dussap. A fully predictive model for one-dimensional light attenuation by chlamydomonas reinhardtii in a torus photobioreactor. *Biotechnol Bioeng*, 91(5):569–82, 2005. ISSN 0006-3592 (Print) 0006-3592 (Linking). doi: 10.1002/bit.20475. URL https://www.ncbi.nlm.nih.gov/pubmed/16025533. Pottier, L Pruvost, J Deremetz, J Cornet, J-F Legrand, J Dussap, C G eng Biotechnol Bioeng. 2005 Sep 5;91(5):569-82. doi: 10.1002/bit.20475.

[118] Benchling [biology software], 2021. URL Retrievedfromhttps://benchling.com.

[119] Addgene, 2021. URL www.addgene.org.

[120] Eurofins genomics, 2021. URL https://eurofinsgenomics.com/en/home/.

[121] Genscript, 2021. URL https://www.genscript.com/.

[122] Kegg. URL https://www.genome.jp/kegg/genes.html.

[123] Tiago Toscano Selão, Artur Włodarczyk, Peter J Nixon, and Birgitta Norling. Growth and selection of the cyanobacterium synechococcus sp. pcc 7002 using alternative nitrogen and phosphorus sources. *Metabolic engineering*, 54:255–263, 2019. ISSN 1096-7176.

APPENDIX A

EXPERIMENTAL PROCEDURES

A.1 Growth Conditions

A.1.1 *E. coli*

Culture volume: 5-10 mL

Culture vessel: 14 mL culture tubes

Agitation rate: 220 rpm

Media: LB broth

Light intensity: N/A

Optimal temperature: 37°C

A.1.2 *Synechococcus* 7002

Culture volume: 100-200 mL

Culture vessel: Beveled Erlenmeyer flasks, 100 mL culture in a 250 mL flask or 200 mL culture in a 500 mL flask

Agitation rate: 180 rpm

Media: A+ media or BG-11 with 4 μg/L vitamin B12

Light intensity: up to 250 μmol m^{-2} s^{-1}

Optimal temperature: 37°C

CO_2: Atmospheric concentration or 1%v/v

A.1.3 *Synechocystis* 6803

Culture volume: 100 mL

Culture vessel: 250 mL beveled Erlenmeyer flasks

Agitation rate: 120 rpm

Media: BG-11

Light intensity: up to 100 μmol m^{-2} s^{-1}

Optimal temperature: 30°C

CO_2: 1%v/v

A.2 Plasmid Construction and Screening

GOLDEN GATE RESTRICTION-LIGATION REACTIONS

MATERIALS:

- Plasmids of known concentration containing required acceptor vectors, linkers, modular parts, etc.
- Type II Restriction Enzyme and buffer
- T4 ligase and buffer (with 10 mM ATP)
- Ultrapure water
- 100 uL PCR tubes

METHOD:

1. Label PCR tubes and add the appropriate amount of water first *calculate amount of water needed before-hand.
    a. Enzymes are sensitive to buffer concentrations so it is imperative to be exact in volumes
2. Add 100-200 ng of acceptor vector
3. Add required DNA parts at between a 1:2 and 1:6 molar ratio (start with 1:2 and increase as needed)
    a. Concentrations depend on exact reaction, optimization likely needed, depending on final efficiency obtained
4. Add 2 ul each of RE buffer and T4 buffer to a 20uL reaction. Scale up as needed
5. Add 1ul of each enzyme (10u RE, 200 units T4 DNA ligase)
6. Run Thermocycler at following cycle:
    a. 37°C for 10 minutes
    b. 16°C for 10 minutes
        i. 5 rounds
    c. 37°C for 20 minutes
7. Cycle time can be optimized by increasing cycles and/or decreasing cycle length of steps 6.a and 6.b

Figure A.1 Protocol for restriction/ligation reactions to assemble modular level 0 parts into level 1 constructs for transformation into *E. coli* and blue/white screening.

LB ANTIBIOTIC PLATES FOR BLUE/WHITE SCREENING (CYANOGATE)

MATERIALS:

- *LB*
- Appropriate antibiotic stock solutions
- Two 500 mL Pyrex containers
- Agar
- Sodium Thiosulfate
- IPTG
- X-Gal
- 20 plates (labeled in clean hood prior to pouring)

METHOD:

Makes approx. 20 1.5%(w/v) plates (25 mL each)

1.) Add 7.5 g agar to 250 mL Ultra-pure water in one container.
2.) In a second container, add 10 g LB broth to 200 mL of water, then bring total volume to 250 mL.
3.) Cover and autoclave both solutions.
4.) Allow solutions to cool to 45-50 °C
5.) Add Appropriate Antibiotic, IPTG, and X-gal in clean hood to LB broth

Chemical	Stock Concentration (mg/mL)	Amount added (for total V of 500mL)	Working Concentration
IPTG (Not necessary for DH5 alpha strain)	238.3 (1 M)	0.5 mL (500µL)	1 mM
X-Gal	20	0.5 mL (500µL)	40 µg/mL
Spectinomycin dihydrocholoride pentahydrate (Level 0)	50	1 mL (1000µL)	100 µg/mL
Carbenicillin disodium (Level 1)	50	1 mL (1000µL)	100 µg/mL
Kanamycin Sulfate (Level T, may also use Spec)	50	2500??	50 µg/mL
Sodium Thiosulfate	24..8g/100mL	0.5 ml (500 µL)	

*for making individual AB plates into plates compatible for Blue White Screening:
Add 40uL X-Gal (stock concentration)
Add 4uL IPTG (stock concentration)
Spread evenly across surface of plate with sterile cell scrapers and let absorb dry for at least 30 minutes

6.) Combine both agar and liquid solution, mix well. Note the agar can solidify quickly.
7.) Pour plates with haste until the bottom of the plate is completely filled with liquid. Use flame thrower to pop bubbles immediately after pouring.
8.) Dry opened LB plates at room temperature under UV light for about 30 minutes.

Figure A.2 Protocol for LB plates with the appropriate concentrations of various antibiotics and other necessary ingredients for compatibility with *E. coli* blue-white screening procedures as described in Gale et al.[69].

COLONY PCR FOR CYANOBACTERIA

METHOD:

1. Streak strain of interest on agar plate to isolate single colonies. Grow until single colonies are clearly visible.
    a. Scoop lawn growth cyano plate with clean loop, then streak as shown by black line. Without changing loops or re-scooping cells, streak as shown by purple line, single colonies should appear.
    b. 
2. Pick single colony with a sterile loop and restreak on new plate
    a. Allow the single colony to grow.
3. After colony has grown up more, transfer a good sized scoop to 20 uL 100% DMSO in a pcr tube
4. Incubate at 95°C for 5 minutes in the thermocycler.
5. Transfer 1 uL of this mixture as the template to a new labeled PCR tube with appropriate primers, buffers and polymerase.
    a. 20 uL reaction is ideal, but volumes can be altered to fit application.
    b. Example Reaction
        i. 1 ul template
        ii. 1 ul each verification primer (10 mM stock)
        iii. 2 ul thermopol polymerase buffer
        iv. 1 ul Vent polymerase
        v. 1 ul dNTPs
        vi. 13 ul nuclease free MilliQ water
6. Run gel on PCR product as normal, adjust agarose percentage based on length of products and ladder.

Figure A.3 protocol for colony PCR in cyanobacteria to test for segregation of genes in a single colony of transformants.

A.3 Cyanobacterial Transformation

Synechococcus sp. PCC 7002 Transformation Method

Natural Transformation

Phase 1

Materials:

- *Synechococcus* sp. PCC 7002 cell culture in late exponential phase (OD_{730} = 0.7-0.9)
- 100 mL sterile A+ medium with Trace element added in a 250 mL baffled flask

Method:

1.) Inoculate 100 mL sterile A+ medium with trace elements to OD_{730} = 0.1 using *Synechococcus* sp. PCC 7002 cells in late exponential phase.
2.) Incubate the 100 mL cell culture at 180 rpm, 37°C, and 250 µE light until cells reach early/mid exponential phase (OD_{730} = 0.4-0.6; ~2 days).

Phase 2

Materials:

- 100 mL of *Synechococcus* sp. PCC 7002 cell culture in early/mid exponential phase (OD_{730} = 0.4-0.6)
- DNA samples of known concentration
- A+ agar plates
- A+ antibiotic plates
- 15 mL cell culture tubes
- Sterile A+ medium
- Sterile trace elements
- Sterile glass beads

Method:

3.) Spin down *Synechococcus* sp. PCC 7002 cells in early/mid exponential phase at 1449 x *g* for 10 minutes. Decant the supernatant.
4.) Resuspend the pellet in sterile A+ medium with trace elements to yield a final OD_{730} of 2.5.
5.) Aliquot 0.5 mL of the resuspended cells into sterile culture tubes.
6.) Add enough volume of DNA solution to yield 1 pmole of DNA to the cell suspension.
7.) Add the same volume of nuclease free water to the negative control.
8.) Place the tubes containing the DNA/cell suspension in the incubator under the following conditions: 180 rpm; 37°C; 250 µE light
9.) Allow suspension to incubate for at least 6 hours.
10.) Plate 3 150 µL of cells onto 3 A+ antibiotic marker plates using 5-7 sterile glass beads.
11.) Plate 50 µL of cells onto one A+ plates using 5-7 sterile glass beads.
12.) Allow cells to grow at 37°C, 1% CO_2, and 250 µE light until colonies appear.
13.) Pick colonies to streak onto selective plates until cells are homogenous.
14.) Scrape cells from streak plates and inoculate 5 mL liquid culture with antibiotic.
15.) Grow cells up in larger volumes until enough cells are available to make freezer stocks.

Figure A.4 Natural transformation of *Synechococcus* 7002

SYNECHOCYSTIS TRANSFORMATION BY ELECTROPORATION WITH PLASMID DNA

MATERIALS:

- *Synechocystis* sp. PCC 6803 (early exponential phase, OD_{750}~0.3-0.5)
- Ice-water bath
- Microcentrifuge tubes, chilled on ice
- Sterile DI water, ice cold
- DNA
- Electroporator
- Electroporation cuvettes (1mm gap)
- Sterile Ice-cold BG11 for washing
- Sterile BG11, 5 mM glucose for recovery
- 14 mL Culture tubes

METHOD:

1.) Perform Allow the culture to reach early-exponential phase (OD_{750}~0.3-0.5).
THE FOLLOWING STEPS MUST BE PERFORMED AT 4°C! KEEP EVERYTHING ON ICE!
2.) Transfer 1.5 mL culture to centrifuge tubes and submerse in ice bath for 15 minutes. Swirl occasionally to ensure even cooling. Always prepare more than you think you need in case arcing occurs.
3.) Pellet 1.5 mL cells by centrifugation at 6,000 xg for 5 minute at 4°C. Decant the supernatant and resuspend the cell pellet in 1 mL of sterile ice-cold BG-11 (no glucose).
4.) Harvest the washed cells by centrifugation at 6,000 xg for 5 minutes at 4°C.Decant the supernatant and re-spin the cells at 6,000 xg for 5 minute at 4°C and carefully pipette off all excess liquid.
5.) Add 5 µL (of 1 µg/mL concentration) of chilled plasmid DNA in water to the cell pellet and then add 45 µl sterile ice-cold water and pipette up and down to resuspend. Add 5 µL of chilled DI water to one of the cell suspensions to act as a negative control.
6.) Transfer the entire bacterial/DNA suspension (50 µL) to the chilled electroporation cuvette. Be sure that no bubbles are present (by taping the cuvette on the table quickly) and that the liquid forms a complete bridge between the two electrodes. Cap the cuvette. Wipe moisture from the cuvette and insert the cuvette into the electroporator.
7.) Electroporate the cuvette under the Prokaryotes setting at 1500V for 5 ms.
8.) As quickly as possible after the pulse, remove the electroporation cuvette and add 1 mL of warm BG-11 with 5 mM glucose medium.
9.) Allow cells to recover for 2 hours at 30°C, 180 rpm Make sure that you do not stress cells by adding bubbles or pipetting up/down too much during transfer.
10.) After incubation, plate 200-400 µL of cells on non-selective BG-11 agar plates with a 0.45 um filter paper overlaying the agar.
11.) Store the plates at room temperature until all of the liquid has been absorbed.
12.) Invert the plates and incubate at 30°C, 1% CO2, and 100 uE light for 24 hours.
13.) Using flame-sterilized tweezers, transfer the filter paper to a new, selective BG-11 plate.
14.) Invert the plates and incubate at 30°C, 1% CO2, and 100 uE light until colonies appear (about 4-7 days).

Figure A.5 Electroporation of *Synechocystis* 6803.

SYNECHOCYSTIS TRANSFORMATION BY CONJUGATION

MATERIALS:

- *Synechocystis* sp. PCC 6803 (early exponential phase, OD_{750}~0.5)
- *E. coli* DH5α with compatible plasmid (MOB and target construct)
- 14 mL culture tubes
- 2 mL microcentrifuge tubes
- BG-11 media
- LB broth
- LB-BG-11 plates (BG-11 with 5% v/v LB broth)
- BG-11 plates
- Appropriate antibiotics
- Swinging bucket and tabletop centrifuges
- Flame-sterilized forceps

METHOD:

1.) Allow *Synechocystis* sp. PCC 6803 culture to reach mid-exponential phase (OD_{750}~0.5). Grow about 2 days
2.) Allow *E. coli* strain with appropriate MOB gene and target plasmid to grow to steady state in overnight culture of 5 mL in a 14 mL culture tube. (1 mL culture is required per conjugation event)
3.) Prepare *E. coli* culture for conjugation.
    a. Centrifuge *E. coli* overnight cultures at 3,000 x g for 10 min at room temperature. Discard the supernatant.
    b. Wash cell pellet with 5 mL fresh LB broth without antibiotics, gently pipetting up and down to resuspend pellet, and repeat step 3.a.
        i. Repeat this process three times .
4.) Prepare *Synechocystis* sp. PCC 6803 culture for conjugation.
    a. Centrifuge the required volume of culture at 1500 x g for 10 min at room temperature. Discard the supernatant.
    b. Wash pellet with same volume of fresh BG-11 as used in step 4.a, gently pipetting up and down to resuspend pellet, and repeat step 4.a.
        i. Repeat this process three times.
5.) Aliquot 900 µL of cyanobacteial culture with 900 µL *E. coli* culture in a 2 mL tube. Mix by gently pipetting up and down.
6.) Incubate this mixture at room temperature for 30 min.
7.) Centrifuge mixed culture at 1500 x g for 10 minutes at room temperature. Discard all supernatant but 200 µL, and resuspend pellet in remaining supernatant by gentle pipetting.
8.) Spread 200 µL combined culture onto a 0.45 µm filter on BG-11 plates with 5% v/v LB broth without antibiotics.
    a. Incubate culture for 24 hours at 30°C and 100 µE light for 24 hours.
9.) After 24 hours, transfer the membrane using flame-sterilized forceps to a new BG-11 plate with the appropriate antibiotics, and incubate until cyanobacterial colonies appear (7-14 days).
10.) Replate single colonies on new BG-11 plates with the appropriate antibiotic to isolate transformant strains.
    a. Multiple rounds of replating may be needed to obtain monoculture

Figure A.6 Conjugation in *Synechocystis* 6803.

APPENDIX B

PLASMIDS, PRIMERS, AND DNA SEQUENCES

All vectors constructed for this thesis were designed first in the online DNA editing software, Benchling[118]. DNA sequences for standard Cyanogate and MoClo parts were retrieved from Addgene[119]. I designed primers for sequence amplification, verification, and more using tools in Benchling, and all primers were ordered from Eurofins[120] and re-suspended in water to stock concentration of 10μM for use with various applications. Custom gene sequences were synthesized by Genscript[121] and integrated into the golden gate modular cloning infrastructure. Gene sequences for *dxr* and *fbp1* can be found in the KEGG database [122] by searching the gene names slr00119 and SYNPCC7002_A1301, respectively. Supporting materials for the construction of these cyanobacterial mutants can be found here.

Table B.1 List of final Level T plasmids transformed into either *Synechococcus* 7002 or *Synechocystis* 6803 by electroporation, conjugation, or natural transformation. Ligation between parts are denoted by dashes, with the first part indicating the most upstream sequence, and the last part representing the acceptor vector. For example:
Part_1-Part_2-Part_3-Linker-Acceptor_vector-.

Plasmid name	Source	Description	Selection Marker
SBP_J23119T	This Study	Level T construct: Integrative vector for cyanobacterial transformation and insertion of the SBPase gene promoted by the J23119 promoter into NS1 of *Synechococcus* 7002. SBPL1P1-J23119L1-SBPL1P3-SBPL1P4-pICH41780-pCAT.334-	Spectinomycin
SBP_J23109T	This Study	Level T construct: Integrative vector for cyanobacterial transformation and insertion of the SBPase gene promoted by the J23109 promoter into NS1 of *Synechococcus* 7002. SBPL1P1-J23109L1-SBPL1P3-SBPL1P4-pICH41780-pCAT.334-	Spectinomycin
SBP_J23108T	This Study	Level T construct: Integrative vector for cyanobacterial transformation and insertion of the SBPase gene promoted by the J23108 promoter into NS1 of *Synechococcus* 7002. SBPL1P1-J23108L1-SBPL1P3-SBPL1P4-pICH41780-pCAT.334-	Spectinomycin
CrLT69	This Study	Level T construct: CRISPRi system for inducible repression of the DXR gene in *Synechocystis* 6803 on a self-replicating plasmid. Targets base pair 69 from the beginning of the ORF of the DXR gene. CrL1P1-69r_L1P2-pICH41744-pCAT.000-	Carbenicillin, Kanamycin
CrLT178	This Study	Level T construct: CRISPRi system for inducible repression of the DXR gene in *Synechocystis* 6803 on a self-replicating plasmid. Targets base pair 178 from the beginning of the ORF of the DXR gene. CrL1P1-178f_L1P2-pICH41744-pCAT.000-	Carbenicillin, Kanamycin

Table B.1 Continued.

Plasmid name	Source	Description	Selection Marker
DST	This Study	Level T construct: Integrative vector for cyanobacterial transformation and disruption of the genomic DXR gene in the *Synechocystis* 6803 genome. DSL1P1-pICH41722-pCAT.334-	Spectinomycin
DRT	This Study	Level T construct: Self-replicating vector for inducible expression of DXR in *Synechocystis* 6803. Counterselectable marker (SacB) present for counterselection of plasmid. DRL1P1-DRL1P2-pICH41744-pCAT.000	Carbenicillin, Kanamycin
NirAT_eYFP	This Study	Level T construct: Self-replicating vector for inducible expression of the eYFP reporter protein using the NirA promoter for promoter strength characterization. NirAL1-pICH41722-pCAT.000	Carbenicillin, Kanamycin
J23119T_eYFP	This Study	Level T construct: Self-replicating vector for expression of the eYFP reporter protein using the J23119_TSS promoter custom assembled with the same 5'-UTR as the NirA promoter for promoter strength characterization. NirAL1-pICH41722-pCAT.000	Carbenicillin, Kanamycin

Table B.2 List of plasmids, acceptor vectors, modular parts and level 1 constructs used and synthesized by golden gate cloning techniques using the Cyanogate and MoClo toolkits.

Plasmid name	Source	Description	Selection Marker
pCAT.000	Cyanogate Kit [59]	Level T part: Self-replicating level T acceptor vector for cyanobacterial transformation	Carbenicillin, Kanamycin
pCAT.334	Cyanogate Kit [59]	Level T part: Integrative level T acceptor vector for cyanobacterial transformation	Spectinomycin
pICH47732	MoClo Kit [60] [61]	Level 1 Part: Level 1 Position 1 (L1P1) acceptor vector	Carbenicillin
pICH47742	MoClo Kit [60] [61]	Level 1 Part: Level 1 Position 2 (L1P2) acceptor vector	Carbenicillin
pICH47751	MoClo Kit [60] [61]	Level 1 Part: Level 1 Position 3 (L1P3) acceptor vector	Carbenicillin
pICH47761	MoClo Kit [60] [61]	Level 1 Part: Level 1 Position 4 (L1P4) acceptor vector	Carbenicillin
pICH41722	MoClo Kit [60] [61]	Level 1 part: end linker for L1P1 ligation	Spectinomycin
pICH41744	MoClo Kit [60] [61]	Level 1 part: end linker for L1P2 ligation	Spectinomycin
pICH41766	MoClo Kit [60] [61]	Level 1 part: end linker for L1P3 ligation	Spectinomycin
pICH41780	MoClo Kit [60] [61]	Level 1 part: end linker for L1P4 ligation	Spectinomycin
pC0.053	Cyanogate Kit [59]	Level 0 part: NirA nitrogen inducible promoter	Spectinomycin
pC0.027	Cyanogate Kit [59]	Level 0 part: Kanamycin resistance cassette	Spectinomycin
pC0.082	Cyanogate Kit [59]	Level 0 part: double terminator	Spectinomycin
pC0.119	Cyanogate Kit [59]	Level 0 part: SacB uplinker	Spectinomycin

Table B.2 Continued.

Plasmid name	Source	Description	Selection Marker
pC0.026	Cyanogate Kit [59]	Level 0 part: SacB cassette	Spectinomycin
pC0.028	Cyanogate Kit [59]	Level 0 part: Spectinomycin resistance cassette	Spectinomycin
pC0.017	Cyanogate Kit [59]	Level 0 part: dCas9 sequence	Spectinomycin
pC0.219	Cyanogate Kit [59]	Level 0 part: J23119 promoter truncated to the Transcription start site for use with sgRNA	Spectinomycin
pC0.122	Cyanogate Kit [59]	Level 0 part: sgRNA scaffold	Spectinomycin
pC0.117	Cyanogate Kit [59]	Level 0 part: Upstream neutral cite homology arm linker	Spectinomycin
pC0.118	Cyanogate Kit [59]	Level 0 part: Downstream neutral cite homology arm linker	Spectinomycin
pC0.283	Cyanogate Kit [59]	Level 0 part: Upflanking homology to Neutral site 1 (NS1) in the *Synechococcus* 7002 synechococcus genome	Spectinomycin
pC0.284	Cyanogate Kit [59]	Level 0 part: downflanking homology to Neutral site 1 (NS1) in the *Synechococcus* 7002 synechococcus genome	Spectinomycin
pC0.121	Cyanogate Kit [59]	Level 0 part: Antibiotic resistance cassette uplinker	Spectinomycin
pC0.120	Cyanogate Kit [59]	Level 0 part: Antibiotic resistance cassette downlinker	Spectinomycin
pC0.008	Cyanogate Kit [59]	Level 0 part: eYFP open reading frame	Spectinomycin

Table B.2 Continued.

Plasmid name	Source	Description	Selection Marker
SBPL1P1	This Study	Level 1 Construct: Neutral site upstream homology region for insertion into *Synechococcus* 7002. pC0.283-pC0.117-pICH47732-	Carbenicillin
J23119L1	This Study	Level 1 Construct: SBPase expression cassette using the J23119 promoter. 7002_J23119&RBS-SBP_ORF-pC0.082-pICH47742	Carbenicillin
J23109L1	This Study	Level 1 Construct: SBPase expression cassette using the J23109 promoter. 7002_J23109&RBS-SBP_ORF-pC0.082-pICH47743	Carbenicillin
J23108L1	This Study	Level 1 Construct: SBPase expression cassette using the J23108 promoter. 7002_J23108&RBS-SBP_ORF-pC0.082-pICH47744	Carbenicillin
SBPL1P3	This Study	Level 1 Construct: Kanamycin resistance cassette for insertion marker. pC0.121-pC0.027-pC0.120-pICH47751	Carbenicillin
SBPL1P4	This Study	Level 1 Construct: Neutral site downstream homology region for insertion into *Synechococcus* 7002. pC0.118-pC0.284-pICH47761-	Carbenicillin
CrL1P1	This Study	Level 1 Construct: dCas9 expression cassette using the NirA promoter. pC0.053-pC0.017-pC0.082-pICH47732-	Carbenicillin

Table B.2 Continued.

Plasmid name	Source	Description	Selection Marker
69r_L1P2	This Study	Level 1 Construct: sgRNA expression cassette targeting the DXR gene at base pair 69 from the beginning of the open reading frame, promoted by the J23119 promoter truncated to the transcription start site. pC0.219-6803_DXR_69r_sgRNA-pC0.122-pICH47742-	Carbenicillin
178f_L1P2	This Study	Level 1 Construct: sgRNA expression cassette targeting the DXR gene at base pair 178 from the beginning of the open reading frame, promoted by the J23119 promoter truncated to the transcription start site. pC0.219-6803_DXR_178f_sgRNA-pC0.122-pICH47742-	Carbenicillin
DRL1P1	This Study	Level 1 Construct: DXR expression cassette using the NirA promoter. pC0.053-DXR_ORF-pC0.082-pICH47732-	Carbenicillin
DRL1P2	This Study	Level 1 Construct: SacB cassette for counterselection of the final self replicating plasmid. Custom linkers were used to construct the vector. pC0.119-pC0.026-specdummy-pICH47742-	Carbenicillin
DSL1P1	This Study	Level 1 Construct: Knockout cassette for the DXR gene. DXR_UP_homology-pC0.027-DXR_DOWN_homology-pICH47732	Carbenicillin
NirAL1	This Study	Level 1 Construct: eYFP promoted by the NirA promoter. pC0.053-pC0.008-pC0.082-pICH47732-	Carbenicillin

Table B.2 Continued.

Plasmid name	Source	Description	Selection Marker
J23119_5UTR_L1	This Study	Level 1 Construct: eYFP promoted by the J23119 promoter customized with the same 5' untranslated region as the NirA promoter. J23119_TSS+5UTR-pC0.008-pC0.082-pICH47732-	Carbenicillin

Table B.3 List of primers

Primer Name	Purpose	Sequence (5'-3')	Source
DXR_verif_F	Forward primer for verification of genomic DXR knockout	ACTACGCCGCTAAATATGCC	This study
Spec_V_R	Reverse primer for verification of genomic DXR knockout	AGTTGAGGTGACCATCGTAG	This study
DXR_V_R	Reverse primer for verification of genomic DXR knockout	ACAACCGACAATACCTGTGAC	This study
SBP_verif_F	Forward primer for verification of genomic SBPase overexpression	CGCTATCTAGTCACGCTTTTG	This study
SBP_verif_R	Reverse primer for verification of genomic SBPase overexpression	TGAATGACCTCATCGGACAC	This study
NSI_us_F	Forward primer for verification of genomic Limonene Synthase expression	CTAGCACAAATGAAGCCCGAC	[31]
NSI_ds_R	Reverse primer for verification of genomic Limonene Synthase expression	GCAGATATAAGCAACGGTACAG	[31]

Table B.3 Continued.

Primer Name	Purpose	Sequence (5'-3')	Source
U250Forward	Primer to amplify upstream homology arm of DXR	TTTTTGGTCTCAGG AGAAATCAAGCAAT TGACCTTGGATG	This study
U250Reverse	Primer to amplify upstream homology arm of DXR	AAAAAGGTCTCAA CCTTACCGCCGTT GCTTAAGCTAAAAC	This study
D250Forward	Primer to amplify downstream homology arm of DXR	TTTTTGGTCTCAG CTTAGTCTAGTTG GCTTCAACTTTGAC	This study
D250Reverse	Primer to amplify downstream homology arm of DXR	AAAAAGGTCTCA AGCGCTGTGGGG TTTTCCTCACCTCAAC	This study
SpecdummyForward	Primer used to make custom linker in self-replicating vector DRT	TTTTTGGTCTCAAG GTAAATCAAGCAAT TGACCTTGG	This study
SpecdummyReverse	Primer used to make custom linker in self-replicating vector DRT	AAAAAGGTCTCAAG CGCCAAGGTCAATT GCTTGATTT	This study
69rForward	Primer used to make 6803_DXR_69r_sgRNA custom part by oligonucleotide overlap synthesis	TTTTTGGTCTCTT AGCACCACCTGAA AAGCATCAGGATGATGG	This study

Table B.3 Continued.

Primer Name	Purpose	Sequence (5'-3')	Source
69rReverse	Primer used to make 6803_DXR_69r_sgRNA custom part by oligonucleotide overlap synthesis	GGGAAGGTCTCTA AACCCATCATCC TGATGCTTTTCAGGTGGT	This study
178fForward	Primer used to make 6803_DXR_178f_sgRNA custom part by oligonucleotide overlap synthesis	TTTTTGGTCTCTTA GCAGAGATTGTTGC GATTCGTCAGG	This study
178fReverse	Primer used to make 6803_DXR_178f_sgRNA custom part by oligonucleotide overlap synthesis	GGGAAGGTCTCTA AACCCTGACGAA TCGCAACAATCTCT	This study
L1_4254_F	External sequencing primer for level one constructs	TGGCTGGTGGCAGGATATATTG	This study
L1_120_R	External sequencing primer for level one constructs	TACAAATGGACGAACGGATAAACC	This study
SBPL1P2_4731_F	Internal sequencing primer for SBPL1P2 construct	CCCGATGAACTGATCGAAATTGAC	This study
SBPL1P2_5182_F	Internal sequencing primer for SBPL1P2 construct	TGGTCACTTCCAAGGGCAAC	This study

Table B.3 Continued.

Primer Name	Purpose	Sequence (5'-3')	Source
SBPL1P2_4722_R	Internal sequencing primer for SBPL1P2 construct	GGGTCAACGGCGATGTCAATTTCG	This study
SBPL1P2_5215_R	Internal sequencing primer for SBPL1P2 construct	CGATTCCAGTCCGCACTTTC	This study
SBPL1P3_4783_F	Internal sequencing primer for SBPL1P3 construct	AAAGCCGTTTCTGTAATGAAGG	This study
SBPL1P3_5143_F	Internal sequencing primer for SBPL1P3 construct	AACACTGCCAGCGCATCAAC	This study
SBPL1P3_4826_R	Internal sequencing primer for SBPL1P3 construct	AGTCGGAATCGCAGACCGATAC	This study
SBPL1P3_5223_R	Internal sequencing primer for SBPL1P3 construct	TTTATCCGTACTCCTGATGATGC	This study
CrL1P1_6359_R	Internal sequencing primer for CrL1P1 construct	CAACAATGGCTTTCTTCTGTTC	This study
CrL1P1_6197_F	Internal sequencing primer for CrL1P1 construct	GTCGATAAAGGTGCTTCAGCTC	This study
CrL1P1_8209_R	Internal sequencing primer for CrL1P1 construct	GTGATCCCTAGTAACTCTTTAACG	This study

Table B.3 Continued.

Primer Name	Purpose	Sequence (5'-3')	Source
CrL1P1_7831_F	Internal sequencing primer for CrL1P1 construct	CAAGAAATAGGCAAAGCAACC	This study
DRL1P1_5045_F	Internal sequencing primer for DRL1P1 construct	TGCTTTAGCCAATAAGGAAACG	This study
DRL1P1_5290_R	Internal sequencing primer for DRL1P1 construct	GTTACAAACGGTAATCTTTCCACC	This study
DRL1P2_5858_R	Internal sequencing primer for DRL1P1 construct	GCGCGTTCAATTTCATCTGTTAC	This study
DRL1P2_5651_F	Internal sequencing primer for DRL1P1 construct	TGAAGCAAACACTGGAACTG	This study
eYFP_F	Internal sequencing primer for both eYFP constructs	ACCACATGAAGCAGCACGAC	This study
eYFP_R	Internal sequencing primer for both eYFP constructs	GTTGTGGCTGTTGTAGTTGTACTC	This study
Cr_ext_F	External sequencing primer for level T constructs using the pCAT.000 acceptor vector	AAATAGGCGTATCACGAGGC	This study

Table B.3 Continued.

Primer Name	Purpose	Sequence (5'-3')	Source
Cr_ext_R	External sequencing primer for level T constructs using the pCAT.000 acceptor vector	CGTGACAGTTAGTACGGGAG	This study
CrL1P1_6197_F	Internal sequencing primer for CR69 and CR178 level T constructs	GTCGATAAAGGTGCTTCAGCTC	This study
CrL1P1_6359_R	Internal sequencing primer for CR69 and CR178 level T constructs	CAACAATGGCTTTCTTCTGTTC	This study
CrL1P1_8209_R	Internal sequencing primer for CR69 and CR178 level T constructs	GTGATCCCTAGTAACTCTTTAACG	This study
CrL1P1_7831_F	Internal sequencing primer for CR69 and CR178 level T constructs	CAAGAAATAGGCAAAGCAACC	This study
CrT11479_F	Internal sequencing primer for CR69 and CR178 level T constructs	CAGTCCTAGTGGTTGCTAAGG	This study
CrT11655_R	Internal sequencing primer for CR69 and CR178 level T constructs	TTTGTAATTCTCCGGCACTAGC	This study

Table B.3 Continued.

Primer Name	Purpose	Sequence (5'-3')	Source
SBPT_ext_F	External sequencing primer for level T SBPT constructs	GTTAGCTCACTCATTAGGCAC	This study
SBPT_ext_R	External sequencing primer for level T SBPT constructs	TTAAGTTGGGTAACGCCAGGG	This study
SBPL1P2_4722_R	Internal sequencing primer for level T SBPT constructs	GGGTCAACGGCGATGTCAATTTCG	This study
SBPT_3898_F	Internal sequencing primer for level T SBPT constructs	AGTTGTCGAACAAGCGGCGA	This study
SBPL1P3_5223_R	Internal sequencing primer for level T SBPT constructs	TTTATCCGTACTCCTGATGATGC	This study
SBPL1P3_5143_F	Internal sequencing primer for level T SBPT constructs	AACACTGCCAGCGCATCAAC	This study
DST_3556_F	Internal sequencing primer for level T DST constructs	ACAGGCCAGCCATTACGCTC	This study
DST_3658_R	Internal sequencing primer for level T DST constructs	GCGCCGGTTGCATTCGATTC	This study
DRL1P1_5045_F	Internal sequencing primer for level T DST constructs	TGCTTTAGCCAATAAGGAAACG	This study

Table B.3 Continued.

Primer Name	Purpose	Sequence (5'-3')	Source
DXR_9888_R	Internal sequencing primer for level T DST constructs	CTTTCGCAAACGCTTGAGTTG	This study
DRL1P2_5858_R	Internal sequencing primer for level T DST constructs	GCGCGTTCAATTTCATCTGTTAC	This study
DRL1P2_5651_F	Internal sequencing primer for level T DST constructs	TGAAGCAAACACTGGAACTG	This study

Table B.4 List of custom sequences needed to construct the final vectors used for cyanobacterial transformation in these studies.

Plasmid name Sequence (5'-3')	Source Source	Description Name	Description
6803_DXR_69r_sgRNA	small guide RNA sequence targeting base pair 69 from the beginning of the open reading frame, for guiding dCas9 to the DXR gene for transcription repression. Outfitted with the appropriate restriction sites and four base pair overhangs for direct use with the Cyanogate Kit.	TTTTTGGTCTCTTAGCAC CACCTGAAAAGCATCAGGA TGATGGGTTTAGAGACCTTCCC	This study

Table B.4 Continued.

Plasmid name	Source	Description	Selection Marker
6803_DXR_178f_sgRNA	small guide RNA sequence targeting base pair 178 from the beginning of the open reading frame, for guiding dCas9 to the DXR gene for transcription repression. Outfitted with the appropriate restriction sites and four base pair overhangs for direct use with the Cyanogate Kit.	TTTTTGGTCTCTTAGCAGA GATTGTTGCGATTCGTCAG GGTTTAGAGACCTTCCC	This study

Table B.4 Continued.

Plasmid name	Source	Description	Selection Marker
7002_J23119&RBS	J23119 Synthetic promoter outfitted with RBS used for characterization of the promoter in *Synechococcus* 7002 in previous studies. BpiI restriction sites flank both ends of the promoting sequence for insertion into the level zero acceptor vector as a promoter part.	AGCAGTTACAGACCTTGA AGACATGGAGTTGACAGC TAGCTCAGTCCTAGGTAT AATGCTAGCTACTAGTGC ATCGCTATCGCGTATACT ATTTAGGGATCACATACA ATGTTGTCTTCTTTTCC	This study, someone else too

Table B.4 Continued.

Plasmid name	Source	Description	Selection Marker
7002_J23109&RBS	J23109 Synthetic promoter outfitted with RBS used for characterization of the promoter in *Synechococcus* 7002 in previous studies. BpiI restriction sites flank both ends of the promoting sequence for insertion into the level zero acceptor vector as a promoter part.	AGCAGTTACAGACCTTGA AGACATGGAGTTTACAGC TAGCTCAGTCCTAGGGAC TGTGCTAGCTACTAGTGC ATCGCTATCGCGTATACTA TTTAGGGATCACATACAAT GTTGTCTTCTTTTCC	This study, someone else too

Table B.4 Continued.

Plasmid name	Source	Description	Selection Marker
7002_J23108&RBS	J23108 Synthetic promoter outfitted with RBS used for characterization of the promoter in *Synechococcus* 7002 in previous studies. BpiI restriction sites flank both ends of the promoting sequence for insertion into the level zero acceptor vector as a promoter part.	AGCAGTTACAGACCTTGA AGACATGGAGCTGACAGC TAGCTCAGTCCTAGGTAT AATGCTAGCTACTAGTGC ATCGCTATCGCGTATACT ATTTAGGGATCACATACA ATGTTGTCTTCTTTTCC	This study
specdummy	custom part for use in DRL1P2 to link SacB gene to the end of the L1P2 acceptor without an antibiotic resistance cassette.	TTTTTGGTCTCAAGGTAA ATCAAGCAATTGACCTTG GCGCTTGAGACCTTTTT	This Study

Table B.4 Continued.

Plasmid name	Source	Description	Selection Marker
J23119_TSS+5UTR	Custom sequence for the J23119 promoter outfitted with the same 5'UTR as the NirA promoter (pC0.053) for consistency in promoter characterization.	TGGCCGATTCATTAATCA CTCTGTGGTCTCTGGAGT TGACAGCTAGCTCAGTCC TAGGTATAATGCTAGCTG TTATCTGGCTAGTGGAGG TTACTAGAATGTGAGACC ACGAA	This Study
DXR_UP_homology	Approximately 250 homologous basepairs within the DXR gene in *Synechocystis* 6803 for disruption of the gene by an antibiotic cassette. The homology arms are flanked with the appropriate restriction enzyme sites and four base pair overhangs for direct use with the Cyanogate kit and MoClo modular cloning kits	TTTTTGGTCTCAGGAGAA ATCAAGCAATTGACCTTG GATGACTACGCCGCTAAA TATGCCAAAGGTGAATTA ACCGCCACCTCCCGCACC TCCGTTGCTGTGTAGATT GAAGTTAATTTTTCGTTT CTAAGTTTTGCCTTAGTA AAAACAAGAGAATAAATA ATTTTGCTCCTCCTTGGT TCAATCCTGGGGGAGTTT TTTCTTCTCAGATGGGCG GCAACCCCGTAAGATTGG GAAGATTAGTTTTAGCTT AAGCAACGGCGGTAAGGT TGAGACCTTTTT	This Study

Table B.4 Continued.

Plasmid name	Source	Description	Selection Marker
DXR_DOWN_homology	Approximately 250 homologous basepairs within the DXR gene in *Synechocystis* 6803 for disruption of the gene by an antibiotic cassette. The homology arms are flanked with the appropriate restriction enzyme sites and four base pair overhangs for direct use with the Cyanogate kit and MoClo modular cloning kits	TTTTTGGTCTCAGCTTAG TCTAGTTGGCTTCAACTT TGACCGGAATTATTTACC CAAGGATGGTGGGGGATT CTGGTTAGTTTTAGCGGG TCATCAGGCGATCGCCAA AATATTTCTGATAATTTC ACTAAGTTTGACTGAAAT TTAACTAATCAAAACGGG GATCACCCATTGCTCTAT GTCCACTGATTCTGTTAA CTGTCGGGGTCAAAAACA GGGAATCTGGGCACAGGA TTATGGCGGTTGAGGTGA GGAAAACCCCACAGCGCT TGAGACCTTTTT	This Study
	Se		

APPENDIX C

COPYRIGHT PERMISSIONS

C.1 Copyright Permission for NOAA Data

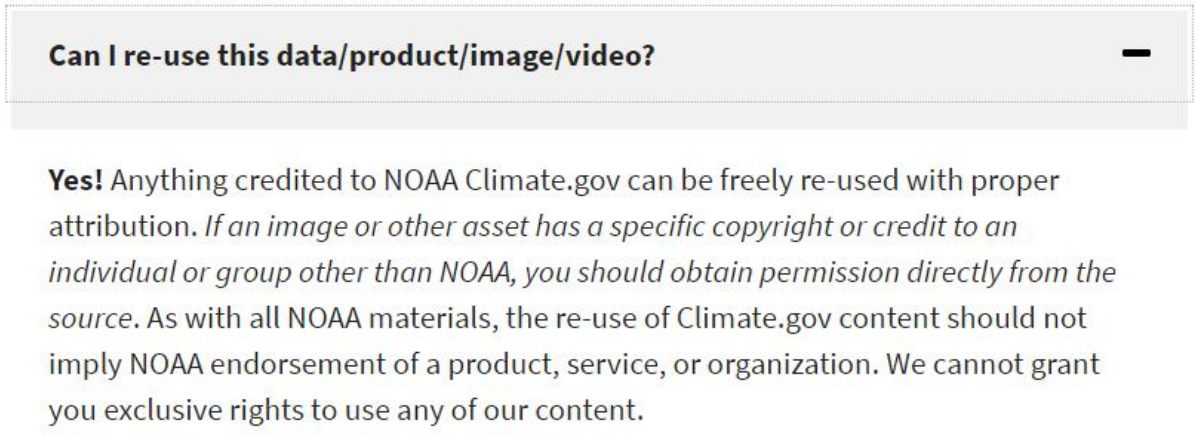

Figure C.1 Copyright permission for NOAA data. Copy right permission stated on the NOAA website for use of Figure 1.1 and Figure 1.2(https://www.climate.gov/faqs)

C.2 Copyright Permission for ^{13}C Workflow from Sake et al.

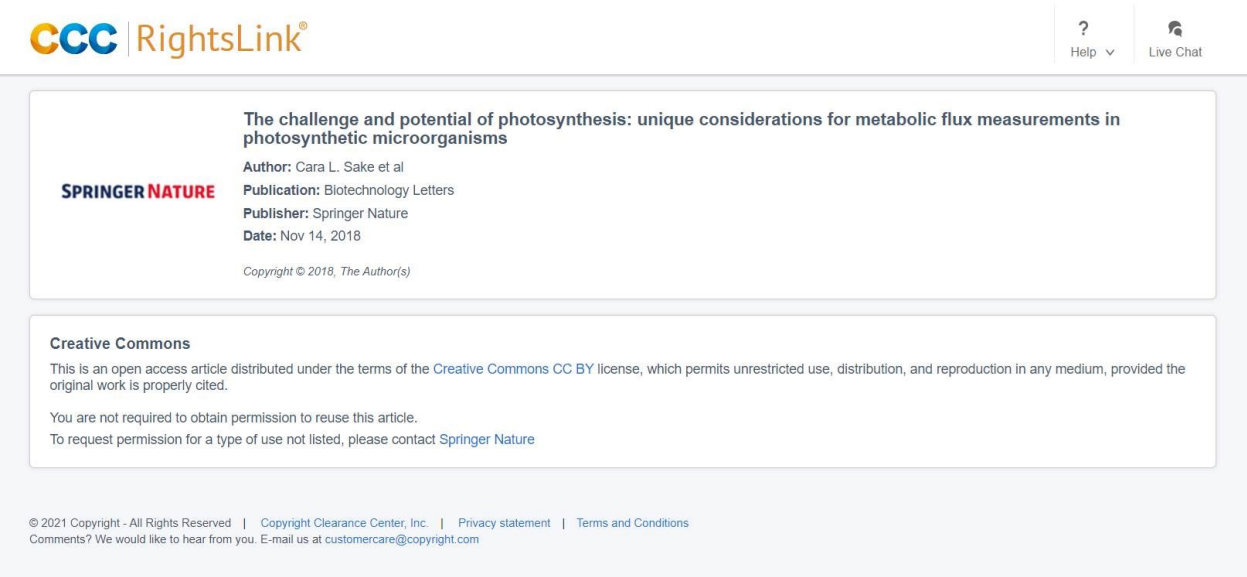

Figure C.2 Copyright permission for ^{13}C workflow figure. The paper titled "The challenges and potential of photosynthesis: unique considerations for metabolic flux measurements in photosynthetic microorganisms" by Sake et al. [77] is an Open Access article, distributed under the Creative Commons CC BY license (http://creativecommons.org/licenses/by/4.0/) and available for unrestricted reuse.

C.3 Copyright Permission for CRISPRi Description Figure from Hogan et al.

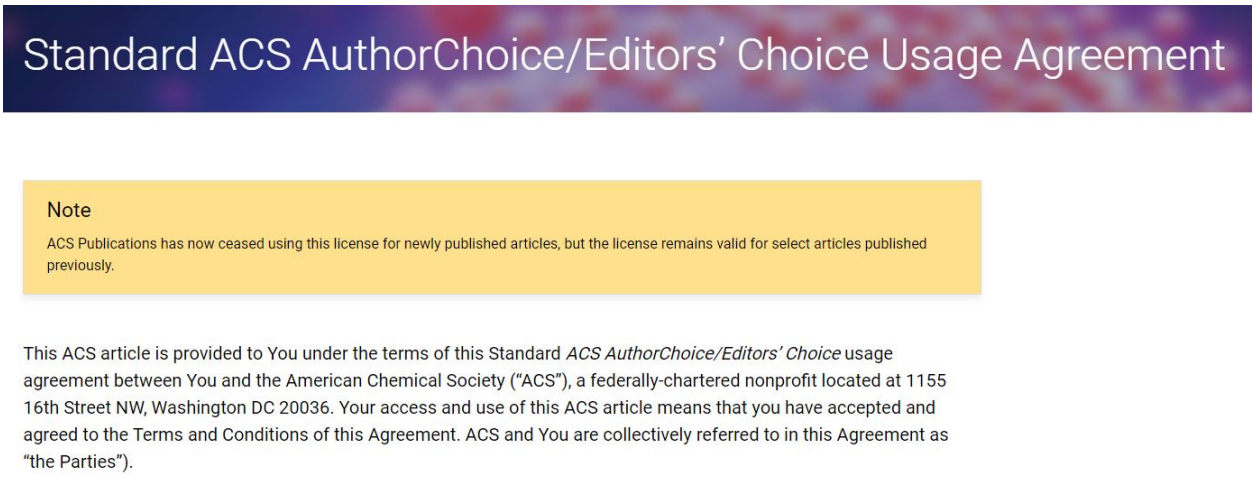

Figure C.3 Copyright permission for CRISPRi Description Figure. This is an unofficial adaptation of an article that appeared in an ACS publication. ACS has not endorsed the content of this adaptation or the context of its use. Figure 3.8 was published in the ACS Synthetic Biology Journal in 2019 by Hogan et al.[68] and is available to be used for non-commerical purposes under the ACS AuthorChoice License (https://pubs.acs.org/page/policy/authorchoice$_{t}ermsofuse.html$)

APPENDIX D

SUPPLEMENTARY INFORMATION FOR CHAPTER 4

Table D.1 Metabolic network and Associated Atom Transitions. The main reactions of cyanobacterial central metabolism and their atom transitions supplied to the INCA model.

RUBP (abcde) + CO2 (f) ->3PG (cde) + 3PG (fba)
3PG (abc) <->GAP (abc)
GAP (abc) <->DHAP (abc)
FBP (abcdef) <->GAP (abc) + DHAP (abc)
FBP (abcdef) <->F6P (abcdef)
F6P (abcdef) <->G6P (abcdef)
G6P (abcdef) ->RU5P (bcdef) + CO2 (a)
DHAP (abc) + E4P (defg) ->SBP (cbadefg)
SBP (abcdefg) ->S7P (abcdefg)
F6P (abcdef) <->GAP (def) + EC3 (abc)
S7P (abcdefg) <->E4P (defg) + EC3 (abc)
F6P (abcdef) <->E4P (cdef) + EC2 (ab)
S7P (abcdefg) <->R5P (cdefg) + EC2 (ab)
X5P (abcde) <->GAP (cde) + EC2 (ab)
RU5P (abcde) <->X5P (abcde)
RU5P (abcde) <->R5P (abcde)
RU5P (abcde) ->RUBP (abcde)
RUBP (abcde) ->3PG (cde) + 2PG (ba)
2PG (ab) ->GLYC (ab)
GLYC (ab) ->GOX (ab)
GOX (ab) + GOX (cd) ->GA (abd) + CO2 (c)
GA (abc) <->2PGA (abc)
3PG (abc) <->2PGA (abc)
2PGA (abc) <->PEP (abc)
PEP (abc) ->PYR (abc)
PYR (abc) ->ACA (bc) + CO2 (a)
OAA (abcd) + ACA (ef) ->CIT (dcbfea)
CIT (abcdef) <->ICI (abcdef)
ICI (abcdef) ->AKG (abcde) + CO2 (f)
AKG (abcde) ->SSA (bcde) + CO2 (a)
SSA (abcd) ->SUC (abcd)
SUC (abcd) <->FUM (abcd)
FUM (abcd) <->MAL (abcd)

Table D.1 Continued.

MAL (abcd) <->OAA (abcd)
PEP (abc) + CO2 (d) ->OAA (abcd)
MAL (abcd) ->PYR (abc) + CO2 (d)
0.4197*R5P + 3.579*ACA + 0.2171*E4P + 1.07*3PG + 0.5718*PEP + 2.728*PYR + 0.7506*OAA (abcd) + 0.7473*AKG + 0.21*GAP + 1.279*G1P ->34.22*Biomass + 0.6313*FUM (abcd) + 1.536*CO2
G6P (abcdef) + dummy ->RU5P (bcdef) + CO2 (a)
GOX (ab) + GOX (cd) + dummy ->GA (abd) + CO2 (c)
PYR (abc) + dummy ->ACA (bc) + CO2 (a)
ICI (abcdef) + dummy <->AKG (abcde) + CO2 (f)
AKG (abcde) + dummy ->SSA (bcde) + CO2 (a)
PEP (abc) + CO2 (d) ->OAA (abcd) + dummy
MAL (abcd) + dummy ->PYR (abc) + CO2 (d)
0*3PG (abc) ->3PG.s (abc)
0*3PG.u (abc) ->3PG.s (abc)
3PG.s ->sink
0*RU5P (abcde) ->RU5P.s (abcde)
0*RU5P.u (abcde) ->RU5P.s (abcde)
RU5P.s ->sink
0*PEP (abc) ->PEP.s (abc)
0*PEP.u (abc) ->PEP.s (abc)
PEP.s ->sink
0*GAP (abc) ->GAP.s (abc)
0*GAP.u (abc) ->GAP.s (abc)
GAP.s ->sink
G6P (abcdef) <->G1P (abcdef)
0*DHAP (abc) ->DHAP.s (abc)
0*DHAP.u (abc) ->DHAP.s (abc)
DHAP.s ->sink
CO2.l (a) ->CO2.x (a)
CO2.u (a) ->CO2.x (a)
[7]GAP (def) + PYR (abc) ->DOXP (defba) + CO2 (c)
[7]DOXP (abcde) + DOXP (fghij) ->LIM (abcdefghij)
CO2.x (a) ->CO2 (a)
CO2.u (a) + dummy ->CO2 (a)

[7]Applies only to the LS strain

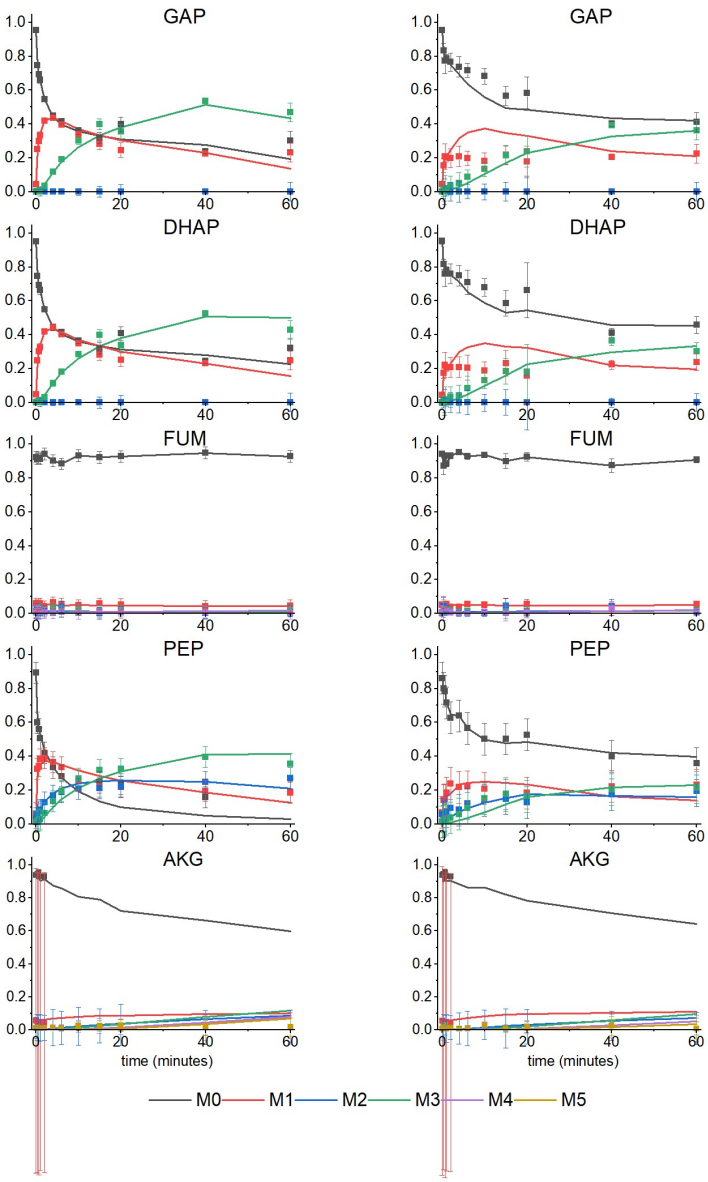

Figure D.1 Labeling dynamics of measured metabolites GAP, DHAP, FUM, PEP and AKG. Mass isotopomer distributions are shown by symbols over time and are calculated as the mean of three biological replicates (n=3). Error bars represent the highest value of either standard error between replicates (n=3) or to the error required to correct the zero timepoint value to the expected distribution vector. Lines represent the model fit to the experimental data in the solved flux map (Figure 4.6.)

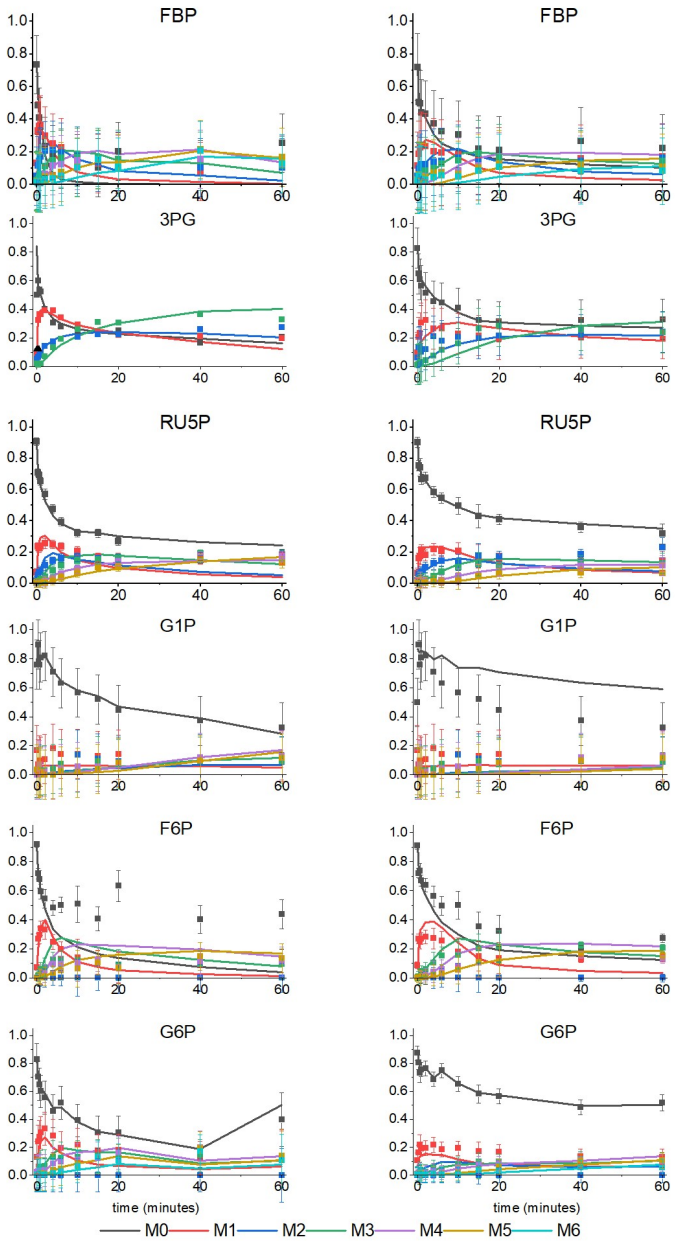

Figure D.2 Labeling dynamics of measured metabolites: FBP, 3PG, RU5P, G1P, FBP, G6P. Mass isotopomer distributions are shown by symbols over time and are calculated as the mean of three biological replicates (n=3). Error bars represent the highest value of either standard error between replicates (n=3) or to the error required to correct the zero timepoint value to the expected distribution vector. Lines represent the model fit to the experimental data in the solved flux map (Figure 4.6.)

Table D.2 Simulated Flux Values and Bounds. Parameter continuation was used to determine the upper and lower bound of each reaction flux to a 95% confidence interval. Biomass: 0.4197*R5P + 3.579*ACA + 0.2171*E4P + 1.07*3PG + 0.5718*PEP + 2.728*PYR + 0.7506*OAA + 0.7473*AKG + 0.21*GAP + 1.279*G1P -¿ 34.22*Biomass + 0.6313*FUM + 1.536*dummy.

Reaction	WT Flux	WT StdErr	WT LB	WT UB	LS Flux	LS StdErr	LS LB	LS UB
RUBP + CO2 ->3PG + 3PG	72.68	3.71	63.99	82.30	70.96	3.65	63.08	78.96
3PG <-> GAP	127.97	6.53	112.80	143.73	124.96	6.43	111.03	139.18
GAP <-> DHAP	51.42	2.63	45.26	57.89	50.19	2.59	44.63	56.02
FBP <->DHAP + GAP	-27.07	1.38	-30.53	-23.82	-26.42	1.36	-29.42	-23.48
FBP <->F6P	27.07	1.38	23.82	30.53	26.42	1.36	23.48	29.42
F6P <->G6P	2.33	0.12	2.05	2.78	2.26	0.12	2.01	2.53
G6P ->RU5P + CO2	0.00	0.00	0.00	0.38	0.00	0.00	0.00	0.16
DHAP + E4P ->SBP	24.35	1.24	21.31	27.51	23.77	1.22	21.14	26.48
SBP ->S7P	24.35	1.24	21.31	27.51	23.77	1.22	21.14	26.48
F6P <->GAP + EC3	0.00	0.00	0.00	0.61	0.00	0.00	0.00	0.51
S7P <->E4P + EC3	0.00	0.00	-0.61	0.00	0.00	0.00	-0.51	0.00
F6P <->E4P + EC2	24.74	1.26	21.80	27.93	24.16	1.24	21.47	26.90
S7P <->R5P + EC2	24.35	1.24	21.46	27.26	23.77	1.22	21.12	26.49
X5P <->GAP + EC2	-49.09	2.51	-55.51	-43.32	-47.93	2.47	-53.33	-42.60
RU5P <->X5P	-49.09	2.51	-55.51	-43.32	-47.93	2.47	-53.33	-42.60
RU5P <->R5P	-23.59	1.20	-26.69	-20.79	-23.03	1.19	-25.64	-20.47
RU5P ->RUBP	72.68	3.71	64.11	81.98	70.96	3.65	63.08	78.99
RUBP ->3PG + 2PG	0.00	0.00	0.00	0.46	0.00	0.00	0.00	0.83
2PG ->GLYC	0.00	0.00	0.00	0.46	0.00	0.00	0.00	0.83
GLYC ->GOX	0.00	0.00	0.00	0.46	0.00	0.00	0.00	0.83
GOX + GOX ->GA + CO2	0.00	0.00	0.00	0.23	0.00	0.00	0.00	0.41
GA <->2PGA	0.00	0.00	0.00	0.23	0.00	0.00	0.00	0.41
3PG <->2PGA	15.45	0.79	13.51	17.46	15.07	0.78	13.37	16.74

Table D.2 Continued.

Reaction	WT Flux	WT stdErr	WT LB	WT UB	LS Flux	LS StdErr	LS LB	LS UB
2PGA <->PEP	15.45	0.79	13.58	17.32	15.07	0.78	13.39	16.78
PEP ->PYR	9.86	2.04	7.95	11.68	0.00	0.00	NaN	12.15
PYR ->ACA + CO2	7.87	0.40	6.92	8.82	7.66	0.40	6.80	8.52
OAA + ACA ->CIT	1.36	0.07	1.19	1.59	1.32	0.07	1.17	1.49
CIT <->ICI	1.36	0.07	1.19	1.59	1.32	0.07	1.17	1.49
ICI ->AKG + CO2	1.36	0.07	1.19	1.59	1.32	0.07	1.17	1.47
AKG ->SSA + CO2	0.00	0.00	0.00	0.13	0.00	0.00	0.00	0.09
SSA ->SUC	0.00	0.00	0.00	0.13	0.00	0.00	0.00	0.09
SUC <->FUM	0.00	0.00	0.00	0.13	0.00	0.00	0.00	0.11
FUM <->MAL	1.15	0.06	1.01	1.32	1.12	0.06	0.99	1.27
MAL <->OAA	-1.82	1.97	-3.46	-0.53	-11.41	0.59	-12.67	0.05
PEP + CO2 ->OAA	4.55	1.98	3.20	6.42	14.06	0.72	3.57	15.66
MAL ->PYR + CO2	2.97	1.97	1.64	4.94	12.52	0.65	1.67	13.95
Biomass	1.82	0.09	1.60	2.06	1.77	0.09	1.57	1.97
0*3PG ->3PG.s	0.86	0.04	0.78	0.96	0.77	0.06	0.64	0.89
0*3PG.u ->3PG.s	0.14	0.04	0.04	0.22	0.23	0.06	0.11	0.36
3PG.s ->sink	1.00	0.00	1.00	1.00	1.00	0.00	1.00	1.00
0*RU5P ->RU5P.s	0.68	0.01	0.66	0.71	0.58	0.02	0.54	0.62
0*RU5P.u ->RU5P.s	0.32	0.01	0.29	0.34	0.42	0.02	0.38	0.46
RU5P.s ->sink	1.00	0.00	1.00	1.00	1.00	0.00	1.00	1.00
0*PEP ->PEP.s	0.86	0.02	0.81	0.90	0.60	0.04	0.51	0.68
0*PEP.u ->PEP.s	0.15	0.02	0.10	0.19	0.40	0.04	0.32	0.49
PEP.s ->sink	1.00	0.00	1.00	1.00	1.00	0.00	1.00	1.00
0*GAP ->GAP.s	0.81	0.01	0.80	0.83	0.70	0.01	0.67	0.72
0*GAP.u ->GAP.s	0.19	0.01	0.17	0.20	0.30	0.01	0.28	0.33
GAP.s ->sink	1.00	0.00	1.00	1.00	1.00	0.00	1.00	1.00
G6P <->G1P	2.33	0.12	2.05	2.63	2.26	0.12	2.01	2.52

Table D.2 Continued.

Reaction	WT Flux	WT stdErr	WT LB	WT UB	LS Flux	LS StdErr	LS LB	LS UB
0*DHAP ->DHAP.s	0.81	0.01	0.80	0.82	0.66	0.02	0.62	0.69
0*DHAP.u ->DHAP.s	0.19	0.01	0.18	0.20	0.34	0.02	0.31	0.38
DHAP.s ->sink	1.00	0.00	1.00	1.00	1.00	0.00	1.00	1.00
CO2.l ->CO2.x	62.23	3.18	54.61	69.67	60.76	3.13	54.03	67.53
CO2.u ->CO2.x	0.00	0.00	0.00	0.34	0.00	0.00	0.00	0.32
GAP + PYR ->DOXP + CO2	N/A	N/A	N/A	N/A	0.04	0.00	0.04	0.04
DOXP + DOXP ->LIM	N/A	N/A	N/A	N/A	0.02	0.00	0.02	0.02
CO2.x ->CO2	62.23	3.18	54.87	70.38	60.76	3.13	53.94	67.52
CO2.u + dummy ->CO2	2.79	0.14	2.46	3.16	2.72	0.14	2.41	3.02

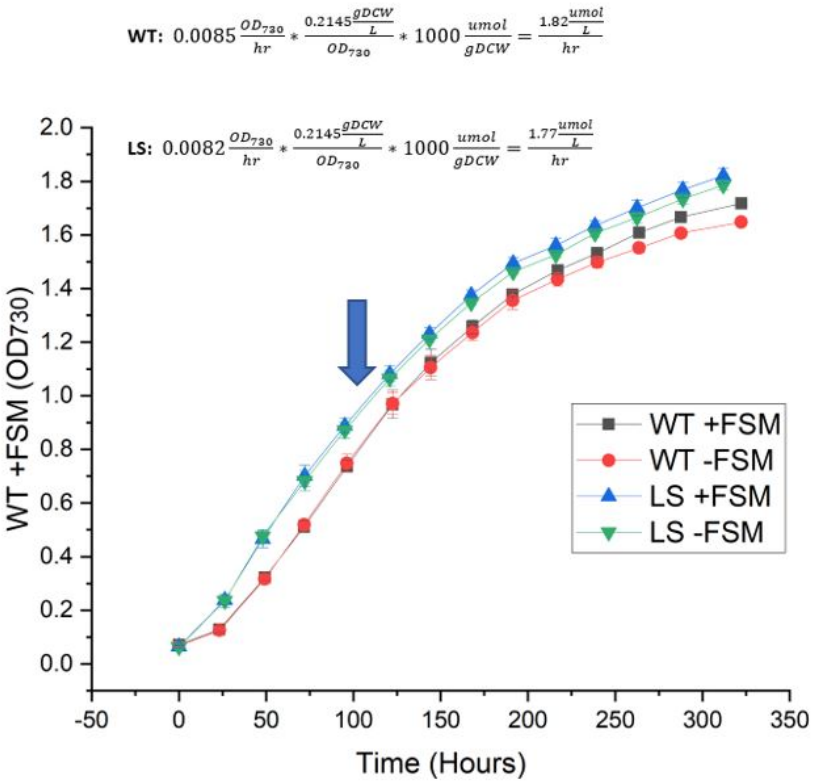

Figure D.3 Growth curve of *Synechococcus* 7002 WT strain and LS strain. The labeling and quenching experiment was performed at an OD_{730} of around 0.8. We converted the average growth rate between the data points indicated by the arrow to a biomass accumulation rate in terms of μmol L^{-1} hr^{-1} using a conversion factor derived by [123].

APPENDIX E

SUPPLEMENTARY INFORMATION FOR CHAPTER 5

Table E.1 Exchange reactions for simulations run to predict growth rate and biomass yield. Every biomass formation equation constructed from the various sources and organisms were set as the objective if the iCre1355 model and grown in a carbon limiting environment. The photon emission value for each simulation represents the saturation photon flux. Column headers: P-phosphate, NH4-ammonium, S-sulfate, Mg-magnesium, Na-sodium, Photon-photon emission, O2-oxygen, CO2-carbon dioxide, H+-proton.

Organism	P	NH4	S	Mg	Na	Photon	O2	CO2	H+
C. reinhardtii[8]	-0.02371	-0.27711	-0.00125	-0.00111	-0.49315	-31.36	-3.25922	-1.60533	0.191077
C. reinhardtii (M)[8]	-0.03927	-0.12945	-0.00163	-0.00091	-0.2816	-31.28	-3.26154	-1.60533	0.111257
C. reinhardtii[9]	-0.07033	-0.25847	-0.00079	-0.00069	-0.83014	-22.75	-1.88423	-1.60533	0.500548
C. reinhardtii (M)[9]	-0.0113	-0.13983	-0.00131	-0.00069	-0.82266	-22.55	-1.65631	-1.60533	0.670208
C. reinhardtii (H)[9]	-0.01119	-0.1098	-0.00124	-0.00089	-0.80868	-22.52	-1.64519	-1.60533	0.686445
C. prototheco-ides[10]	-0.02321	-0.29937	-0.00126	-0.00043	-0.93099	-22.73	-1.79659	-1.60533	0.607154
C. prototheco-ides (H)[10]	-0.02155	-0.08432	-0.00199	-0.00097	-1.38336	-19.7	-0.91558	-1.60533	1.275505
Synechococcus sp PCC 7002[11]	-0.02443	-0.32839	-0.00095	-0.00165	-0.78562	-26.02	-2.41778	-1.60533	0.431845

[8]Biomass formation equation sourced from[112]
[9]Biomass formation equation sourced from[113]
[10]Biomass formation equation sourced from[101]
[11]Biomass formation equation sourced from[115]

Table E.1 Continued.

Synechocystis sp PCC 6803[12]	-0.04444	-0.29211	-0.00103	-0.00117	-0.79367	-26.86	-2.52426	-1.60533	0.456084

[12]Biomass formation equation sourced from[116]

Table E.2 Exchange reactions for simulations run to predict growth rate and biomass yield. Every biomass formation equation constructed from the various sources and organisms were set as the objective if the iCre1355 model and grown in a carbon limiting environment. The photon emission value for each simulation represents the saturation photon flux. Column headers: P-phosphate, NH4-ammonium, S-sulfate, Mg-magnesium, Na-sodium, Photon-photon emission, O2-oxygen, CO2-carbon dioxide, H+-proton.

Organism	P	NH4	S	Mg	Na	Photon	O2	CO2	H+
C. reinhardtii[13] 0.072298	-0.85186	-0.0214	-0.2498	-0.00113	-0.001	-0.34359	-29.1567	-3.09715	-1.44677
C. reinhardtii (M)[13] 0.004882	-1.06968	-0.0358	-0.11774	-0.00149	-0.00083	-0.15991	-29.2886	-3.11282	-1.46096
C. reinhardtii[14] 0.395561	-1.45095	-0.01118	-0.12996	-0.00097	-0.00085	-0.53767	-23.051	-1.79332	-1.59916
C. reinhardtii (M)[14] 0.594224	-1.54127	-0.01157	-0.14317	-0.00134	-0.00071	-0.7503	-22.9963	-1.67448	-1.64344
C. reinhardtii (H)[14] 0.58385	-1.61934	-0.0116	-0.11393	-0.00129	-0.00092	-0.71067	-23.486	-1.66513	-1.66513
C. prototheocoides[15] 0.372676	-0.89513	-0.01908	-0.24556	-0.00103	-0.00035	-0.63835	-20.2322	-1.75596	-1.31444
C. prototheocoides (H)[15] 1.176265	-1.88004	-0.02221	-0.08702	-0.00205	-0.001	-1.28755	-21.5763	-0.91916	-1.65577

[13]Biomass formation equation sourced from[112]
[14]Biomass formation equation sourced from[113]
[15]Biomass formation equation sourced from[101]

Table E.2 Continued.

Synechococcus sp PCC 7002[16] 0.107781	-0.72176	-0.02048	-0.27469	-0.0008	-0.00139	-0.40374	-23.2154	-2.31054	-1.34039
Synechocystis sp PCC 6803[17] 0.072516	-0.76244	-0.0379	-0.24863	-0.00088	-0.001	-0.35992	-24.1864	-2.42965	-1.36444

[16]Biomass formation equation sourced from[115]
[17]Biomass formation equation sourced from[116]

Table E.3 Reactants and products consumed and formed in the biomass formation equation and their coefficients for each of the equations constructed for this study.Model species and conditions are as follows, with (M) indicating mixotrophic growth conditions, (H) indicating heterotrophic growth conditions, and the absence of a marker indicating phototrophic growth conditions. 1- C. reinhardtii[112] (native equation to iCre1355) 2- C. reinhardtii (M)[112] 3- C reinhardtii[113] 4- C. reinhardtii (M)[113] 5- C. reinhardtii (H)[113] 6- C. protothecoides[101] 7- C. protothecoides (H)[101] 8- Synechococcus sp. PCC 7002[115] 9- Synechocystis sp. PCC 6803[116].

Metabolite	Metabolite ID	1	2	3	4	5	6	7	8	9
ATP	atp_c	-92.4316	-92.4316	-29.9486	-29.9486	-29.9486	-24.0614	-7.7833	-45.8071	-53.4073
H2O	h2o_c	-92.40	-92.40	-29.89	-29.89	-29.89	-24.0332	-7.7579	-45.7318	-53.35
L-Alanyl-tRNA(Ala)	alatrna_c	-0.86603	-0.27926	-0.40838	-0.47409	-0.34736	-0.87449	-0.21501	-0.95460	-0.77548
L-Arginyl-tRNA(Arg)	argtrna_c	-0.47517	-0.09366	-0.22407	-0.26012	-0.19058	-0.47981	-0.11797	-0.52376	-0.42548
L-Asparaginyl-tRNA(Asn)	asntrna_c	-0.21459	-0.06954	-0.10119	-0.11747	-0.08607	-0.21669	-0.05328	-0.23654	-0.19215
L-Aspartyl-tRNA(Asp)	asptrna_c	-0.21459	-0.06954	-0.10119	-0.11747	-0.08607	-0.21669	-0.05328	-0.23654	-0.19215
L-Cysteinyl-tRNA(Cys)	cystrna_c	-0.00766	-0.01224	-0.00361	-0.00420	-0.00307	-0.00774	-0.00190	-0.00845	-0.00686
L-Glutaminyl-tRNA(Gln)	glntrna_c	-0.25674	-0.09182	-0.12107	-0.14055	-0.10298	-0.25925	-0.06374	-0.28300	-0.22990
L-Glutamyl-tRNA(Glu)	glutrna_c	-0.25674	-0.09182	-0.12107	-0.14055	-0.10298	-0.25925	-0.06374	-0.28300	-0.22990
Glycyl-tRNA(Gly)	glytrna_c	-0.32572	-0.11386	-0.15359	-0.17831	-0.13064	-0.32890	-0.08086	-0.35903	-0.29166
L-Histidyl-tRNA(His)	histrna_c	-0.00383	-0.01273	-0.00181	-0.00210	-0.00154	-0.00387	-0.00095	-0.00422	-0.00343
L-Isoleucyl-tRNA(Ile)	iletrna_c	-0.10346	-0.03795	-0.04879	-0.05664	-0.04150	-0.10447	-0.02569	-0.11405	-0.09265

Table E.3 Continued.

L-Leucyl-tRNA(Leu)	leutrna_c	-0.26058	-0.09304	-0.12287	-0.14265	-0.10451	-0.26312	-0.06469	-0.28723	-0.23333
L-Lysine-tRNA (Lys)	lystrna_c	-0.05748	-0.03061	-0.02710	-0.03147	-0.02305	-0.05804	-0.01427	-0.06336	-0.05147
L-Methionyl-tRNA (Met)	mettrna_c	-0.00766	-0.01273	-0.00361	-0.00420	-0.00307	-0.00774	-0.00190	-0.00845	-0.00686
L-Phenylalanyl-tRNA(Phe)	phetrna_c	-0.10730	-0.04003	-0.05060	-0.05874	-0.04304	-0.10834	-0.02664	-0.11827	-0.09608
L-Prolyl-tRNA(Pro)	protrna_c	-0.14945	-0.05191	-0.07047	-0.08181	-0.05994	-0.15091	-0.03710	-0.16473	-0.13382
L-Seryl-tRNA(Ser)	sertrna_c	-0.06514	-0.02081	-0.03072	-0.03566	-0.02613	-0.06578	-0.01617	-0.07181	-0.05833
L-Threonyl-tRNA(Thr)	thrtrna_c	-0.26058	-0.03452	-0.12287	-0.14265	-0.10451	-0.26312	-0.06469	-0.28723	-0.23333
L-Tryptophanyl-tRNA(Trp)	trptrna_c	-0.00383	-0.00159	-0.00181	-0.00210	-0.00154	-0.00387	-0.00095	-0.00422	-0.00343
L-Tyrosyl-tRNA(Tyr)	tyrtrna_c	-0.00383	-0.00159	-0.00181	-0.00210	-0.00154	-0.00387	-0.00095	-0.00422	-0.00343
L-Valyl-tRNA(Val)	valtrna_c	-0.18777	-0.06427	-0.08854	-0.10279	-0.07531	-0.18960	-0.04662	-0.20697	-0.16813
dATP	datp_c	-0.00122	-0.00218	-0.00060	-0.00060	-0.00060	-0.00109	-0.00117	-0.00083	-0.00221
dCTP	dctp_c	-0.00218	-0.00388	-0.00108	-0.00108	-0.00108	-0.00194	-0.00209	-0.00149	-0.00395
dGTP	dgtp_c	-0.00218	-0.00388	-0.00108	-0.00108	-0.00108	-0.00194	-0.00209	-0.00149	-0.00395
dTTP	dttp_c	-0.00122	-0.00218	-0.00060	-0.00060	-0.00060	-0.00109	-0.00117	-0.00083	-0.00221
CTP	ctp_c	-0.05638	-0.10421	-0.02787	-0.02787	-0.02787	-0.05033	-0.05423	-0.03852	-0.10222

Table E.3 Continued.

GTP	gtp_c	-0.05634	-0.10421	-0.02785	-0.02785	-0.02785	-0.05029	-0.05419	-0.03850	-0.10214
UTP	utp_c	-0.03161	-0.05862	-0.01562	-0.01562	-0.01562	-0.02821	-0.03040	-0.02159	-0.05730
starch n=300 repeat units (80 repeat units amylose, 220 repeat units amylopectin, corresponds to maize starch)	starch300_h	-0.00320	-0.00641	-0.00320	-0.00320	-0.00320	-0.00320	-0.00320	-0.00320	-0.00320
D-Mannose	man_c	-0.16418	-0.32836	-0.50981	-0.38236	-0.44960	-0.12976	-0.15146	-0.15911	-0.18530
L-Arabinose	arab_L_c	-0.26207	-0.52414	-0.81378	-0.61033	-0.71766	-0.20713	-0.24176	-0.25398	-0.29578
D-Galactose	gal_c	-0.34850	-0.69700	-1.08215	-0.81161	-0.95434	-0.27544	-0.32150	-0.33774	-0.39333
Monogalactosyldiacylglycerol (1-(9Z,12Z,15Z)-octadecatrienoyl,2-(4Z,7Z,10Z,13Z)-hexadecatetraenoyl, 18:3(9Z,12Z,15Z) / 16:4(4Z,7Z,10Z,13Z))	mgdg1839 Z12Z 15Z1644Z7 Z10 Z13Z_h	-0.02845	-0.02845	-0.03645	-0.05381	-0.05536	-0.02334	-0.10047	-0.00794	-0.01874

Table E.3 Continued.

Monogalactosyldiacylglycerol (1-(9Z,12Z,15Z)-octadecatrienoyl,2-(7Z,10Z,13Z)-hexadecatrienoyl, 18:3(9Z,12Z,15Z) / 16:3(7Z,10Z,13Z))	mgdg1839Z 12Z15Z163 7Z10Z13Z_h	-0.00324	-0.00324	-0.00415	-0.00613	-0.00631	-0.00266	-0.01145	-0.00090	-0.00214
Monogalactosyldiacylglycerol (1-(9Z,12Z,15Z)-octadecatrienoyl,2-(4Z,7Z,10Z)-hexadecatrienoyl, 18:3(9Z,12Z,15Z) /16:3(4Z,7Z,10Z))	mgdg183 9Z12Z15Z 163 4Z7Z10Z_h	-0.00324	-0.00324	-0.00415	-0.00613	-0.00631	-0.00266	-0.01145	-0.00090	-0.00214
Monogalactosyldiacylglycerol (1-(9Z,12Z)-octadecadienoyl,2-(4Z,7Z,10Z,13Z)-hexadecat etraenoyl, 18:2(9Z,12Z) /16:4(4Z, 7Z,10Z,13Z))	mgdg1829Z 12Z1644 Z7Z10Z13Z_h	-0.00324	-0.00324	-0.00415	-0.00613	-0.00631	-0.00266	-0.01145	-0.00090	-0.00214

Table E.3 Continued.

Monogalactosyldiacyl glycerol (1-(9Z,12Z)-octadecadienoyl,2 -(7Z,10Z,13Z)-hexadecatrienoyl, 18:2(9Z,1 2Z) /16:3(7Z,10Z, 13Z))	mgdg18 29Z12Z16 37Z10Z 13Z_h	- 0.00040	- 0.00040	- 0.00052	- 0.00076	- 0.00079	- 0.00033	- 0.00143	- 0.00011	- 0.00027
Monogalac tosyldiacylgl ycerol (1-(9Z,1 2Z)-octadecadienoyl,2-(4Z,7Z ,10Z)-hexadecat rienoyl, 18:2(9Z, 12Z) /16 :3(4Z,7Z,10Z))	mgdg1829Z 12Z1634Z7 Z10Z_h	- 0.00040	- 0.00040	- 0.00052	- 0.00076	- 0.00079	- 0.00033	- 0.00143	- 0.00011	- 0.00027
Monogalac tosyldiacylgly cerol (1-(9Z,12Z,15Z)-octade catrienoyl,2-(7Z,10Z)-hexadecadienoyl, 18:3(9Z,12Z ,15Z) /16:2(7Z,10Z))	mgdg1839 Z12Z15Z16 27Z10Z_h	- 0.00040	- 0.00040	- 0.00052	- 0.00076	- 0.00079	- 0.00033	- 0.00143	- 0.00011	- 0.00027

Table E.3 Continued.

Monogalac tosyldiacylg lycerol (1-(9Z,12 Z)-octadecadieno yl,2-(7Z,10Z)-h exadecadienoyl, 18:2(9Z,12Z) /16:2(7Z,10Z))	mgdg1829Z 12Z1627Z 10Z_h	- 0.00040	- 0.00040	- 0.00052	- 0.00076	- 0.00078	- 0.00033	- 0.00142	- 0.00011	- 0.00027
Monogalactosyl diacylglycerol (1-(9Z,12Z)-o ctadecadienoyl,2- (7Z)-hex adecenoyl, 18:2 (9Z,12Z) /16:1(7Z))	mgdg1829Z 12Z161 7Z_h	- 0.00020	- 0.00020	- 0.00026	- 0.00038	- 0.00039	- 0.00016	- 0.00071	- 0.00006	- 0.00013
Monogalactosyld iacylglycerol (1-(9Z,12 Z)-octadecadien oyl,2-(9Z)-hexa decenoyl, 18:2(9Z ,12Z) /16:1(9Z))	mgdg182 9Z12Z16 19Z_h	- 0.00020	- 0.00020	- 0.00026	- 0.00038	- 0.00039	- 0.00016	- 0.00071	- 0.00006	- 0.00013
Monogalactosyldi acylglycerol (1-(9Z,12Z, 15Z)-octadecat rienoyl,2-hexade canoyl, 18:3(9Z, 12Z,15Z) /16:0)	mgdg1839Z 12Z15Z 160_h	- 0.00020	- 0.00020	- 0.00026	- 0.00038	- 0.00039	- 0.00016	- 0.00071	- 0.00006	- 0.00013

Table E.3 Continued.

Monogalacto syldiacylg lycerol (1-(9Z,12Z)-octadecadienoyl,2-hexade canoyl, 18:2(9Z, 12Z) /16:0)	mgdg1829Z 12Z160_h	-0.00020	-0.00020	-0.00026	-0.00038	-0.00039	-0.00016	-0.00071	-0.00006	-0.00013
Digalactos yldiacylg lycerol (1-(9Z,12Z,15 Z)-octadecatrienoy l,2-(4Z,7Z,10Z,13Z)-hexa decatetraenoyl, 18:3(9Z, 12Z,15Z) /16:4(4Z,7Z,1 0Z,13Z))	dgdg183 9Z12Z15 Z1644Z7 Z10Z13 Z_h	-0.00027	-0.00027	-0.00035	-0.00051	-0.00052	-0.00022	-0.00095	-0.00008	-0.00018
Digalacto syldiacylg lycerol (1-(9Z ,12Z,15Z)-oct adecatrienoy l,2-(7Z,10Z,13 Z)-hexadecatr ienoyl, 18:3(9 Z,12Z,15Z) /16:3(7Z ,10Z,13Z))	dgdg183 9Z12Z1 5Z1637 Z10Z1 3Z_h	-0.00074	-0.00074	-0.00095	-0.00140	-0.00144	-0.00061	-0.00261	-0.00021	-0.00049

Table E.3 Continued.

Digalacto syldiacylglycerol (1-(9Z,12Z,15Z)-octadecatrienoyl,2-(4Z,7Z,10Z)-hexadecatrienoyl, 18:3(9Z,12Z,15Z)/16:3(4Z,7Z,10Z))	dgdg1839 Z12Z15 Z1634Z7 Z10Z_h	-0.00074	-0.00074	-0.00095	-0.00140	-0.00144	-0.00061	-0.00261	-0.00021	-0.00049
Digalactosyldiacylglycerol (1-(9Z,12Z,15Z)-octadecatrienoyl,2-(7Z,10Z)-hexadecadienoyl, 18:3(9Z,12Z,15Z)/16:2(7Z,10Z))	dgdg1839 Z12Z15Z 1627Z1 0Z_h	-0.00054	-0.00054	-0.00069	-0.00101	-0.00104	-0.00044	-0.00189	-0.00015	-0.00035
Digalacto syldiacylglycerol (1-(9Z,12Z)-octadecadienoyl,2-(7Z,10Z,13Z)-hexadecatrienoyl, 18:2(9Z,12Z) /16:3(7Z,10Z,13Z))	dgdg1829 Z12Z1637 Z10Z1 3Z_h	-0.00027	-0.00027	-0.00034	-0.00051	-0.00052	-0.00022	-0.00095	-0.00007	-0.00018

Table E.3 Continued.

Digalact osyldiacy lglycerol (1-(9Z,12 Z)-octadecadienoy l,2-(4Z,7Z,10Z)-he xadecatrienoyl, 18:2(9Z,12Z) /16:3(4Z,7Z, 10Z))	dgdg182 9Z12Z1 634Z7Z 10Z_h	- 0.00027	- 0.00027	- 0.00034	- 0.00051	- 0.00052	- 0.00022	- 0.00095	- 0.00007	- 0.00018
Digalact osyldiacy lglycerol (1-(9Z,1 2Z)-octadecad ienoyl,2-(7Z,10Z)-h exadecadienoyl, 18:2(9 Z,12Z) /16: 2(7Z,10Z))	dgdg182 9Z12Z1 627Z1 0Z_h	- 0.00054	- 0.00054	- 0.00069	- 0.00101	- 0.00104	- 0.00044	- 0.00189	- 0.00015	- 0.00035
Digalacto syldiacylg lycerol (1-(9Z)- octadecenoyl,2-(7Z,10Z,13Z)-hexade catrienoyl, 18:1(9Z) /16: 3(7Z,10Z,13Z))	dgdg1 819Z1 637Z10 Z13Z_h	- 0.00020	- 0.00020	- 0.00026	- 0.00038	- 0.00039	- 0.00016	- 0.00071	- 0.00006	- 0.00013
Digalactosyld iacylglyce rol (1-(9Z)- octadecenoyl,2-(4Z, 7Z,10Z)-hexadecatr ienoyl, 18:1(9Z) /1 6:3(4Z,7Z, 10Z))	dgdg1819 Z1634Z7Z 10Z_h	- 0.00020	- 0.00020	- 0.00026	- 0.00038	- 0.00039	- 0.00016	- 0.00071	- 0.00006	- 0.00013

Table E.3 Continued.

Digalactosyldi acylglycerol (1-(9Z)-octade cenoyl,2-(7Z,10Z)-hex adecadi enoyl, 18:1 (9Z) /16:2(7 Z,10Z))	dgdg181 9Z1627 Z10Z_h	- 0.00040	- 0.00040	- 0.00051	- 0.00076	- 0.00078	- 0.00033	- 0.00141	- 0.00011	- 0.00026
Digalactosyl diacylgly cerol (1-(9Z,12Z ,15Z)-octadec atrienoyl,2-hexade canoyl, 18:3(9Z,1 2Z,15Z)/16:0)	dgdg1 839Z1 2Z15Z 160_h	- 0.00240	- 0.00240	- 0.00308	- 0.00455	- 0.00468	- 0.00197	- 0.00849	- 0.00067	- 0.00158
Digalact osyldiacylg lycerol (1-(9Z, 12Z)-octadeca dienoyl,2-(7 Z)-hexadecen oyl, 18:2(9Z,1 2Z)/16:1(7Z))	dgdg1829 Z12Z16 17Z_h	- 0.00030	- 0.00030	- 0.00038	- 0.00057	- 0.00058	- 0.00025	- 0.00106	- 0.00008	- 0.00020
Digalact osyldiacylgl ycerol (1-(9Z,12Z)-octadecadieno yl,2-(9Z)-hexade cenoyl, 18:2(9 Z,12Z)/16 :1(9Z))	dgdg1829 Z12Z161 9Z_h	- 0.00030	- 0.00030	- 0.00038	- 0.00057	- 0.00058	- 0.00025	- 0.00106	- 0.00008	- 0.00020

Table E.3 Continued.

Digalact osyldiacyl glycerol (1-(9Z,12Z)-oc tadecadienoyl, 2-hexade canoyl, 18 :2(9Z,12Z)/16:0)	dgdg 1829Z 12Z16 0_h	-0.00333	-0.00333	-0.00427	-0.00630	-0.00648	-0.00273	-0.01176	-0.00093	-0.00219
Digalac tosyldiacyl glycerol (1-(9Z)-o ctadeceno yl,2-(7Z)-hexade cenoyl, 18:1(9Z) /16:1(7Z))	dgdg18 19Z1617 Z_h	-0.00030	-0.00030	-0.00038	-0.00057	-0.00058	0.00025	-0.00106	-0.00008	-0.00020
Digalactosy ldiacylglycerol (1-(9Z) -octadecen oyl,2-(9Z)-hex adecenoyl, 18:1(9 Z)/16 :1(9Z))	dgdg18 19Z1619 Z_h	-0.00030	-0.00030	-0.00038	-0.00057	-0.00058	0.00025	-0.00106	-0.00008	-0.00020
Digalacto syldiacyl glycerol (1-(9Z)-o ctadecenoy l,2-hexade canoyl, 18 :1(9Z)/16:0)	dgdg1 819Z16 0_h	-0.00173	-0.00173	-0.00221	-0.00327	-0.00336	0.00142	-0.00610	-0.00048	-0.00114
diacylgl yceryl-N,N,N -trimethylhomo serine (18:3(9Z,12 Z,15Z)/18:4(5 Z,9Z,12Z,15Z))	dgts183 9Z12 Z15Z184 5Z9Z12 Z15Z_c	-0.00041	-0.00041	-0.00052	-0.00077	-0.00079	0.00033	-0.00144	-0.00011	-0.00027

Table E.3 Continued.

diacylglycery l-N,N,N-tri methylhomos erine (18:3(9 Z,12Z,15Z)/18: 3(5Z,9Z,12Z))	dgts1 839Z 12Z15Z18 35Z9Z1 2Z_c	- 0.00108	- 0.00108	- 0.00139	- 0.00205	- 0.00211	- 0.00089	- 0.00382	- 0.00030	- 0.00071
diacylgly ceryl-N,N, N-trimethylh omoserine (18:2(9Z,12Z)/18:4(5Z,9Z ,12Z,15Z))	dgts1829 Z12Z1845 Z9Z12Z15 Z_c	- 0.00008	- 0.00008	- 0.00010	- 0.00014	- 0.00015	- 0.00006	- 0.00027	- 0.00002	- 0.00005
diacylglyce ryl-N,N,N- trimethylho moserine (18:2(9Z,12 Z)/18:3(5Z,9 Z,12Z))	dgts1829Z 12Z1835Z9 Z12Z_c	- 0.00162	- 0.00162	- 0.00207	- 0.00306	- 0.00315	- 0.00133	- 0.00572	- 0.00045	- 0.00107
diacylglyc eryl-N,N,N -trimethylh omoserine (18:1(9Z)/ 18:4(5Z,9Z, 12Z,15Z))	dgts181 9Z1845Z 9Z12Z15 Z_c	- 0.00027	- 0.00027	- 0.00035	- 0.00051	- 0.00052	- 0.00022	- 0.00095	- 0.00008	- 0.00018
diacylglyceryl - N,N,N-trimethy lhomoserine (18:1(11Z)/18 :4(5Z,9Z,12Z,1 5Z))	dgts18111 Z1845Z9Z1 2Z15Z_c	- 0.00027	- 0.00027	- 0.00035	- 0.00051	- 0.00052	- 0.00022	- 0.00095	- 0.00008	- 0.00018

Table E.3 Continued.

diacylglyc eryl-N,N,N -trimethyl homoserine (16:0/18:4(5Z ,9Z,12Z,15Z))	dgts1601 845Z9Z12 Z15Z_c	- 0.00209	- 0.00209	- 0.00268	- 0.00396	- 0.00408	- 0.00172	- 0.00740	- 0.00058	- 0.00138
diacylglyceryl -N,N,N-trimethyl homoserine (18:2(9Z,12Z) /18:2(9Z,12Z))	dgts182 9Z12Z18 29Z12Z $_c$ |	- 0.00040	- 0.00040	- 0.00052	- 0.00076	- 0.00079	- 0.00033	- 0.00143	- 0.00011	- 0.00027
diacylglyceryl -N,N,N-trimethyl homoserine (18:3(9Z,12Z,15Z) /18:1(9Z))	dgts1839 Z12Z15Z 1819Z_c	- 0.00034	- 0.00034	- 0.00043	- 0.00064	- 0.00065	- 0.00028	- 0.00119	- 0.00009	- 0.00022
diacylglyceryl -N,N,N-trimethyl homoserine (18:2(9Z,12Z) /18:1(9Z))	dgts182 9Z12Z18 19Z_c	- 0.00007	- 0.00007	- 0.00010	- 0.00014	- 0.00015	- 0.00006	- 0.00026	- 0.00002	- 0.00005
diacylglyceryl -N,N,N-trimethyl homoserine (18:3(9Z,12Z,15Z) /18:1(11Z))	dgts18 39Z12Z1 5Z18111 Z_c	- 0.00034	- 0.00034	- 0.00043	- 0.00064	- 0.00065	- 0.00028	- 0.00119	- 0.00009	- 0.00022

Table E.3 Continued.

diacylglyceryl -N,N,N-trimethyl homoserine (18:2(9Z,12Z) /18:1(11Z))	dgts182 9Z12Z18 111Z_c	- 0.00007	- 0.00007	- 0.00010	- 0.00014	- 0.00015	- 0.00006	- 0.00026	- 0.00002	- 0.00005
diacylglyceryl -N,N,N-trimethyl homoserine (18:1(9Z) /18:3(5Z,9Z,12Z))	dgts181 9Z1835Z 9Z12Z_c	- 0.00040	- 0.00040	- 0.00052	- 0.00076	- 0.00079	- 0.00033	- 0.00143	- 0.00011	- 0.00027
diacylglyceryl -N,N,N-trimethyl homoserine (18:1(11Z) /18:3(5Z,9Z,12Z))	dgts181 11Z1835 Z9Z12Z _c	- 0.00040	- 0.00040	- 0.00052	- 0.00076	- 0.00079	- 0.00033	- 0.00143	- 0.00011	- 0.00027
diacylglyceryl -N,N,N-trimethyl homoserine (16:0/18:3(5Z,9Z,12Z))	dgts160 1835Z9 Z12Z_c	- 0.00390	- 0.00390	- 0.00500	- 0.00738	- 0.00759	- 0.00320	- 0.01377	- 0.00109	- 0.00257
diacylglyceryl -N,N,N-trimethyl homoserine (18:1(9Z) /18:2(9Z,12Z))	dgts18 19Z182 9Z12Z_c	- 0.00020	- 0.00020	- 0.00026	- 0.00038	- 0.00039	- 0.00017	- 0.00071	- 0.00006	- 0.00013
diacylglyceryl -N,N,N-trimethyl homoserine (18:1(11Z) /18:2(9Z,12Z))	dgts181 11Z1829 Z12Z_c	- 0.00020	- 0.00020	- 0.00026	- 0.00038	- 0.00039	- 0.00017	- 0.00071	- 0.00006	- 0.00013

Table E.3 Continued.

diacylglyceryl -N,N,N-trimethyl homoserine (18:1(9Z) /18:1(9Z))	dgts18 19Z181 9Z_c	- 0.00007	- 0.00007	- 0.00010	- 0.00014	- 0.00014	- 0.00006	- 0.00026	- 0.00002	- 0.00005
diacylglyceryl -N,N,N-trimethyl homoserine (18:1(9Z) /18:1(11Z))	dgts18 19Z1811 1Z_c	- 0.00007	- 0.00007	- 0.00010	- 0.00014	- 0.00014	- 0.00006	- 0.00026	- 0.00002	- 0.00005
diacylglyceryl -N,N,N-trimethyl homoserine (18:1(11Z) /18:1(9Z))	dgts181 11Z181 9Z_c	- 0.00007	- 0.00007	- 0.00010	- 0.00014	- 0.00014	- 0.00006	- 0.00026	- 0.00002	- 0.00005
diacylglyceryl -N,N,N-trimethyl homoserine (18:1(11Z) /18:1(11Z))	dgts1811 1Z181 11Z_c	- 0.00007	- 0.00007	- 0.00010	- 0.00014	- 0.00014	- 0.00006	- 0.00026	- 0.00002	- 0.00005
diacylglyceryl -N,N,N-trimethyl homoserine (16:0/18:2(9Z,12Z))	dgts16 1829Z1 2Z_c	- 0.00111	- 0.00111	- 0.00142	- 0.00210	- 0.00216	- 0.00091	- 0.00392	- 0.00031	- 0.00073
diacylglyceryl -N,N,N-trimethyl homoserine (16:0/18:1(9Z))	dgts16 01819 Z_c	- 0.00008	- 0.00008	- 0.00010	- 0.00015	- 0.00015	- 0.00006	- 0.00027	- 0.00002	- 0.00005

Table E.3 Continued.

diacylglyceryl -N,N,N-trimethyl homoserine (16:0/18:1(11Z))	dgts16 018111 Z_c	-0.00008	-0.00008	-0.00010	-0.00015	-0.00015	-0.00006	-0.00027	-0.00002	-0.00005
sulfoquin ovosyldiacyl glycerol (1-(9Z,12Z,15Z)-octadecatrienoyl,2-hexadecanoyl, 18:3(9Z,12Z,15Z) /16:0)	sqdg18 39Z12Z1 5Z160_h	-0.00078	-0.00078	-0.00100	-0.00147	-0.00151	-0.00064	-0.00274	-0.00022	-0.00051
sulfoquin ovosyldiacyl glycerol (1-(9Z,12Z)-octadecadienoyl,2-hexadecanoyl, 18:2(9Z,12Z) /16:0)	sqdg18 29Z12Z 160_h	-0.00073	-0.00073	-0.00093	-0.00137	-0.00141	-0.00060	-0.00257	-0.00020	-0.00048
sulfoquin ovosyldiacyl glycerol (1-(9Z)-octadecenoyl,2-hexadecanoyl, 18:1(9Z) /16:0)	sqdg18 19Z160 _h	-0.00048	-0.00048	-0.00062	-0.00091	-0.00094	-0.00040	-0.00171	-0.00013	-0.00032
sulfoquin ovosyldiacyl glycerol (1-(11Z)-octadecenoyl,2-hexadecanoyl, 18:1(11Z) /16:0)	sqdg18 111Z16 0_h	-0.00048	-0.00048	-0.00062	-0.00091	-0.00094	-0.00040	-0.00171	-0.00013	-0.00032

Table E.3 Continued.

sulfoquin ovosyldiacyl glycerol (dihexadecanoyl, n-C16:0)	sqdg160_h	-0.00245	-0.00245	-0.00313	-0.00463	-0.00476	-0.00201	-0.00864	-0.00068	-0.00161
2'-O-all-cis-5,9,12-octadecatrienoyl-sulfoquin ovosyldiacyl glycerol (2'-18:3(5,9,12) /18:1(9Z) /16:0)	asqdpa 1819Z 160_c	-0.00118	-0.00118	-0.00152	-0.00224	-0.00230	-0.00097	-0.00418	-0.00033	-0.00078
2'-O-all-cis-5,9,12-octadecatrienoyl-sulfoquin ovosyldiacyl glycerol (2'-18:3(5,9,12) /18:1(11Z) /16:0)	asqdpa 18111Z 160_c	-0.00118	-0.00118	-0.00152	-0.00224	-0.00230	-0.00097	-0.00418	-0.00033	-0.00078
2'-O-all-cis-5,9,12-octadecatrienoyl-sulfoquin ovosyldiacyl glycerol (2'-18:3(5,9,12) /18:2(9Z,12Z) /16:0)	asqdpa 1829Z1 2Z160_c	-0.00118	-0.00118	-0.00152	-0.00224	-0.00231	-0.00097	-0.00418	-0.00033	-0.00078
2'-O-all-cis-5,9,12-octadecatrienoyl-sulfoquin ovosyldiacyl glycerol (2'-18:3(5,9,12) /18:3(9Z,12Z,15Z) /16:0)	asqdpa 1839Z1 2Z15Z1 60_c	-0.00119	-0.00119	-0.00152	-0.00225	-0.00231	-0.00097	-0.00419	-0.00033	-0.00078

Table E.3 Continued.

2'-O-all-cis-5,9,12,15-octadecatetraenoyl-sulfoquinovosyldiacyl glycerol (2'-18:4(5,9,12,15) /18:1(9Z) /16:0)	asqdca 1819Z1 60_c	- 0.00118	- 0.00118	- 0.00152	- 0.00224	- 0.00231	- 0.00097	- 0.00418	- 0.00033	- 0.00078
2'-O-all-cis-5,9,12,15-octadecatetraenoyl-sulfoquinovosyldiacyl glycerol (2'-18:4(5,9,12,15) /18:1(11Z) /16:0)	asqdca 18111Z1 60_c	- 0.00118	- 0.00118	- 0.00152	- 0.00224	- 0.00231	- 0.00097	- 0.00418	- 0.00033	- 0.00078
2'-O-all-cis-5,9,12,15-octadecatetraenoyl-sulfoquinovosyldiacyl glycerol (2'-18:4(5,9,12,15) /18:2(9Z,12Z) /16:0)	asqdca1 829Z12Z 160_c	- 0.00119	- 0.00119	- 0.00152	- 0.00225	- 0.00231	- 0.00097	- 0.00419	- 0.00033	- 0.00078
2'-O-all-cis-5,9,12,15-octadecatetraenoyl-sulfoquinovosyldiacyl glycerol (2'-18:4(5,9,12,15) /18:3(9Z,12Z,15Z) /16:0)	asqdca 1839Z1 2Z15Z160_c	- 0.00119	- 0.00119	- 0.00152	- 0.00225	- 0.00231	- 0.00098	- 0.00420	- 0.00033	- 0.00078

Table E.3 Continued.

Phosphatidylglycerol (1-(9Z,12Z,15Z)-octadecatrienoyl,2-(3E)-hexadecenoyl, 18:3(9Z,12Z,15Z) /16:1(3E))	pg1839Z12Z15Z1613E_h	-0.00123	-0.00123	-0.00158	-0.00233	-0.00240	-0.00101	-0.00435	-0.00034	-0.00081
Phosphatidylglycerol (1-(9Z,12Z,15Z)-octadecatrienoyl,2-hexadecanoyl, 18:3(9Z,12Z,15Z) /16:0)	pg1839Z12Z15Z160_h	-0.00074	-0.00074	-0.00094	-0.00139	-0.00143	0.00060	-0.00260	-0.00021	-0.00049
Phosphatidylglycerol (1-(9Z,12Z)-octadecadienoyl,2-(3E)-hexadecenoyl, 18:2(9Z,12Z) /16:1(3E))	pg1829Z12Z161 3E_h	-0.00336	-0.00336	-0.00430	-0.00635	-0.00654	0.00276	-0.01186	-0.00094	-0.00221
Phosphatidylglycerol (1-(9Z,12Z)-octadecadienoyl,2-hexadecanoyl, 18:2(9Z,12Z) /16:0)	pg1829Z12Z160 _h	-0.00074	-0.00074	-0.00094	-0.00139	-0.00143	0.00060	-0.00260	-0.00021	-0.00048
Phosphatidylglycerol (1-(9Z)-octadecenoyl,2-(3E)-hexadecenoyl, 18:1(9Z) /16:1(3E))	pg181 9Z1613E_h	-0.00045	-0.00045	-0.00058	-0.00085	-0.00087	0.00037	-0.00159	-0.00013	-0.00030

Table E.3 Continued.

Phosphatidylglycerol (1-(11Z)-octadecenoyl,2-(3E)-hexadecenoyl, 18:1(11Z) /16:1(3E))	pg1811 1Z161 3E_h	-0.00045	-0.00045	-0.00058	-0.00085	-0.00087	-0.00037	-0.00159	-0.00013	-0.00030
Phosphatidylglycerol (1-(9Z)-octadecenoyl,2-hexadecanoyl, 18:1(9Z) /16:0)	pg1819 Z160_h	-0.00061	-0.00061	-0.00078	-0.00116	-0.00119	-0.00050	-0.00216	-0.00017	-0.00040
Phosphatidylglycerol (1-(11Z)-octadecenoyl,2-hexadecanoyl, 18:1(11Z) /16:0)	pg1811 1Z160_h	-0.00061	-0.00061	-0.00078	-0.00116	-0.00119	-0.00050	-0.00216	-0.00017	-0.00040
phosphatidyl ethanol amine (18:2(9Z,12Z) /18:3(5Z,9Z ,12Z))	pe1829Z1 2Z1835Z 9Z12Z_c	-0.00020	-0.00020	-0.00025	-0.00037	-0.00038	-0.00016	-0.00069	-0.00005	-0.00013
phosphatidyl ethanol amine (18:1(9Z) /18:4(5Z,9Z ,12Z,15Z))	pe1819Z1 845Z9Z12 Z15Z_c	0.00000	0.00000	0.00000	-0.00001	-0.00001	0.00000	-0.00001	0.00000	0.00000
phosphatidyl ethanol amine (18:1(9Z) /18:3(5Z,9 Z,12Z))	pe1819Z 1835Z9Z 12Z_c	-0.00009	-0.00009	-0.00012	-0.00018	-0.00018	-0.00008	-0.00033	-0.00003	-0.00006
phosphatidyl ethanol amine (18:1(11Z) /18:4(5Z,9 Z,12Z,15Z))	pe18111 Z1845Z9Z 12Z15Z_c	-0.00013	-0.00013	-0.00016	-0.00024	-0.00025	-0.00010	-0.00045	-0.00004	-0.00008

Table E.3 Continued.

phosphatidyl ethanol amine (18:1(11Z) /18:3(5 Z,9Z,12Z))	pe18111Z 1835Z9Z1 2Z_c	-0.00311	-0.00311	-0.00398	-0.00588	-0.00605	-0.00255	-0.01097	-0.00087	-0.00205
phosphatidyl ethanol amine (18:0/18:4(5Z,9Z, 12Z,15Z))	pe180184 5Z9Z12Z1 5Z_c	-0.00065	-0.00065	-0.00084	-0.00124	-0.00127	-0.00054	-0.00231	-0.00018	-0.00043
phosphatidyl ethanol amine (18:0/18:3(5Z ,9Z,12Z))	pe18018 35Z9Z12 Z_c	-0.00235	-0.00235	-0.00301	-0.00444	-0.00456	-0.00192	-0.00828	-0.00065	-0.00155
1-Phosphatidyl-D-myo-inositol (1-(11Z)-octadecenoyl,2-hexadecanoyl, 18:1(11Z) /16:0)	pail181 11Z160_ c	-0.00192	-0.00192	-0.00246	-0.00363	-0.00373	-0.00157	-0.00678	-0.00054	-0.00126
1-Phosphatidyl-D-myo-inositol (1-(9Z)-octadecenoyl,2-hexadecanoyl, 18:1(9Z) /16:0)	pail1819 Z160_c	-0.00026	-0.00026	-0.00033	-0.00049	-0.00050	-0.00021	-0.00091	-0.00007	-0.00017
Triacylglycerol (16:0/18:1(11Z) /16:0)	tag16018 111Z160_c	-0.00133	-0.00133	-0.00170	-0.00251	-0.00259	-0.00109	-0.00469	-0.00037	-0.00088
Triacylglycerol (16:0/18:1(9Z) /16:0)	tag160181 9Z160_c	-0.00133	-0.00133	-0.00170	-0.00251	-0.00259	-0.00109	-0.00469	-0.00037	-0.00088

Table E.3 Continued.

Triacylglycerol (18:0/18:1(9Z) /16:0)	tag180181 9Z160_c	- 0.00129	- 0.00129	- 0.00165	- 0.00243	- 0.00250	- 0.00105	- 0.00454	- 0.00036	- 0.00085
Triacylglycerol (18:1(11Z) /18:1(11Z) /16:0)	tag18111Z 18111Z160_c	- 0.00129	- 0.00129	- 0.00165	- 0.00244	- 0.00251	- 0.00106	- 0.00455	- 0.00036	- 0.00085
Triacylglycerol (18:1(11Z) /18:1(9Z) /16:0)	tag18111Z 1819Z160_c	- 0.00129	- 0.00129	- 0.00165	- 0.00244	- 0.00251	- 0.00106	- 0.00455	- 0.00036	- 0.00085
Triacylglycerol (18:1(9Z) /18:1(11Z) /16:0)	tag1819Z 8111Z16 0_c	- 0.00129	- 0.00129	- 0.00165	- 0.00244	- 0.00251	- 0.00106	- 0.00455	- 0.00036	- 0.00085
Triacylglycerol (18:1(9Z) /18:1(9Z) /16:0)	tag1819Z 1819Z1 60_c	- 0.00129	- 0.00129	- 0.00165	- 0.00244	- 0.00251	- 0.00106	- 0.00455	- 0.00036	- 0.00085
Triacylglycerol (16:0/18:1(11Z) /18:0)	tag1601 8111Z18 0_c	- 0.00129	- 0.00129	- 0.00165	- 0.00243	- 0.00250	- 0.00105	- 0.00454	- 0.00036	- 0.00085
Triacylglycerol (16:0/18:1(9Z) /18:0)	tag1601 819Z18 0_c	- 0.00129	- 0.00129	- 0.00165	- 0.00243	- 0.00250	- 0.00105	- 0.00454	- 0.00036	- 0.00085
Triacylglycerol (18:0/18:1(9Z) /18:0)	tag18018 19Z180 $_c$ |	- 0.00124	- 0.00124	- 0.00160	- 0.00235	- 0.00242	- 0.00102	- 0.00440	- 0.00035	- 0.00082
Triacylglycerol (18:1(11Z) /18:1(11Z) /18:0)	tag18111 Z18111Z 180_c	- 0.00125	- 0.00125	- 0.00160	- 0.00236	- 0.00243	- 0.00102	- 0.00441	- 0.00035	- 0.00082
Triacylglycerol (18:1(11Z) /18:1(9Z) /18:0)	tag1811 1Z1819Z 180_c	- 0.00125	- 0.00125	- 0.00160	- 0.00236	- 0.00243	- 0.00102	- 0.00441	- 0.00035	- 0.00082

Table E.3 Continued.

Triacylglycerol (18:1(9Z) /18:1(11Z) /18:0)	tag181 9Z18111 Z180_c	- 0.00125	- 0.00125	- 0.00160	- 0.00236	- 0.00243	- 0.00102	- 0.00441	- 0.00035	- 0.00082
Triacylglycerol (18:1(9Z) /18:1(9Z) /18:0)	tag1819 Z1819Z 180_c	- 0.00125	- 0.00125	- 0.00160	- 0.00236	- 0.00243	- 0.00102	- 0.00441	- 0.00035	- 0.00082
Triacylglycerol (16:0/18:1(11Z) /18:1(11Z))	tag160 18111Z 18111 Z_c	- 0.00129	- 0.00129	- 0.00165	- 0.00244	- 0.00251	- 0.00106	- 0.00455	- 0.00036	- 0.00085
Triacylglycerol (16:0/18:1(9Z) /18:1(11Z))	tag160 1819Z18 111Z_c	- 0.00129	- 0.00129	- 0.00165	- 0.00244	- 0.00251	- 0.00106	- 0.00455	- 0.00036	- 0.00085
Triacylglycerol (18:0/18:1(9Z) /18:1(11Z))	tag1801 819Z181 11Z_c	- 0.00125	- 0.00125	- 0.00160	- 0.00236	- 0.00243	- 0.00102	- 0.00441	- 0.00035	- 0.00082
Triacylglycerol (18:1(11Z) /18:1(11Z) /18:1(11Z))	tag1811 1Z18111 Z18111 Z_c	- 0.00125	- 0.00125	- 0.00160	- 0.00237	- 0.00243	- 0.00103	- 0.00442	- 0.00035	- 0.00082
Triacylglycerol (18:1(11Z) /18:1(9Z) /18:1(11Z))	tag18111 Z1819Z1 8111Z_c	- 0.00125	- 0.00125	- 0.00160	- 0.00237	- 0.00243	- 0.00103	- 0.00442	- 0.00035	- 0.00082
Triacylglycerol (18:1(9Z) /18:1(11Z) /18:1(11Z))	tag1819 Z18111Z 18111Z_c	- 0.00125	- 0.00125	- 0.00160	- 0.00237	- 0.00243	- 0.00103	- 0.00442	- 0.00035	- 0.00082
Triacylglycerol (18:1(9Z) /18:1(9Z) /18:1(11Z))	tag1819Z 1819Z181 11Z_c	- 0.00125	- 0.00125	- 0.00160	- 0.00237	- 0.00243	- 0.00103	- 0.00442	- 0.00035	- 0.00082

Table E.3 Continued.

Triacylglycerol (16:0/18:1(11Z) /18:1(9Z))	tag16018 111Z1819 Z_c	- 0.00129	- 0.00129	- 0.00165	- 0.00244	- 0.00251	- 0.00106	- 0.00455	- 0.00036	- 0.00085
Triacylglycerol (16:0/18:1(9Z) /18:1(9Z))	tag1601 819Z1819 Z_c	- 0.00129	- 0.00129	- 0.00165	- 0.00244	- 0.00251	- 0.00106	- 0.00455	- 0.00036	- 0.00085
Triacylglycerol (18:0/18:1(9Z) /18:1(9Z))	tag1801 819Z181 9Z_c	- 0.00125	- 0.00125	- 0.00160	- 0.00236	- 0.00243	- 0.00102	- 0.00441	- 0.00035	- 0.00082
Triacylglycerol (18:1(11Z) /18:1(11Z) /18:1(9Z))	tag1811 1Z18111Z 1819Z_c	- 0.00125	- 0.00125	- 0.00160	- 0.00237	- 0.00243	- 0.00103	- 0.00442	- 0.00035	- 0.00082
Triacylglycerol (18:1(11Z) /18:1(9Z) /18:1(9Z))	tag1811 1Z1819Z 1819Z_c	- 0.00125	- 0.00125	- 0.00160	- 0.00237	- 0.00243	- 0.00103	- 0.00442	- 0.00035	- 0.00082
Triacylglycerol (18:1(9Z) /18:1(11Z) /18:1(9Z))	tag1819Z 18111Z1 819Z_c	- 0.00125	- 0.00125	- 0.00160	- 0.00237	- 0.00243	- 0.00103	- 0.00442	- 0.00035	- 0.00082
Triacylglycerol (18:1(9Z) /18:1(9Z) /18:1(9Z))	tag1819 Z1819Z1 819Z_c	- 0.00125	- 0.00125	- 0.00160	- 0.00237	- 0.00243	- 0.00103	- 0.00442	- 0.00035	- 0.00082
Triacylglycerol (16:0/18:1(11Z) /18:3(5Z,9Z,12Z))	tag16018 111Z18 35Z9Z12Z $_c$	- 0.00129	- 0.00129	- 0.00166	- 0.00245	- 0.00252	- 0.00106	- 0.00457	- 0.00036	- 0.00085
Triacylglycerol (16:0/18:1(9Z) /18:3(5Z,9Z,12Z))	tag160181 9Z1835Z9 Z12Z_c	- 0.00129	- 0.00129	- 0.00166	- 0.00245	- 0.00252	- 0.00106	- 0.00457	- 0.00036	- 0.00085

Table E.3 Continued.

Triacylglycerol (18:0/18:1(9Z) /18:3(5Z,9Z,12Z))	tag18018 19Z1835Z 9Z12Z_c	- 0.00125	- 0.00125	- 0.00161	- 0.00237	- 0.00244	- 0.00103	- 0.00443	- 0.00035	- 0.00083
Triacylglycerol (18:1(11Z) /18:1(11Z) /18:3(5Z,9Z,12Z))	tag18111 Z18111Z 1835Z9Z 12Z_c	- 0.00126	- 0.00126	- 0.00161	- 0.00238	- 0.00244	- 0.00103	- 0.00444	- 0.00035	- 0.00083
Triacylglycerol (18:1(11Z) /18:1(9Z) /18:3(5Z,9Z,12Z))	tag18111 Z1819Z1 835Z9Z12 Z_c	- 0.00126	- 0.00126	- 0.00161	- 0.00238	- 0.00244	- 0.00103	- 0.00444	- 0.00035	- 0.00083
Triacylglycerol (18:1(9Z) /18:1(11Z) /18:3(5Z,9Z,12Z))	tag1819Z 18111Z1 835Z9Z1 2Z_c	- 0.00126	- 0.00126	- 0.00161	- 0.00238	- 0.00244	- 0.00103	- 0.00444	- 0.00035	- 0.00083
Triacylglycerol (18:1(9Z) /18:1(9Z) /18:3(5Z,9Z,12Z))	tag1819Z 1819Z183 5Z9Z12 Z_c	- 0.00126	- 0.00126	- 0.00161	- 0.00238	- 0.00244	- 0.00103	- 0.00444	- 0.00035	- 0.00083
Triacylglycerol (16:0/18:1(11Z) /18:4(5Z,9Z,12Z,15Z))	tag1601 8111Z18 45Z9Z12 Z15Z_c	- 0.00130	- 0.00130	- 0.00166	- 0.00245	- 0.00252	- 0.00106	- 0.00458	- 0.00036	- 0.00085
Triacylglycerol (16:0/18:1(9Z) /18:4(5Z,9Z,12Z,15Z))	tag1601 819Z184 5Z9Z12 Z15Z_c	- 0.00130	- 0.00130	- 0.00166	- 0.00245	- 0.00252	- 0.00106	- 0.00458	- 0.00036	- 0.00085
Triacylglycerol (18:0/18:1(9Z) /18:4(5Z,9Z,12Z,15Z))	tag1801 819Z184 5Z9Z12Z 15Z_c	- 0.00126	- 0.00126	- 0.00161	- 0.00238	- 0.00244	- 0.00103	- 0.00444	- 0.00035	- 0.00083

Table E.3 Continued.

Triacylglycerol (18:1(11Z) /18:1(11Z) /18:4(5Z,9Z,12Z,15Z))	tag18111 Z18111Z1 845Z9Z12Z 15Z_c	-0.00126	-0.00126	-0.00161	-0.00238	-0.00245	-0.00103	-0.00445	-0.00035	-0.00083
Triacylglycerol (18:1(11Z) /18:1(9Z) /18:4(5Z,9Z,12Z,15Z))	tag18111 Z1819Z18 45Z9Z12 Z15Z_c	-0.00126	-0.00126	-0.00161	-0.00238	-0.00245	-0.00103	-0.00445	-0.00035	-0.00083
Triacylglycerol (18:1(9Z) /18:1(11Z) /18:4(5Z,9Z,12Z,15Z))	tag1819Z 18111Z18 45Z9Z12Z 15Z_c	-0.00126	-0.00126	-0.00161	-0.00238	-0.00245	-0.00103	-0.00445	-0.00035	-0.00083
Triacylglycerol (18:1(9Z) /18:1(9Z) /18:4(5Z,9Z,12Z,15Z))	tag1819Z1 819Z1845 Z9Z12Z1 5Z_c	-0.00126	-0.00126	-0.00161	-0.00238	-0.00245	-0.00103	-0.00445	-0.00035	-0.00083
Acetate	ac_c	-0.03706	-0.03706	-0.11508	-0.08631	-0.10149	-0.02929	-0.03419	-0.03592	-0.04183
Propionate (n-C3:0)	ppa_c	-0.03005	-0.03005	-0.09330	-0.06997	-0.08228	-0.02375	-0.02772	-0.02912	-0.03391
Butyrate (n-C4:0)	but_c	-0.02526	-0.02526	-0.07845	-0.05884	-0.06918	-0.01997	-0.02331	-0.02448	-0.02851
Glycerol	glyc_c	-0.01208	-0.01208	-0.03752	-0.02814	-0.03309	-0.00955	-0.01115	-0.01171	-0.01364
Chlorophyll a	chla_u	-0.01008	-0.00784	-0.00858	-0.00715	-0.00930	-0.00358	-0.01008	-0.01400	-0.01008
Chlorophyll b	chlb_u	-0.01655	-0.01434	-0.01408	-0.01174	-0.01526	-0.00587	-0.01655	-0.02297	-0.01655
Rhodopsin	rhodopsin_s	0.00000	0.00000	0.00000	0.00000	0.00000	0.00000	0.00000	0.00000	0.00000
alpha-Carotene	acaro_h	-0.00050	0.00000	-0.00050	-0.00050	-0.00050	-0.00050	-0.00050	-0.00161	-0.00050

Table E.3 Continued.

Antheraxanthin	anxan_u	-0.00010	0.00000	-0.00010	-0.00010	-0.00010	-0.00010	-0.00010	-0.00032	-0.00010
beta-Carotene	caro_u	-0.00141	-0.00001	-0.00141	-0.00141	-0.00141	-0.00141	-0.00141	-0.00451	-0.00141
Loroxanthin	loroxan_u	-0.00066	-0.00001	-0.00066	-0.00066	-0.00066	-0.00066	-0.00066	-0.00209	-0.00066
Lutein	lut_u	-0.00126	-0.00001	-0.00126	-0.00126	-0.00126	-0.00126	-0.00126	-0.00402	-0.00126
Neoxanthin	neoxan_u	-0.00055	0.00000	-0.00055	-0.00055	-0.00055	-0.00055	-0.00055	-0.00177	-0.00055
Violaxanthin	vioxan_u	-0.00035	0.00000	-0.00035	-0.00035	-0.00035	-0.00035	-0.00035	-0.00113	-0.00035
Zeaxanthin	zaxan_u	-0.00030	0.00000	-0.00030	-0.00030	-0.00030	-0.00030	-0.00030	-0.00097	-0.00030
Nicotinamide adenine dinucleotide	nad_c	-0.00179	-0.00179	-0.00179	-0.00179	-0.00179	-0.00179	-0.00179	-0.00179	-0.00179
Nicotinamide adenine dinucleotide - reduced	nadh_c	-0.00005	-0.00005	-0.00005	-0.00005	-0.00005	-0.00005	-0.00005	-0.00005	-0.00005
Nicotinamide adenine dinucleotide phosphate	nadp_c	-0.00011	-0.00011	-0.00011	-0.00011	-0.00011	-0.00011	-0.00011	-0.00011	-0.00011
Nicotinamide adenine dinucleotide phosphate - reduced	nadph_c	-0.00034	-0.00034	-0.00034	-0.00034	-0.00034	-0.00034	-0.00034	-0.00034	-0.00034
Biotin	btn_c	0.00000	0.00000	0.00000	0.00000	0.00000	0.00000	0.00000	0.00000	0.00000
Thiamine monophosphate	thmmp_c	-0.00022	-0.00022	-0.00011	-0.00012	-0.00009	-0.00023	-0.00006	-0.00025	-0.00020
Flavin adenine dinucleotide oxidized	fad_c	-0.00022	-0.00022	-0.00022	-0.00022	-0.00022	-0.00022	-0.00022	-0.00022	-0.00022

Table E.3 Continued.

Reduced glutathione	gthrd_c	-0.00006	-0.00006	-0.00006	-0.00006	-0.00006	-0.00006	-0.00006	-0.00006	-0.00006
	Products									
ADP	adp_c	92.40	92.40	29.89	29.89	29.89	24.0332	7.7579	45.7318	53.35
H+	h_c	92.40	92.40	29.89	29.89	29.89	24.0332	7.7579	45.7318	53.35
Phosphate	pi_c	92.40	92.40	29.89	29.89	29.89	24.0332	7.7579	45.7318	53.35
tRNA(Ala)	trnaala_c	0.86603	0.27926	0.40838	0.47409	0.34736	0.87449	0.21501	0.95460	0.77548
tRNA(Arg)	trnaarg_c	0.47517	0.09366	0.22407	0.26012	0.19058	0.47981	0.11797	0.52376	0.42548
tRNA(Asn)	trnaasn_c	0.21459	0.06954	0.10119	0.11747	0.08607	0.21669	0.05328	0.23654	0.19215
tRNA(Asp)	trnaasp_c	0.21459	0.06954	0.10119	0.11747	0.08607	0.21669	0.05328	0.23654	0.19215
tRNA(Cys)	trnacys_c	0.00766	0.01224	0.00361	0.00420	0.00307	0.00774	0.00190	0.00845	0.00686
tRNA(Gln)	trnagln_c	0.25674	0.09182	0.12107	0.14055	0.10298	0.25925	0.06374	0.28300	0.22990
tRNA(Glu)	trnaglu_c	0.25674	0.09182	0.12107	0.14055	0.10298	0.25925	0.06374	0.28300	0.22990
tRNA(Gly)	trnagly_c	0.32572	0.11386	0.15359	0.17831	0.13064	0.32890	0.08086	0.35903	0.29166
tRNA(His)	trnahis_c	0.00383	0.01273	0.00181	0.00210	0.00154	0.00387	0.00095	0.00422	0.00343
tRNA(Ile)	trnaile_c	0.10346	0.03795	0.04879	0.05664	0.04150	0.10447	0.02569	0.11405	0.09265
tRNA(Leu)	trnaleu_c	0.26058	0.09304	0.12287	0.14265	0.10451	0.26312	0.06469	0.28723	0.23333
tRNA(Lys)	trnalys_c	0.05748	0.03061	0.02710	0.03147	0.02305	0.05804	0.01427	0.06336	0.05147
tRNA(Met)	trnamet_c	0.00766	0.01273	0.00361	0.00420	0.00307	0.00774	0.00190	0.00845	0.00686
tRNA(Phe)	trnaphe_c	0.10730	0.04003	0.05060	0.05874	0.04304	0.10834	0.02664	0.11827	0.09608
tRNA(Pro)	trnapro_c	0.14945	0.05191	0.07047	0.08181	0.05994	0.15091	0.03710	0.16473	0.13382
tRNA(Ser)	trnaser_c	0.06514	0.02081	0.03072	0.03566	0.02613	0.06578	0.01617	0.07181	0.05833
tRNA(Thr)	trnathr_c	0.26058	0.03452	0.12287	0.14265	0.10451	0.26312	0.06469	0.28723	0.23333
tRNA(Trp)	trnatrp_c	0.00383	0.00159	0.00181	0.00210	0.00154	0.00387	0.00095	0.00422	0.00343
tRNA(Tyr)	trnatyr_c	0.00383	0.00159	0.00181	0.00210	0.00154	0.00387	0.00095	0.00422	0.00343
tRNA(Val)	trnaval_c	0.18777	0.06427	0.08854	0.10279	0.07531	0.18960	0.04662	0.20697	0.16813